THÈSE

En vue de l'obtention du

DOCTORAT DE L'UNIVERSITÉ DE TOULOUSE

Délivré par :

Institut National Polytechnique de Toulouse (INP Toulouse)

Discipline ou spécialité :

Génie Électrique

Présentée et soutenue par :

M. LUKASZ KRZYSZTOF SIENKIEWICZ

le mardi 7 juin 2016

Titre :

CONCEPT, IMPLEMENTATION AND ANALYSIS OF THE
PIEZOELECTRIC RESONANT SENSOR/ACTUATOR FOR MEASURING
THE AGING PROCESS OF HUMAN SKIN

Ecole doctorale :

Génie Electrique, Electronique, Télécommunications (GEET)

Unité de recherche :

Laboratoire Plasma et Conversion d'Energie (LAPLACE)

Directeur(s) de Thèse :

M. JEAN FRANCOIS ROUCHON

M. MIECZYSLAW RONKOWSKI

Rapporteurs :

M. LIONEL PETIT, INSA LYON

M. SLAWOMIR WIAK, TECHNICAL UNIVERSITY OF LODZ

Membre(s) du jury :

M. JANUSZ NIEZNANSKI, POLITECHNIKA GDANSK POLOGNE, Président

M. FRANCOIS PIGACHE, INP TOULOUSE, Membre

M. GRZEGORZ KOSTRO, POLITECHNIKA GDANSK POLOGNE, Membre

M. JEAN FRANCOIS ROUCHON, INP TOULOUSE, Membre

M. MIECZYSLAW RONKOWSKI, POLITECHNIKA GDANSK POLOGNE, Membre

CONTENTS

The most exciting phrase to hear in science, the one that heralds new discoveries, is not 'Eureka!' but 'That's funny...'

Isaac Asimov

PRAGNĘ SERDECZNIE PODZIĘKOWAĆ

ACKNOWLEDGEMENTS

REMERCIEMENTS

Je voudrais remercier le Professeur Jean-François Rouchon, pour ses conseils et soutien pendant mon séjour en France. Pour de nombreux conseils et discussions techniques précieux tout au long de ce projet, mais surtout pour créer une atmosphère très amicale et agréable au laboratoire.

Je tiens à remercier vivement le Professeur Mieczysław Ronkowski pour encouragement et d'inspiration pour débuter les études de doctorat à Gdańsk et plus tard à Toulouse. Prof. Ronkowski a été un grand conseiller à la fois, les questions de la science et de la vie.

Je voudrais remercier tout particulièrement la Professeur Maria Pietrzak-Dawid pour son attitude amicale et énergique. Elle a été une grande aide pendant de mes études et de travaux de recherche à Toulouse, depuis le début. Il serait impossible sans Elle.

Je voudrais remercier mon co-directeur, le Docteur Grzegorz Kostro pour toute l'aide et des conseils et des discussions techniques au cours de mes études de doctorat.

Je voudrais remercier mon co-directeur, le Docteur François Pigache pour toute l'aide et des conseils précieux, particulièrement pendant les dernières étapes de mon travail.

Je voudrais exprimer ma gratitude à ingénieur Dominique Harribey pour me présenter le laboratoire et aider de nombreux aspects techniques et mécaniques des expériences.

Je tiens à remercier ma famille pour la compréhension et leur soutien par mes études en Pologne et en France.

Je remercie également mes collègues du département: Michał, Filip, Roland, Dominik et tous mes collègues d'Erasmus et N7 en particulier: Carlos, Dries, Elena, Fernanda, Faycel, Hemza, Max, Remi, Marcin et Maciek. Ce était le temps vraiment magiques.

Ania, mon amour, je te remercie pour ton soutien, de compréhension et de patience quand je ne suis pas avec toi.

STRESZCZENIE

Podstawowym celem rozprawy doktorskiej było opracowanie koncepcji, modelu analitycznego, modelu wirtualnego, modelu numerycznego, realizacja i weryfikacja eksperymentalna piezoelektrycznego rezonansowego sensora/aktuatora do pomiaru procesu starzenia się ludzkiej skóry. Rozprawę zrealizowano jako wspólny doktorat Politechniki Gdańskiej z uczelnią INP- ENSEEIHT-LAPLACE w Tuluzie, Francja. Praca doktorska jest kontynuacją dotychczasowych badań nad przetwornikami piezoelektrycznymi prowadzonymi w Katedrze Energoelektroniki i Maszyn Elektrycznych Politechniki Gdańskiej. Pracę częściowo zrealizowano w ramach staży naukowych w laboratorium LAPLACE w Tuluzie.

Opracowano koncepcję przetwornika do pomiaru właściwości mechanicznych charakteryzujących tkanki miękkie, w tym skórę. Rezonansowy, przetwornik piezoelektryczny zginający, zwany dalej przetwornikiem typu „unimorph", został wybrany na podstawie wymagań, które sformułowano w aspekcie właściwości ludzkiej skóry. W świetle metod opisu właściwości ludzkiej skóry zaproponowano nowatorskie podejście, wykorzystując dynamiczną metodę wgłębienia. Innowacyjność koncepcji polega na wsparciu dynamicznej metody wgłębienia przez zastosowanie rezonansowego sensora/aktuatora piezoelektrycznego jako wgłębnika (ang. indentation device). Takie rozwiązanie pozwala wykorzystać szereg atrakcyjnych właściwości piezoelektrycznych przetworników elektromechanicznych.

Rozprawa jest podzielona na siedem rozdziałów. Rozdział 1 opisuje tezę i cele pracy doktorskiej. Rozdział 2 przedstawia opis zjawiska piezoelektrycznego i jego zastosowania w dziedzinie medycyny i bioinżynierii. W rozdział 3 sformułowano wymagania stawiane rozważanemu przetwornikowi. Uzasadniono wybór przetwornika typu unimorph. W rozdziale 4 przedstawiono model analityczny przetwornika unimorph, uwzględniający statyczne obliczenia odkształceń, schemat zastępczy przetwornika oraz opis warunków pracy kontaktu pomiędzy przetwornikiem a badanymi materiałami. Rozdział 5 zawiera analizę numeryczną przetwornika unimorph z wykorzystaniem opracowanego modelu wirtualnego i metod polowych (FEM). Rozdział 6 opisuje realizację weryfikacji eksperymentalnej opracowanych modeli przetwornika unimorph, a w szczególności pomiarów zbudowanych prototypów przetwornika unimorph. Ostatni rozdział zawiera ogólne wnioski i osiągnięcia rozprawy, sformułowane na podstawie przeprowadzonych rozważań i wyników badań, a także wskazania celów przyszłych prac badawczych.

<u>ABSTRACT</u>

The main goal of the dissertation was following: preparation of a new concept, implementation and analysis of the piezoelectric resonant sensor/actuator for measuring the aging process of human skin. The research work has been carried out in the framework of cooperation between the INP-ENSEEIHT-LAPLACE, Toulouse, France, and at the Gdansk University of Technology, Faculty of Electrical and Control Engineering, Research Group of Power Electronics and Electrical Machines, Gdańsk, Poland.

A concept of transducer for the characterization of mechanical properties of soft tissues was presented. The piezoelectric resonant, bending transducer, referred to as "unimorph transducer" was chosen from different topologies of piezoelectric benders based on the fulfillment of the stated requirements. The innovation of the project lies in the integration of the dynamic indentation method by using a unimorph as an indentation device. This allows the use of a number of attractive electromechanical properties of piezoelectric transducers.

The thesis is divided into seven chapters. Chapter 1 states the thesis and goals of the dissertation. Chapter 2 presents piezoelectric phenomenon and piezoelectric applications in the fields of medicine and bioengineering. Chapter 3 describes the requirements for the developed transducer. The choice of unimorph transducer is justified. Chapter 4 presents an analytical description of the unimorph transducer, including the calculations of static deformations, equivalent circuit description, and description of the contact conditions between the transducer and the tested materials. Chapter 5 contains the numerical analysis of the unimorph transducer using FEM virtual model. Results of static and modal simulations are described for two considered geometries of the transducer. Chapter 6 describes the experimental verification process of analytic and numerical models developed for unimorph transducer. The final chapter includes general conclusions concerning obtained research results and achievements, as well as possible future works.

RESUME

L'objectif de cet projet est la conception, réalisation et caractérisation d'un actionneur / capteur piézoélectrique piézorésonant destiné à la mesure du vieillissement de la peau humaine. L'étude présentée est le fruit d'une collaboration entre le groupe de recherche de l'Electrodynamique du INP-ENSEEIHT (Toulouse), LAPLACE Laboratoire de Recherche et l'École Polytechnique de Gdańsk, Département Génie Electrique et Automatique.

Un concept d'actionneur / capteur pour la caractérisation des propriétés mécaniques des tissus mous a été présenté. Un actionneur piézoélectrique résonant, appelé "unimorphe" a été choisi parmi les différentes structures piézoélectriques fondées sur le cahier des charges. L'innovation du projet réside dans l'intégration de la méthode d'indentation dynamique en utilisant un unimorphe comme dispositif d'indentation. Ceci permet l'utilisation d'un certain nombre de propriétés électromécaniques favorables des transducteurs piézo-électriques.

Ce mémoire est divisé en 7 chapitres. Le chapitre 1 présente la thèse et ses objectifs. Le chapitre 2 présente le phénomène piézoélectrique et les applications piézoélectriques dans les domaines de la médecine et de la bioingénierie. Le chapitre 3 décrit le cahier des charges pour le transducteur développé. Le choix du transducteur unimorphe est ainsi justifié. Le chapitre 4 présente une description analytique du transducteur unimorphe, y compris les calculs de déformations statiques, la description du circuit équivalent de Mason, et la description des conditions de contact entre la sonde d'indentation et les matériaux testés. Le chapitre 5 contient l'analyse numérique du transducteur unimorphe en utilisant le modèle virtuel MEF. Les résultats de simulations statiques et modales sont décrits par deux géométries considérées du transducteur. Le chapitre 6 décrit le processus de vérification expérimentale des modèles analytiques et numériques développés pour le transducteur unimorphe. Enfin, le dernier chapitre comprend des conclusions générales concernant les résultats de recherche obtenus, ainsi que les travaux futurs possibles.

NOTATIONS

S_{ij}	Strain tensor
T_{kl}	Stress tensor
E_k	Electric field tensor
D_i	Electric displacement tensor
s_{ijkl}, c_{ijkl}	Compliance and stiffness tensors
$\varepsilon_{ij}, \beta_{ij}$	Permeability and impermeability tensors
k	Electromechanical coupling coefficient
E, E^*	Young modulus, reduced Young modulus
d, e, g, h	Piezoelectric constants
u, w	Displacement components
φ	Electric potential
$\widetilde{\varphi}, \psi$	Stress and induction functions
$\delta, \delta_0, \delta_{Ansys}$	Displacement at the free end of the transducer
$p(r), q(r)$	Normal and shear pressure distribution
$1/N$	Transformation ratio for the equivalent circuit
f_R, f_A	Resonance and anti-resonance frequencies
A	Displacement calculated from laser vibrometry
F_N	Normal force applied on the surface of the sample
R_M, C_M, L_M	Parameters of the equivalent circuit modelling the material properties

1   G<small>ENERAL</small> I<small>NTRODUCTION</small>

Among the basic transduction mechanisms that can be used for electricity-to-vibration conversion, and vice-versa, piezoelectric transduction has received the most attention in the existing literature [41], [42], [45]. Piezoelectric phenomenon and piezoelectric materials are preferred in transduction process due to their large power densities and ease of application. One of the best example of such an application is a resonant piezoelectric sensor.

A resonant piezoelectric sensor is a device with an element vibrating at resonance state, which changes its output frequency, i.e., mechanical resonance frequency as a function of a physical parameter; it is proved to have major advantages over other physical resolution principles. Resonant piezoelectric sensors with various excitation and detection techniques have been reported in the available literature [66], and each one has its own advantages and disadvantages. Smart materials, in particular piezoelectric materials for excitation and detection, have numerous advantages like, relatively large power density, relatively large force, low actuation voltage, high energy efficiency, linear behavior, high acoustic quality, high speed and high frequency. In the design of resonant piezoelectric sensors an applications of sensor/actuator in collocation (arrangement) is usually used and provides a stable performance [28].

Nowadays, an increased scientific interest in dynamic measurement methods of soft tissues utilizing piezoelectric sensors can be observed. Such solutions are of the interest in biomedical and pharmaceutical industry (e.g. L'Oréal) applications. The piezoelectric sensors and actuators, due to their favorable characteristics, are likely to replace many of the current solutions for the measurement (assessment) of mechanical quantities characterizing soft tissues, i.e., detection of disease states, determining the aging process of human skin, etc. [71].

1.1 Motivation

The research work described in this thesis has been conducted as part of the European Union sponsored programme ERASMUS [12], and a project *The Center for Advanced Studies - the development of interdisciplinary doctoral studies at the Gdansk University of Technology in the key areas of the Europe 2020 Strategy, referred to as Advanced PhD* [2].

The research work has been carried out in the framework of cooperation between the INP - ENSEEIHT - LAPLACE [34] (Laboratory on Plasma and Conversion of Energy), in Toulouse, France, and the Gdańsk University of Technology, Faculty of Electrical and Control Engineering, Power Electronics and Electrical Machines Research Unit in Gdańsk, Poland [51].

The LAPLACE Laboratory [34] is an inter-university research unit. Its advanced research programs covers the production, the transportation, the management, the conversion and the use of the electricity while concerning all the aspects right from the study of fundamental processes in solid and gas to the development of processes and systems. The major field of study concern the plasma discharges as well as plasma applications, the study of the dielectric materials (polymers, in particular) and their integration into the systems, the study and the design of the electrical systems, the optimization of the controls and the converters. One of the LAPLACE's Laboratory research groups - GREM3 - is a leading research unit in the world in the field of piezoelectric technology and shape-memory alloys technology.

The research process described in this dissertation was divided into two main stages. The first stage was one-year studying and research programme in the frame of ERASMUS, which started in September 2011 at the INP-ENSEEIHT-LAPLACE. This programme, within the specialization of the "Transformation de l'Energie et Mécatronique avancée", covered issues of power electronics, automation and mechatronics systems, and has been completed with the International Master research project and diploma. The first part of the carried out research covered the "Rotating-mode motor – simulations, manufacturing and measurements", and also the "Hybrid piezoelectric motor" topics. The second part was a six-month International Master research project, concerning the piezoelectric sensor/actuator structure, entitled: "Sensor/actuator for measuring the aging process of human skin".

The second stage of the research process was a 10-month research programme in the frame of the Advanced PhD, started in October 2013. It has been divided into 7-month research work carried out at the Power Electronics and Electrical Machines Research Unit, and 3-month internship at the LAPLACE Laboratory. The subject of the research work conducted at the LAPLACE Laboratory was "Analysis and measurement of resonant piezoelectric

sensor/actuator structure", and has covered the performance analysis of a new prototype of unimorph resonant piezoelectric transducer.

It should be emphasized that the research works in the field of piezoelectric technology have not been carried out on a wide scale in Poland, until now. The study carried out in the frame of this thesis can be considered as a pioneer research works in Poland. It focuses on application of piezoelectric transducers for measurement the mechanical properties of soft materials.

1.2 Objectives of the dissertation

A dynamic indentation method for measurement of the mechanical properties characterizing the soft tissues is used in this dissertation. It is based on measurement the normal component of force applied on the surface of the material as a function of the displacement imposed by the indenter. In addition to a static force, vibrations are injected on the surface of the tested sample. Within this method a piezoelectric system is introduced to make use of the electromechanical impedance characterization of resonant piezoelectric actuators [28], [58].

The key aspect of the research work lies in aiding of the dynamic indentation method by using a resonant transducer as an indentation device. This approach allows to use a number of favorable electromechanical properties of piezoelectric transducers: high sensitivity, generation of vibrations in a wide frequency range, control of the measurement conditions by changing the work mode of the transducer, use of the electromechanical impedance methods, simple design and compact dimensions.

Proposition of the thesis is as follows:

The fundamental mechanical properties of a visco-elastic medium resembling a human skin, such as rigidity, flexibility and viscosity, can be determined by measuring the electromechanical impedance variation of the piezoelectric transducer contacting the tested medium.

In order to verify the proposition of the thesis a full research cycle was carried out, that covered: analytical study, numerical analysis (FEM simulations), prototype realization, and experimental verification of the considered (developed) piezoelectric sensor/actuator structures.

The scope of the dissertation included:

- State of the art study of the considered issues in the available literature.
- Development of the concept of piezoelectric sensor/actuator structures.
- Analytical study of the developed/considered piezoelectric sensor/actuator. Application of equivalent circuit representation method (modified Mason's equivalent circuit).
- Application of the electromechanical impedance concept to determine the parameters of the equivalent circuit models of the considered piezoelectric sensor/actuator.
- Development of a virtual model (CAD techniques) of the considered sensor/actuator in operating mode.
- Numerical (FEM ANSYS software) analysis of the virtual model of the considered piezoelectric sensor/actuator.
- Experimental verification of the developed piezoelectric sensor/actuator prototypes.

1.3 Thesis layout

To describe each of the stages of the research work in a systematic way, the thesis is organized into seven chapters.

In chapter 1 the motivation and objectives of the research work are briefly described.

In chapter 2 the piezoelectric phenomenon, history of piezoelectricity, piezoelectric materials and their structures are presented. Examples of piezoelectric applications in the fields of medicine and bioengineering are considered.

In chapter 3 the requirements are formulated for the developed transducer. They are based on the properties of soft tissues, human skin in particular. The structures of piezoelectric bending transducer are presented. Choice of unimorph transducer is justified. Two prototypes of unimorph transducer are described in detail.

In chapter 4 an analytical description of the unimorph transducer is carried out. It includes the calculations of static deformations, equivalent circuit description of the transducer working

near resonance of the system. And finally, the contact conditions between the transducer and the tested materials are described using the Hertz theory.

In chapter 5 the numerical (FEM simulation) analysis of the unimorph transducer virtual model is carried out using Ansys software. Results of static and modal simulations are described for two considered geometries of the transducer.

In chapter 6 experimental verification of the developed piezoelectric sensor/actuator prototypes is presented. Also the results of the experimental analysis are discussed.

In the last chapter 7 the final conclusions concerning obtained research results and achievements, as well as possible future works are presented.

To this dissertation five appendixes are attached.

2 PIEZOELECTRICITY: MATERIALS AND APPLICATIONS

2.1 Physical phenomenon

The piezoelectric effect occurs in materials where an externally applied elastic strain causes a change in electric polarization which generates a charge and a voltage across the material. The converse piezoelectric effect is produced by an externally applied electric field, which changes the electric polarization, which in turn produces an elastic strain.

For a crystal to exhibit the piezoelectric effect, its structure should have no center of symmetry. A stress (tensile or compressive) applied to such a crystal will alter the separation between the positive and negative charge sites in each elementary cell leading to a net polarization at the crystal surface (direct piezoelectric effect). The effect is reciprocal, so that if the crystal is exposed to an electric field, it will experience an elastic strain causing its length to increase or decrease according to field polarity (the converse piezoelectric effect). Both effects are schematically demonstrated in the Figure 2.1:
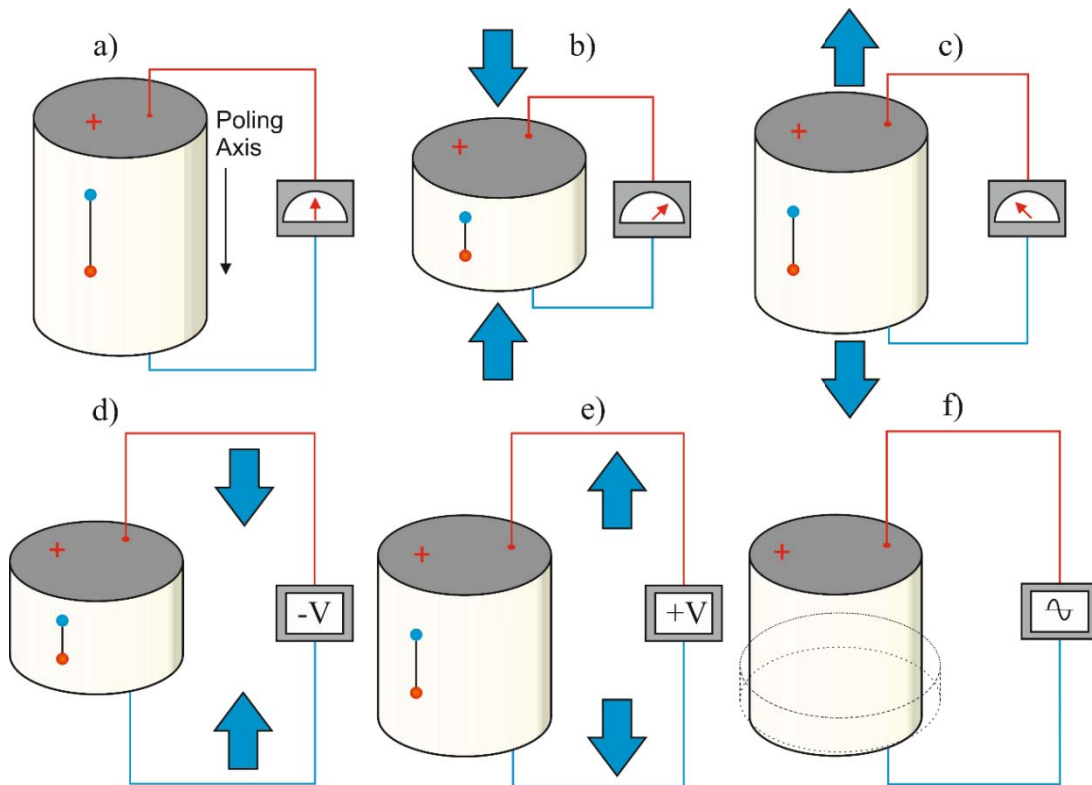
Figure 2.1 Illustrations of piezoelectric effects: direct piezoelectric effect a), b), c) and reverse piezoelectric effect d), e), f); the scale is extended for clarity

2.1.1 History

In the middle of eighteenth century Carolus Linnaeus and Franz Aepinus first observed that certain materials, such as crystals and some ceramics, generate electric charges due to a temperature change. Piezoelectricity as a research field in crystal physics was initiated by the brothers Jacques Curie (1856–1941) and Pierre Curie (1859–1906) with their studies [21], [22]. They discovered an unusual characteristic of certain crystalline minerals as tourmaline, quartz, topaz, cane sugar and Rochelle salt. It was found that tension and compression generated voltages of opposite polarity and proportional to the applied load. This was called by Hankel the piezoelectric effect [67].

The word piezoelectricity comes from Greek and means electricity resulting from pressure (Piezo means pressure in Greek). In the year following the discovery of the direct effect, Gabriel Lippman [16] predicted the existence of the converse effect basing on fundamental thermodynamic principles. Before the end of 1881 the brothers Curies confirmed experimentally the existence of the converse effect. They showed that if one of the voltage-generating crystals was exposed to an electric field it lengthened or shortened according to the polarity of the field, and in proportion to its strength.

Until the beginning of the century, the piezoelectricity did not leave the laboratories. In 1917, Paul Langevin, a French physicist, developed a submarine detector based on the piezoelectric effect, resulting in an improved method for submarine ultrasonic echo detection, namely sonar. This invention was the beginning of practical application of the piezoelectric effect. The success of Langevin's invention opened up opportunities for piezoelectric materials in underwater applications as well as a host of other applications such as ultrasonic transducers, microphones, accelerometers, etc. [46].

In 1945 piezoelectricity was introduced into the global market, thanks to discovery of the mixed oxide compound barium titanate $BaTiO_3$. It was a ferroelectric which could be easily fabricated and shaped at low price and could be made piezoelectric with constants many times higher than natural materials by an electrical poling process. This material was of stable perovskite type, which is one of the fundamental crystal lattice structures (described in chapter 2.1.3). The discovery of lead zirconate titanate (PZT) families of materials in the 1950s was

the beginning of the modern history of piezoelectricity. Until to today, PZT material is one of the most widely used piezoelectric materials [5].

A variety of new areas, such as ultrasonic delay lines, ultrasonic medical therapy and diagnostics, level gauges, devices for continuous industrial control of physical and chemical substance properties, and other devices with wide range of applications were found for piezoelectric transducers. At the same time, more effective electro-acoustic transducers became available. Piezoelectric transducers have been used for measuring wide variety of mechanical and thermal parameters including: effort, pressure, acceleration, weight, angular speed, torques, deformations, temperature etc. Considering accuracy, these devices in many cases surpassed transducers based on other detection principles [66].

Nowadays, piezoelectric transducers are used in various fields of industry, including but not limited to medicine and bioengineering for ultrasonic tomography, pulse measurements, tone measurements, urology, ophthalmology, etc. [31], [36]. The section 2.4 covers the industry applications of piezoelectric materials and transducers in more details.

2.1.2 Materials

Materials that exhibit a significant and useful piezoelectric effect fall into three main groups: natural and synthetic crystals, polarized piezoelectric ceramics, and certain polymer films. The natural Piezoelectric materials are crystals like quartz (SiO_4), Rochelle salt, Tourmaline-group minerals, Topaz, cane sugar, and some organic substances as silk, wood, enamel, dentin, bone, hair, rubber. In the atomic structure of those materials the change in the position of the atoms due to applied stress leads to the formation of net dipole moments that causes polarization and an electric field, respectively.

Since 1935 attempts were made to produce piezoelectric crystals, which could replace quartz. Piezoelectric crystals such as ammonium and potassium salts ($NH_4H_2PO_4 - ADP$, $KH_2PO_4 - KDP$), ethylene diamine tartrate (*EDT*), dipotassium tartrate (*DKT*) and lithium sulphate monohydrate (*LH*) were developed. Many of these materials are no longer in use due to development and production of artificial quartz, ferroelectric crystals or piezoelectric ceramics. With the exception to quartz few single crystals are used in piezoelectric devices. Popular choices are $LiNbO_3$, $LiTaO_3$. The single crystals are anisotropic, exhibiting different

material properties depending on the cut of the materials and the direction of bulk or surface wave propagation [24].

The discovery of the strong piezoelectric properties of ferroelectric ceramics was a major milestone in applications of piezoelectricity. The ferroelectric ceramics are the most common piezoelectric material in today's engineering applications. Among them, polycrystalline ceramics like barium titanate (*BaTiO₃*) and lead zirconate titanate (*PZT*) are the most popular materials, in particular due to the low manufacturing costs and the almost arbitrary shaping possibilities compared to single crystalline piezoelectrics. Furthermore, they exhibit outstanding piezoelectric and dielectric properties, which make them particularly indispensable for the field of actuators [11].

Lead zirconate titanate (PZT) are based on the Perovskite structure of ferroelectric crystals. The general chemical formulae of perovskite crystal structure is ABO_3 , where A are larger metal ions, usually lead or barium, B is a smaller metal ion, usually titanium or zirconium. The perovskite structure is the simplest arrangement where the corner-sharing oxygen octahedra are linked together in a regular cubic array with smaller cations occupying the central octahedral B-site, and larger cations filling the interstices between octahedra in the larger A-site. Figure 2.2 shows the crystal structure of a piezoelectric ceramic (*BaTiO₃*) at temperature above and below Curie point.

a) $T > T_c$ b) $T < T_c$
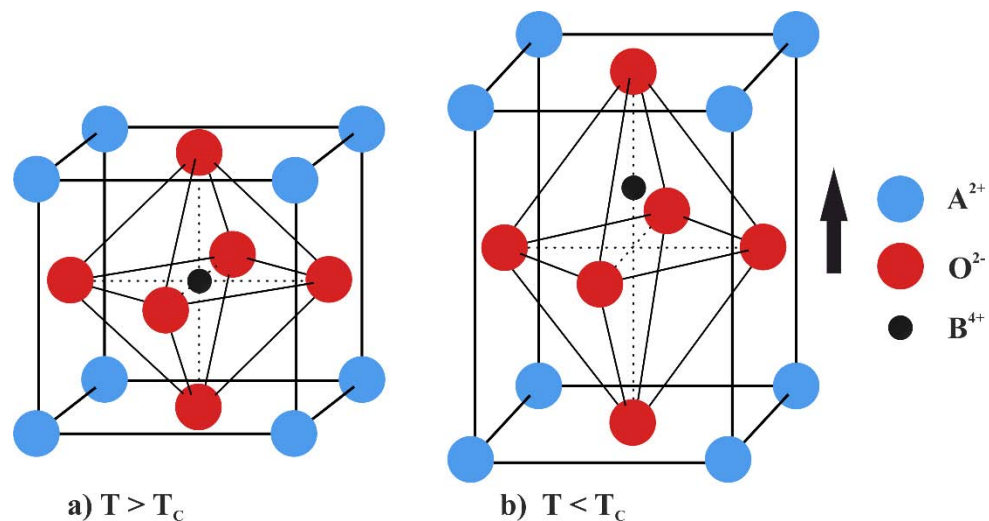
Figure 2.2 Crystal structure of a traditional piezoelectric ceramic (*BaTiO₃*) at temperature a) above, and b) below Curie point

9

Piezoceramics do not have a macroscopic piezoelectric behavior, although the individual single-crystal grain has piezoelectric characteristics. The spontaneous polarization can be reoriented by an external electric filed: ferroelectric ceramics must be artificially polarized by a strong electric field while the material is heated above its Curie point and then slowly cooled with field applied. Remnant polarization being retained, the material exhibits macroscopic piezoelectric effect [49].

"Poling" is the process of generating net remnant polarization in the material by applying sufficiently high electric field. When an electric field is applied to a ferroelectric material, the microscopic ferroelectric domains orient themselves in the direction of the applied field. As the electric field is increased, more and more domains get oriented and, at a sufficiently high electric field, almost all the domains are in the same direction resulting in a single large domain. The material in this state possesses maximum polarization. If the material is maintained at a high temperature (close to the transition temperature) while the electric field is applied, the orientation of the domains is facilitated. The process of poling involves the following steps:

1. The material is heated to a temperature slightly less than the transition temperature and held at the temperature.

2. A sufficiently high electric field is applied to the material for about $2 - 3 \ h$. All the ferroelectric domains get oriented in the direction of the electric field, and the material attains saturation polarization.

3. The material is cooled to room temperature with the electric field kept on. The domains remain frozen in the oriented state.

4. The electric field is now put off. The material remains in the maximum polarization state with most of the domains oriented in the same direction.

The orientation of domains during poling process is illustrated in Figure 2.3.
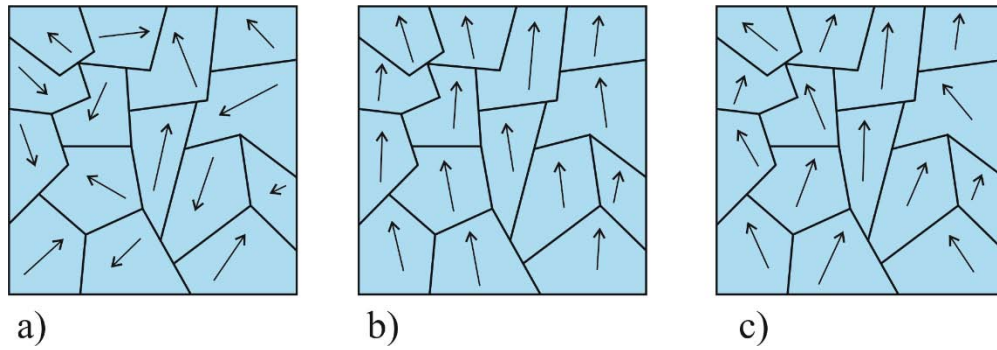
Figure 2.3 Polling of a piezoelectric material: a) the domains are randomly oriented when the material is unpoled; b) The domains are oriented in the direction of the applied electric field, c) relaxation of remnant polarization due to aging

Piezoelectric ceramics are usually divided into two groups. The antonyms "hard" and "soft" doped piezoelectric materials refer to the ferroelectric properties, i.e. the mobility of the dipoles or domains and hence also to the polarization/depolarization behavior. "Hard" piezoelectric materials are those materials whose properties are stable with temperature, electric field, and stress. They are used in applications requiring high power actuation or projection. The applications often have a narrow bandwidth, but are usually operated either at resonance or well under resonance. "Soft" piezoelectric materials are those materials whose properties have been enhanced for sensing, actuation, or both. They have high coupling and high permittivity. Property enhancement was made at the expense of temperature, electric field, and stress stability [13].

The most recent group of piezoelectric materials, PVDF films (polyvinylidene fluoride), was discovered in 1969 in Japan. PVDF can be of two types: piezo-polymer in which the piezoelectric material is immersed in an electrically passive matrix (for instance PZT in epoxy matrix) and piezo-composites that are composite materials made from two different ceramics (for example $BaTiO_3$ fibers reinforcing a PZT matrix).With piezo- and pyroelectric coefficients being less than that of crystalline or ceramic piezoelectrics, polymers have found niche commercial applications in different fields, ranging from sensor systems, accelerometers and non-destructive testing (contactless switches) to fundamental research applications, such as photo-pyroelectric spectroscopy. This class of materials is also used for manufacturing piezo films of low thickness (less than 30 μm), which may be laminated on the structural materials [18].

2.1.3 Physical structure

There are 32 crystal classes which are divided into the following seven groups: triclinic, monoclinic, orthorhombic, tetragonal, trigonal, hexagonal and cubic. These groups are also associated with the elastic nature of the material where triclinic represents an anisotropic material, orthorhombic represents an orthotropic material and cubic are in most cases isotropic materials. Only 20 of the 32 classes allow for piezoelectric properties. Ten of these classes are polar, i.e. show a spontaneous polarization without mechanical stress due to a non-vanishing electric dipole moment associated with their unit cell. The remaining 10 classes are not polar, i.e. polarization appears only after applying a mechanical load.

Figure 2.4 shows a simple molecular model of piezoelectric material. It explains the generating of an electric charge as the result of a force exerted on the material. Before subjecting the material to some external stress, the gravity centers of the negative and positive charges of each molecule coincide. Therefore, the external effects of the negative and positive charges are reciprocally cancelled. As a result, an electrically neutral molecule appears (Figure 2.4a). When exerting some pressure on the material, its internal reticular structure can be deformed, causing the separation of the positive and negative gravity centers of the molecules and generating little dipoles (Figure 2.4b). The facing poles inside the material are mutually cancelled and a distribution of a linked charge appears in the material's surfaces - the material is polarized (Figure 2.4c). This polarization generates an electric field and can be used to transform the mechanical energy used in the material's deformation into electrical energy [7].
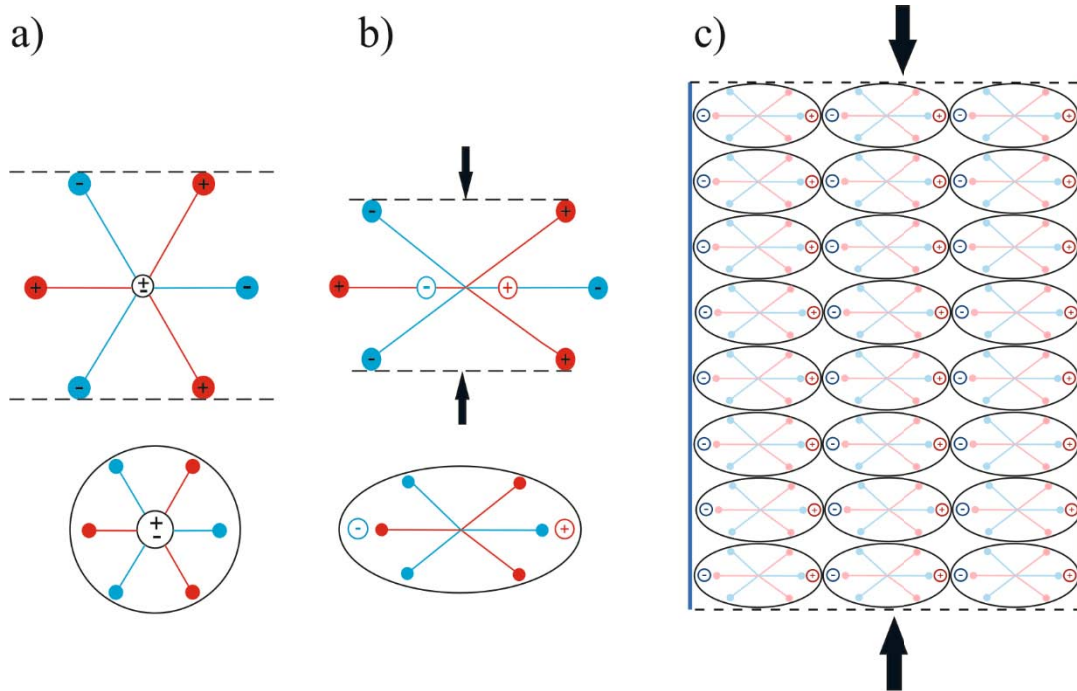
Figure 2.4 Simple molecular model of piezoelectric material: a) an electrically neutral molecule appears, b) generating little dipoles, c) the material is polarized

2.1.4 Manufacturing process

Several techniques have been adopted for fabrication of PZT. The most commonly used techniques are: Solid-state reaction technique, coprecipitation technique and sol–gel technique. PZT in the form of fine powders can be obtained from the above techniques. Other methods such as tape-casting and chemical vapor deposition techniques are used for obtaining PZT in the form of thick or thin films.

In Solid – State Solution technique, the oxides (PbO, TiO_2 and ZrO_2) in suitable proportions are mixed well and subjected to solid-state reaction by the calcination process. The calcination process involves heating the oxides to about 650 $°C$ and maintaining at that temperature for 2 to 3 hours. The product is then heated to about 850 $°C$. The mixture is milled to obtain a particle size of about 1 μm. Ball milling is done using zirconia balls to avoid contamination during milling. The process has been standardized and optimized to get submicron – sized powder with a very narrow particle size distribution [41].

For transducer and actuator applications, PZT is required in the form of discs, cylinders, or plates of different dimensions. The PZT powders fabricated by the techniques mentioned earlier are used to form products of desired shapes and sizes. The powder is initially mixed with a polymer binder and pressed in molds using high pressure. The techniques used for pressing are: uniaxial pressing and isostatic pressing.

In uniaxial pressing, the powder is compacted in a rigid die by applying pressure along a single axis using pistons. In isostatic pressing, the pressure is applied uniformly from all sides. This method gives better uniformity of green density than uniaxial pressing. Isostatic pressing is achieved by keeping the powder in a rubber bag and immersing the bag in a liquid which acts as a pressure transmitter. Hydrostatic pressure is applied on the rubber bag to compact the powder.

The example of manufacturing process based on Ferroperm Piezoceramics involves a number of stages shown schematically in Figure 2.5. The first step is weighing, dry mixing and ball milling of the raw materials. The uniform mixture is then heat treated (calcined), during which the components react to form the polycrystalline phase. The calcined powder is ball milled to increase it' s reactivity, and granulated , with the addition of a binder, to improve its pressing properties. After shaping by dry – pressing, the binder is burnt out by slowly heating the green ceramics to around 700 °C. The parts are transferred to another furnace, where they are sintered between 1200 and 1300 °C. The dimensional tolerance of fired parts (± 3 %) is improved by cutting, grinding, lapping etc.. Electrodes are applied either by screen printing or by vacuum deposition . In the next step, poling is carried out by heating in an oil bath at 130 – 220 °C, and applying an electrical field of 2 – 8 kV/mm to align the domains in the material. The oil bath is used as a heat source and to prevent flash over. Final inspection includes testing of electrode-ceramic bonding as well as measurement of dimensional tolerances, dielectric and piezoelectric properties.
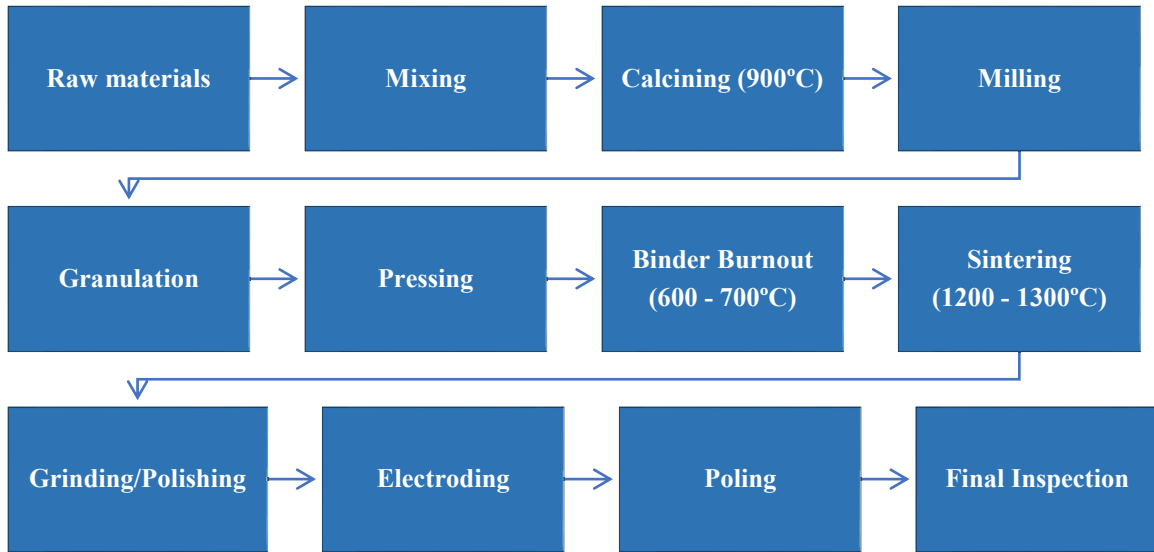
Figure 2.5 The manufacturing process of piezoelectric ceramics [14]

2.2 Constitutive equations

In this section, the constitutive equations for linear piezoelectricity are presented in tensor as well as matrix form. Only the piezoelectric coupling is considered (the thermoelectricity is neglected) and the quasi – electrostatic approach is used (the phase velocities of acoustic waves are several order of magnitude less than the velocities of electromagnetic waves).

2.2.1 Global relations

When writing the constitutive equation for a piezoelectric material, changes of strain and electrical displacement in three orthogonal directions caused by cross – coupling effects due to applied electrical and mechanical stresses must be taken into account. Tensor notation is first adopted, and the reference axes are shown in Figure 2.6. The state of strain is described by a second rank tensor S_{ij} and the state of stress is also described by a second rank tensor T_{kl}. The quantities linking the stress tensor to the strain tensor, compliance s_{ijkl}, and stiffness c_{ijkl}, are then fourth rank tensors. The correlation between the electric field E_k (first rank tensor) and the electric displacement D_i (also a first rank tensor) is the permittivity ε_{ik}, which is a second rank tensor. The piezoelectric equations can be written as:

15

$$S_{ij} = s^E_{ijkl}T_{kl} + d_{ijk}E_k \qquad (2.1)$$

$$D_i = d_{ijk}T_{jk} + \varepsilon^T_{ij}E_j \qquad (2.2)$$

where d_{ijk} is the piezoelectric constant (third rank tensor). Superscripts T and E denote that the dielectric constant ε_{ij} and the elastic constant s_{ijkl} are measured under conditions of constant stress and constant electric field respectively [70].

In general, a first rank tensor has three components, a second rank tensor has nine components, a third rank tensor has 27 components and a fourth rank tensor has 81 components. Not all the tensor components are independent. Both these relations are orientation-dependent; they describe a set of equations that relate these properties in different orientations of the material. The crystal symmetry and the choice of reference axes reduce the number of independent components. A convenient way of describing them is by using axis directions as shown in Figure 2.6.
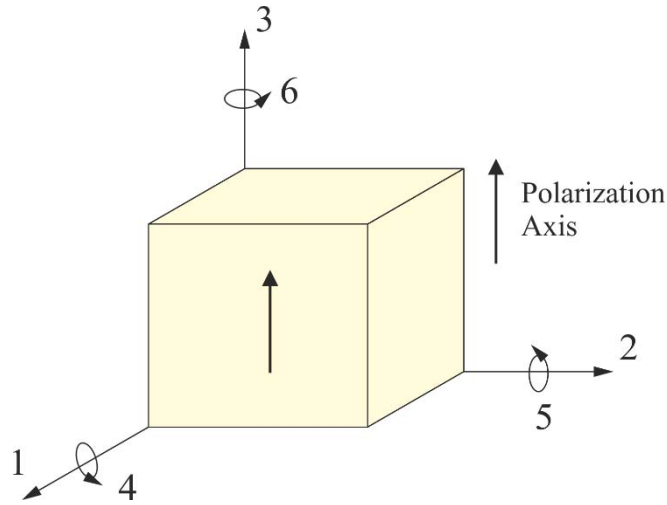
Figure 2.6 Reference axes description

2.2.2 Matrix notation

The convention is to define the poling direction as the 3 – axis, the shear planes are indicated by the subscripts 4, 5 and 6 and are perpendicular to directions 1, 2 and 3 respectively. This simplifies the notations introduced above, where a 3-subscript tensor notation (i,j,k =1,2,3) is replaced by a 2-subscript matrix notation (i=1,2,3 and j=1,2,3,4,5,6), and a 2-subscript tensor notation (i,j =1,2,3) is replaced by a 1-subscript matrix notation (i=1,2,3,4,5,6). See

16

Table 2.1.

$$c_{ijk} = c_{pq} \tag{2.3}$$

$$e_{ikl} = e_{iq} \tag{2.4}$$

$$T_{ij} = T_p \tag{2.5}$$

$$S_{ij} = S_p \text{ when } i = j \tag{2.6}$$

$$2S_{ij} = S_p \text{ when } i \neq j \tag{2.7}$$

Table 2.1 Matrix notation

ij or *kl*	*p* or *q*
11	1
22	2
33	3
23 or 32	4
13 or 31	5
12 or 21	6

With this notations constitutive equations can be written in matrix form:

$$\{S\} = [s]\{T\} + [d]\{E\} \tag{2.8}$$

$$\{D\} = [d]^T\{T\} + [\varepsilon]\{E\} \tag{2.9}$$

where the superscript T stands for the transposed; the other superscripts have been omitted. Assuming that the coordinate system coincides with the orthotropy axes of the material and that the direction of polarization coincides with direction 3, the explicit forms of (2.8) and (2.9) are:

$$\begin{Bmatrix} S_{11} \\ S_{22} \\ S_{33} \\ 2S_{23} \\ 2S_{31} \\ 2S_{12} \end{Bmatrix} = \begin{bmatrix} s_{11} & s_{12} & s_{13} & 0 & 0 & 0 \\ s_{12} & s_{22} & s_{23} & 0 & 0 & 0 \\ s_{13} & s_{23} & s_{33} & 0 & 0 & 0 \\ 0 & 0 & 0 & s_{44} & 0 & 0 \\ 0 & 0 & 0 & 0 & s_{55} & 0 \\ 0 & 0 & 0 & 0 & 0 & s_{66} \end{bmatrix} \begin{Bmatrix} T_{11} \\ T_{22} \\ T_{33} \\ T_{23} \\ T_{31} \\ T_{12} \end{Bmatrix} + \begin{bmatrix} 0 & 0 & d_{31} \\ 0 & 0 & d_{32} \\ 0 & 0 & d_{33} \\ 0 & d_{24} & 0 \\ d_{15} & 0 & 0 \\ 0 & 0 & 0 \end{bmatrix} \begin{Bmatrix} E_1 \\ E_2 \\ E_3 \end{Bmatrix} \quad (2.10)$$
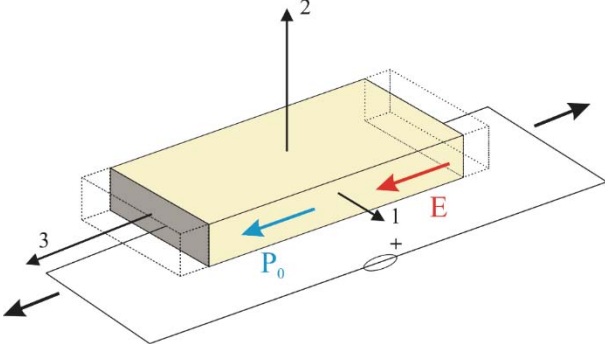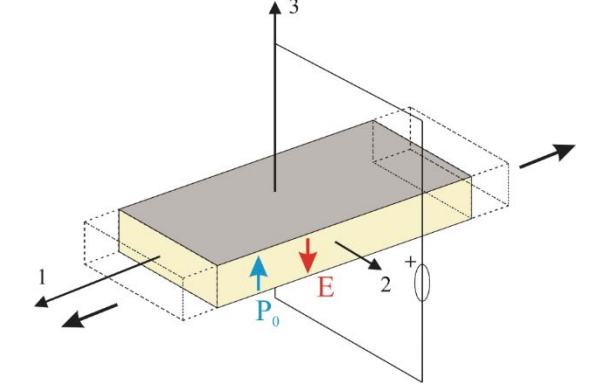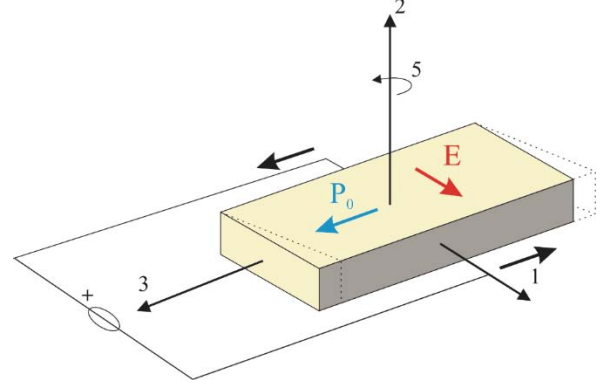
$$\begin{Bmatrix} D_1 \\ D_2 \\ D_3 \end{Bmatrix} = \begin{bmatrix} 0 & 0 & 0 & 0 & d_{15} & 0 \\ 0 & 0 & 0 & d_{24} & 0 & 0 \\ d_{31} & d_{32} & d_{33} & 0 & 0 & 0 \end{bmatrix} \begin{Bmatrix} T_{11} \\ T_{22} \\ T_{33} \\ T_{23} \\ T_{31} \\ T_{12} \end{Bmatrix} + \begin{bmatrix} \varepsilon_{11} & 0 & 0 \\ 0 & \varepsilon_{22} & 0 \\ 0 & 0 & \varepsilon_{33} \end{bmatrix} \begin{Bmatrix} E_1 \\ E_2 \\ E_3 \end{Bmatrix} \quad (2.11)$$

2.2.3 Coupling modes

As can be seen in equations (2.10) and (2.11), the only non-zero elements of piezoelectric constants matrix of ceramic materials are: d_{33}, d_{31} (equal to d_{32}) and d_{15} (equal to d_{24}). Therefore, the electro-elastic coupling operates in three basic modes called longitudinal mode ("33"), transversal mode ("31") and shear mode ("15"). The constitutive equations associated with each of these modes and associated effects, in the case of a rectangular bar, are explained in the Table 2.2.

Thus, a bar polarized along its length and subjected to a difference of potential applied between two electrodes perpendicular to its polarization axis Ox_3 undergoes, by converse piezoelectric effect, a change in length in the same direction. Of course, this assumes that the bar is free to deform, which is particularly the case for unloaded operation ($T_3 = 0$). In a second configuration, the bar can be polarized in its thickness direction and subjected to an external field oriented in the same direction. Due to transverse coupling a change in length perpendicular to the polarization direction can be observed. Finally, the application of an electric field perpendicular to the direction of polarization, for example along the axis Ox_3, tends to turn the elementary dipoles around the axis Ox_2. The resulting deformation can be defined as the shear mode. Similar reasoning can be developed for the direct piezoelectric effect. From these three forms of elementary interaction, a wide variety of configurations can be produced by playing with the sample's geometry (plate, disc, ring, tube, etc.) as well as its polarization type (axial, thickness, etc.). Various types of piezoelectric transducers based on piezoelectric materials are available, thanks to the adaptation of these elementary coupling modes, used independently or in combination.

Table 2.2 Basic electromechanical coupling modes of piezoelectric material

Constitutive equations	**Illustration of the mode**
Longitudinal mode $$\begin{cases} S_3 = s_{33}^E \cdot T_3 + d_{33} \cdot E_3 \\ D_3 = d_{33} \cdot T_3 + \epsilon_{33}^T \cdot E_3 \end{cases}$$	Longitudinal mode of operation: extension along ox3 axis; $d_{33} > 0$; S_3 and E_3 of the same sign; electrode surface represented by grey color
Transversal mode $$\begin{cases} S_3 = s_{11}^E \cdot T_1 + d_{31} \cdot E_3 \\ D_3 = d_{33} \cdot T_3 + \epsilon_{33}^T \cdot E_3 \end{cases}$$	Transversal mode of operation: extension along ox1; $d_{31} < 0$; S_1 and E_3 of opposite sign
Shear mode $$\begin{cases} S_5 = s_{44}^E \cdot T_5 + d_{15} \cdot E_1 \\ D_1 = d_{15} \cdot T_5 + \epsilon_{11}^T \cdot E_1 \end{cases}$$	Shear around ox2 axis; $d_{15} > 0$; S_5 and E_1 of the same sign

2.2.4 Coupling coefficients

Another fundamental parameter used in electromechanical applications is the electromechanical coupling factor k. It is a dimensionless number related to conversion of energy from a mechanical source to electrical work, or vice versa, over an idealized work cycle. It is expressed as:

$$k^2 = \frac{\text{Converted Mechanical Energy}}{\text{Input Electrical Energy}} \qquad (2.12)$$

or:

$$k^2 = \frac{\text{Converted Electrical Energy}}{\text{Input Mechanical Energy}} \qquad (2.13)$$

The (static) coupling factors can be related to series and parallel - resonance frequencies, f_s and f_p respectively, (dynamic behavior) of various specific modes and shapes (Table 2.3).

Table 2.3 Electromechanical coupling factors for different material shapes and polarization directions

Material Coupling Factor	Shape
$k_{31}^2 = \dfrac{A}{1+A}$ or $\dfrac{k_{31}^2}{1-k_{31}^2} = A$ $A = \dfrac{\frac{\pi}{2} f_p}{f_s} \tan\left[\dfrac{\left(\frac{\pi}{2}\right)(f_p - f_s)}{f_s}\right]$	Side electroded bar
$k_p^2 = \dfrac{\left(f_p^2 - f_s^2\right)}{f_p^2}$	Thin-wall sphere, "breathing" mode
$k_{33}^2 = \dfrac{\frac{\pi}{2} f_s}{f_p} \tan\left[\dfrac{\left(\frac{\pi}{2}\right)(f_p - f_s)}{f_p}\right]$	End electroded rod
$k_t^2 = \dfrac{\frac{\pi}{2} f_s}{f_p} \tan\left[\dfrac{\left(\frac{\pi}{2}\right)(f_p - f_s)}{f_p}\right]$	Disc or plate, "33" thickness mode

Effective coupling factor (dynamic), k_{eff} is defined by:

$$k_{eff}^2 = \frac{(f_p^2 - f_s^2)}{f_p^2}$$ (2.14)

It is frequently used to express the effective coupling coefficient of an arbitrary resonator, either at fundamental resonance or at any overtone. The effective coupling factor is equal to the material coupling factor for the sphere working in breathing-mode and the hoop mode ring as in these cases all of the elastic energy is dielectrically coupled. For standing wave modes, k_{eff} is usually lower than the material coupling factor [13].

2.3 Limitations

Limitations for piezoceramics are difficult to define due to the tremendous range of applications requirements and operational environments. Piezoelectric ceramic may be damaged by excessive temperature, mechanical stress, or electric field. Temperature, mechanical stress, and electric field in combination may cause damage that would not have resulted from a single stressor. These stressors may also affect the ageing rates of the ceramic.

2.3.1 Electric field

In ferroelectric ceramics, due to the domain processes, a nonlinear and hysteresis affected correlation exists between the polarization S and the applied electric field H. Depending on the previous history of the material, strongly varying domain configurations can arise, thus for a certain instantaneous value of the electric field different polarization values exist.

Starting from a non-polarized state, the domains orientate themselves to the increasing electric field until they are all aligned with its direction. Thus, the polarization curve represented in Figure 2.7 develops between the points A and B. If the electric field decreases in value to zero, a small part of the domains will fold back due to the mechanical stresses within the ceramics. The remaining polarization is called remanent polarization P_r. This correlation is represented by the curve between the points B and C in Figure 2.7. If an electric field is applied in opposite direction, the domains will be gradually realigned until all of them are aligned with the field direction. For this case, the pair of variables (E, P) passes the curve along the points $C - D - F$. At point D, the electric field reaches a level, the ceramic material is depolarized concerning the external behavior. This electric field level is called coercive field strength E_c .

21

If the electric field is reoriented again, the domains will be gradually realigned until all domains are aligned with the lines of electric flux. In this case, the pair of variables (*E, P*) passes the curve along the points F – G – H – B. The curves along the points B – C – D – F and F – G – H – B form external hysteresis loops. However, if the direction of the external electric field is reversed before all domains are aligned, the pair of variables (*E, P*) branches out to a hysteresis area surrounded by external hysteresis loops. Within this hysteresis area, internal hysteresis loops are formed.
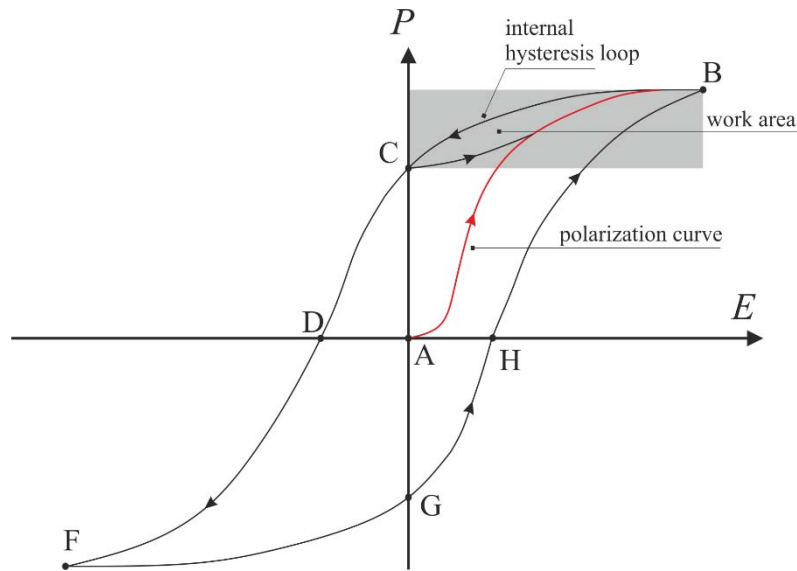
Figure 2.7 *P-E* hysteresis curve and work area of piezoelectric ceramics

The hysteresis affected correlation between the strain S of the ceramics and the electric field *E* applied to it is also present. Due to the characteristic shape of the curve in Figure 2.8 it often called "butterfly" curve:
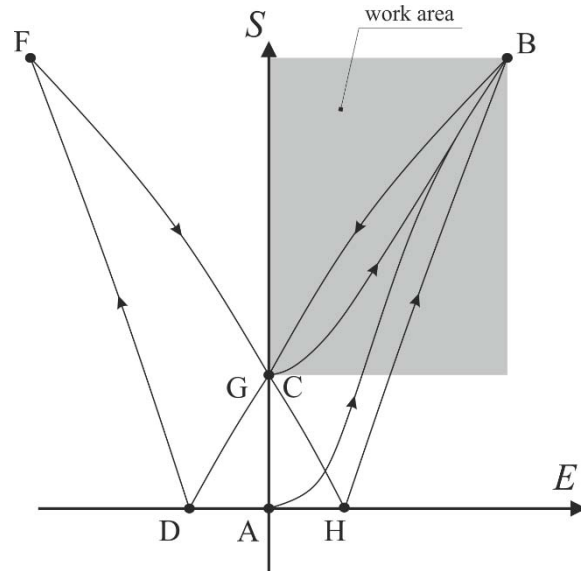
Figure 2.8 *S-E* "butterfly" curve and work area of piezoelectric ceramics

A non-polarized ceramic body represents the starting point of the curve in Figure 2.8 (point A). By applying an external electric field, the domains are aligned with the field direction associated with a strain *S* of the ceramics. Thereby, the pair of variables (*S, E*) passes the curve between the points A – B. If the electric field decreases in value to zero, a small part of domains will fold back, that's why a residual strain S_r of the ceramics is found (point C). If the electric field is applied in opposite direction, all domains will be statistically distributed, and the strain *S* of the ceramics decreases in value to zero at point D. A further increasing of the field strength results in gradual realignment of the domains in field direction, thus the strain of the ceramic body increases again. The pair of variables (*S, E*) passes along the curve C – D – F. If the electric field is reoriented again, the domains will also be realigned. The pair of variables (*S, E*) passes along the curve F – G – H – B, thus the characteristic butterfly curve is formed.

The Coercive field, E_c, of "hard" piezoelectric materials is greater than 10 *kV/cm*; E_c of soft materials is between 1 *kV/cm* and 10 *kV/cm*; and E_c of electrostrictors is less than 1 *kV/cm*. The work area of piezoelectric ceramics is marked by gray rectangle in Figure 2.7 and Figure 2.8. Driving the ceramics within this range, the piezoelectric effect is optimally used, thanks to uniform domain alignment [49].

2.3.2 Temperature

The upper working temperature of ferroelectric ceramics is limited by their ferroelectric to non-ferroelectric transition temperature – the Curie temperature (T_C). Before reaching T_C the dielectric constant peaks, and the net polarization completely disappears at the Curie Temperature. Generally, the operating temperature of piezoelectric ceramics is limited to one-half of T_C, typically at temperatures lower than 200 °C. The temperature limitation may increase with a positive DC bias and may decrease with a high AC field, compressive mechanical bias, or high mechanical loading.

The most commonly used piezoelectric material operating at high temperature is single crystal quartz (SiO_2), which demonstrates a high resistivity and temperature – independent piezoelectric property. However, its piezoelectric coefficient is relatively low ($d_{11} = 2.3\ pC/N$). The most widely used piezoelectric polycrystalline ceramics, based on $Pb(Zr_{1-x}Ti_x)O_3$ (PZT), have a much better piezoelectric coefficients than SiO_2. For example, 150 °C is the upper working temperature for $PbZr_{0.52}Ti_{0.48}O_3$ with a $T_C = 386$ °C [68].

2.3.3 Mechanical Stress

Like all ceramics, piezoelectric ceramics are brittle and have a much higher compressive strength than tensile strength. Tensile loads of piezo actuators are limited to 5 % – 10 % of the compressive load limit. Many piezoelectric transducers are therefore operated under a prestress (also called preload) to maintain it in compression, particularly for high power applications. High mechanical stress may cause depolarization of the ceramic long before the compressive mechanical strength limit is reached. Piezo ceramic materials can withstand pressures up to 250 MPa before they break mechanically. For practical applications, this value must not be approached because depolarization occurs at pressures of the order of 20 to 30% of the mechanical limit. The strength and toughness of the material are highly dependent on its processing conditions. Smaller grain size is associated with greater fracture toughness. Mechanical strength becomes anisotropic after the ceramic is electrically poled. Cracks in unpoled PZT and PMN ceramic have been observed to propagate more readily in a direction perpendicular to an applied electric field. For high hydrostatic pressure, high stress, or squeeze ignition applications, hard piezoelectric materials are suitable. In high dynamic stress applications, such as impact ignition, soft piezoelectric materials may be suitable [13].

2.3.4 Power Limitations

A transducer's ability to meet power output requirements may be limited by dynamic strength, temperature rise, or efficiency. Dynamic strength is usually a limitation only when the transducer has high Q_m and the ceramic is not under compressive mechanical bias (preload). Dielectric, elastic (mechanical), and piezoelectric losses in the ceramic as well as other mechanical losses contribute to temperature rise and inefficiency. Piezoelectric transducers tend to be efficiency limited when operated at low duty cycle and temperature limited when used in continuous operation. For temperature limited transducers, removal of heat is as important as minimizing the generation of heat, as dielectric losses increase as temperature rises. The positive feedback between loss and temperature can result in "thermal runaway" and transducer failure. As ceramic losses at high drive result largely from ceramic domain wall motion, hard ferroelectric ceramics are designated for high output power applications [14].

2.4 Overview of chosen bioengineering and medical applications of piezoelectric materials

Piezoelectric materials convert mechanical energy to electrical energy (direct piezoelectric effect) and electrical energy to mechanical energy (converse piezoelectric effect). Based on these effects, piezoelectric materials have numerous applications in the field of engineering and medicine. The distinctive characteristic of the material, which is a bi-directional energy conversion capability, makes piezoelectric materials highly suited for the design of smart systems. Such system possess the ability to adjust its behavior based on information perceived in real time from its environment. Good examples of smart systems are industrial and medical robots. Piezoelectric materials found applications in this area as: piezoelectric tactile (sensitive to touch) sensors, vibration sensors and ultrasonic detectors for detection and sensing. Piezoelectric motors, benders and vibrators, graspers and precision positioners, on the other hand, are used in robotics for motion control and handling of objects. The main engineering applications of piezoelectric materials with the distinction of the piezoelectric phenomenon used are shown in Figure 2.9 with the distinction of used piezoelectric phenomenon.

```
Applications
of piezoelectric
materials
├── Direct effect
│       Pressure sensor
│       Accelerometer
│       Gyroscope
│       Piezoelectric microphone
│       Ultrasonic detector
│       Hydrophone (sonar)
│       Tactile sensor
│       Energy harvesting
├── Converse effect
│   ├── Low-frequency applications
│   │       Electronic buzzer
│   │       High-frequency speakers
│   │       Actuators
│   └── High-frequency applications
│           Piezoelectric motors
│           Piezoelectric pump
│           Ultrasonic drill
│           Ultrasonic cleaner
│           Ultrasonic generator
│           Projector (sonar)
└── Both effects
        Quartz oscilator
        Quartz balance
        Quartz Atomic Force Microscope (AFM) proe
        Piezoelectric transformer
        Ultrasonic nondestructive testing
        Noise and vibration control
        Structural health monitoring
        Robotics and smart devices
```

Figure 2.9 Chosen applications for piezoelectric materials [41]

This section is focused on the medical and bio-engineering applications of piezoelectric materials, as it coincides with the purpose of the resonant piezoelectric transducer described in this thesis. The sensing and actuation characteristics, the ability to generate and detect ultrasonic frequencies (ultrasound) and the high potential of piezoelectric materials in smart systems make them well suited for medical diagnosis and therapy. Table 2.4 presents some of the piezoelectric applications and devices which are used or still being under research and development (R & D) stage.

Table 2.4 Medical applications of piezoelectric materials

Piezoelectric characteristic used	Medical application
Tactile sensor	▪ Scalpel for minimal invasive surgery
Vibration sensor	▪ Measure of tremors in Parkinson's patients ▪ Monitoring patient's activity ▪ Pace maker control
Pressure sensor	▪ Blood pressure monitor
Sound sensor	▪ Heartbeat monitor (piezoelectric stethoscope)
Pump and valve actuators	▪ Insulin pump ▪ Infusion pump ▪ Valves
Ultrasonic generation	▪ Transdermal drug delivery ▪ Localized drug delivery ▪ Ablation of cancer cells ▪ Cataract surgery ▪ Bone healing and growth ▪ Arthritic and joint inflammation treatment
Ultrasonic detection	▪ Medical imaging (sonography) ▪ Bone density measurement

2.4.1 Tactile sensor

Tactile sensors are devices which sense contact or touch. In the medical field, they are useful in minimally invasive surgery (MIS), in which the scalpel and grasper need to be carefully handled inside the human body. Depending on the working principle, tactile sensors can be divided into: resistive, capacitive, optical and piezoelectric.

Piezoelectric materials used for the tactile sensors are ceramic thin films. It is necessary that such film be flexible, and so PVDF polymers are better suited. In piezoelectric tactile sensors, the direct piezoelectric effect is used where a small pressure on the sensor generates an electrical signal. Another way (more sensitive) is to use the change in resonance frequency of a piezoelectric element in response to a pressure acting on it. A piezoelectric tactile sensor usually consists of a large number of tiny elements arranged in a matrix. Each element is a piezoelectric cantilever or bridge micro – machined on a silicon substrate. The number of elements in the matrix could reach up to 100 elements. The greater number of elements, the better will be the resolution.

The tactile sensors, thanks to micromachining techniques, are small enough to be attached to the end of the graspers or to the tip of the scalpel. They are sensitive enough to detect the presence of soft tissues in the vicinity, which helps to operate the surgical instruments delicately and safely during the surgery. The sensors are capable of detecting the magnitude and position of the pressure on the grasping tool or the scalpel. Piezoelectric tactile sensors are also used in detection of cancerous cells through the study of distributed pressures acting on the surface and their effect on the resonance frequency of the sensor [62].

2.4.2 Piezoelectric accelerometer

The piezoelectric accelerometers operate as very sensitive vibration sensors. In medical applications they are aimed at detecting inertia forces created by body motion. Most of them respond to a particular range of vibration frequencies which have been found to characterize body motion during ordinary physical activities. They monitor activities of patients implanted with pace makers. They are used for detection of involuntary hand tremors in patients with neurological disorders.

A small piezoelectric accelerometer is mounted inside the pacemaker. The accelerometer produces a voltage signal proportional to the activity of the patient. The pacemaker changes the pacing rate in proportion to signals derived from the sensor. The heart rate increases when the patient activity increases and decreases when the patient is resting. In this case, piezoelectric accelerometers should be sensitive to vibration frequencies less than 4 Hz, as this is the upper frequency limit of most physical activities.

Parkinson's disease is a neurodegenerative disease common among middle age and elderly people. The major symptoms are: tremors, rigidity, akinesia, and gait disturbance. Quantitative evaluation of those symptoms is important for dosage of the drugs. The frequencies of the tremor vibrations are normally in the range of about $4 - 12$ Hz. Piezoelectric accelerometers are useful in measuring the vibrations. The measurement system usually consists of 3-axis piezoelectric accelerometers, touch sensors and analog to digital converter (ADC). These sensors are attached to the index finger and thumb with the fingerstall. Single finger-tapping intervals, maximum single finger-tapping velocities, maximum single finger-tapping amplitudes are calculated as the features for diagnosis of Parkinson's disease from the measured acceleration. Such studies help in estimating the severity of the disease and for taking decisions on the type of clinical treatment [50].

2.4.3 Pressure and sound sensor

Piezoelectric pressure sensors are based on using the direct piezoelectric effect. Piezoelectric membrane generates electric voltage proportional to the pressure acting on the membrane. Piezoelectric pressure sensors are designed using quartz, PZT, and ZnO thin films. The pressure sensors are very sensitive and can be used to measure absolute pressures. PZT thin films have been used to design MEMS (Micro Electro-Mechanical Systems) pressure sensors. A typical MEMS PZT pressure sensor consists of a silicon substrate (of about 500 μm thickness) with a silicon oxide coating of about $100 - 200$ nm thickness. On the silicon oxide layer, a sandwich of Pt – PZT – Pt structure is grown. The platinum layers act as electrodes, and the PZT is the active material that senses the pressure. The PZT film thickness is usually in the range of $0.5 - 5$ μm.

The pressure sensor can be used for measuring blood pressure in an continuous manner, for example during heart surgery. For the measurement of blood pressure, the sensor is placed

either on the wrist or the mid – arm. A proper backing and a strap with Velcro is provided to firmly grip the sensor around the wrist or the arm. The electronics required for the sensor such as voltage amplifier and filter may be integrated or may be outside the sensor. Other potential applications of piezoelectric pressure sensors are monitoring of the inflation pressure during the angioplasty (surgical method of opening up blockages in the artery), continuous heart rate monitoring of patients during activities such as walking, running, and treadmill exercises [41].

A piezoelectric sound sensors (microphones) found their applications in medicine as a contact microphones for electronic stethoscopes. The piezoelectric microphone is based on using the direct piezoelectric effect, and is dimensioned to have output signal in the audible frequency range. Such device typically consists of crystal or film held tight in a small enclosure which converts the vibrations transmitted through the flesh into corresponding electrical impulses. The enclosure often contains a microphone preamplifier (use of external preamplifier is also possible) to detect acoustic signals. This device adjusts the volume, filters the noise, and lets medical personnel discriminate sounds in particularly noisy environments such as emergency medical transport vehicles or emergency rooms and triage areas.

2.4.4 Micro pump and valve actuators

Micro pumps are essential components of microfluidic systems, in which extremely small volumes of fluids are transported in a precise manner. Biomedical applications include, among others: drug delivery systems, protein analysis and DNA diagnostics. Typical piezoelectric pump used in bioengineering consists of a pump chamber with a diaphragm, two valves, and an actuator to drive the pump diaphragm. In MEMS – based micro pumps, the chamber is usually formed in a silicon substrate sandwiched between glass plates using micromachining techniques. The chamber contains two one – way valves for input and output. A deformable plate made of silicon, glass, or plastic which acts as the diaphragm is formed on one side of the chamber. When the piezoelectric actuator is operating on the diaphragm, the pressured liquid in chamber propels the valves to open or close according to a certain principle. As a result of this, the liquid moves from the inlet to outlet continuously. The operating frequencies of the various pumps are in the range of 15 – 150 Hz. Piezoelectric materials used for actuation are PZT or piezoelectric polymers (PVDF). The piezoelectric actuators driving micro pumps can be very finely adjusted allowing the pump volumes to be very precisely defined [25].

2.4.5 Ultrasonic generation

The most common use of piezoelectric transducers in medicine is the generation and detection of ultrasonic waves, colloquially called utrasound. Ultrasonic transducers play a key role in today's healthcare, enabling the work of diagnostic testing and surgical devices to treating cancer. The next sections are dedicated to overview of medicine applications of ultrasonic transducers, that can be divided into two main groups: based on the generation and detection functions.

Transdermal drug delivery is a noninvasive technique of administering drug through the skin. The drug delivery system is in the form of patches which are adhered to the skin. The main advantage of this technique over the oral method or injections is the noninvasiveness. On the other hand, only some drugs with relatively small size molecules can be administered through the skin by using patches. Even for those the method has limitations because of the low permeability of the skin. One of the techniques for enhancing drug delivery through skin is the use of ultrasound, which has thermal and mechanical effects, which in turn increase the permeability of the outer skin layer (stratum corneum). The technique is called sonophoresis and it uses single or array of piezoelectric transducers generating ultrasonic waves in the range of $20 - 100$ *kHz*. Pulsed cycle of work is used as continuous ultrasound heats up the area. The intensity of the ultrasound and the pulse frequency must be suitably selected depending on the type of drug and the dosage required [44]. Piezoelectric ultrasonic transducers have also been used for generating ultrasonic fields enhancing the systematic drug delivery in cancer treatment after the main tumor had been removed [44].

High intensity focused ultrasound (HIFU) has been successfully used for treatment of many types of tumors. When high intensity ultrasound is focused at a point on the human tissue, due to absorption, the tissue can reach a high temperature over a very short time. This causes damage or necrosis of the tissue at the precise area without affecting the surroundings. Depending on the power of the transducer and the time of exposure, the high temperatures, sufficient to ablate tumors, can be reached. For ablation of large tumors, the transducer must be moved continuously. The real – time image of the tumor is used for monitoring the movement of the transducer. The best results in destroying tumors were reported for piezoelectric array transducers consisting of piezoelectric composites excited in 1st and 3rd

mode. High intensity transducers made of piezoelectric 1 – 3 composites in the frequency range of 200 *kHz* to 10 *MHz* with acoustic power in the range of 10 – 30 *W/cm²* were fabricated. Those transducers are capable of focusing on small area and generating high temperatures up to 85 *°C* [15].

Low intensity ultrasonic filed generated by a piezoelectric transducers is used for treatment of injuries and aiding in the natural healing of bones. Frequencies of the ultrasound used in the treatments are in the range of 1 – 3 *MHz,* and the intensity is quite low (not more than 3 *W/cm²*). Ultrasonic transducers operate, both, in continuous and pulsed manner. The time of treatment is a few minutes, depending on the type of injury or the cause of pain. Still the scientific evidence of healing properties of ultrasound is still unclear. Some of the theories proposed for confirmation of the therapeutic effects of ultrasound are following:

- high frequency vibrations passing through the tissue generate small temperature fluctuations within the tissue. (some enzymes, such as collagenase, are exquisitely sensitive to these small variations, thus, ultrasound may also facilitate some enzymatic processes);
- ultrasound has a positive effect on collagen by improving its extensibility; thus, helping in the healing of injured tissues;
- ultrasound speeds metabolism, increases blood flow and fluid flow at the fracture site [27].

2.4.6 Ultrasonic detection

The most common use of ultrasonic transducers in the medical field is for the ultrasonic imaging. The image is created using both the echo time of the ultrasound and the Doppler shift of the reflected sound to determine the distance to the targeted internal organ and its movement. Ultrasonic imaging involves the creation of ultrasonic sound waves using a piezoelectric ultrasonic generator and also the conversion of the reflected ultrasound waves into an electric signal using a piezoelectric ultrasonic detector (often the same piezoelectric ceramic). The frequency of the ultrasonic field used is in the range of 10 – 50 *MHz.* The average intensity of the ultrasonic field is normally below 100 *mW/cm²*.

The ultrasonic transducer is placed externally on the skin close to the organ which needs to be imaged. Due to high reflection rate of energy at the transducer – skin boundary it is

necessary to use impedance matching layer, which is usually fixed to the head of the ultrasonic transducer. Moreover, a coupling gel is used on the skin to avoid air getting trapped between the transducer head and the skin. The transducer is scanning over the specific region to be imaged, and the detected signals from different positions are digitized and converted to grey scale. The entire image information is stored in memory and displayed on the monitor.

As the ultrasound gets transmitted, it gets attenuated due to absorption and scattering. High – frequency ultrasonic waves give better resolution, but attenuation is rising with the frequency. Frequencies in the range of 2.5 – 5 *MHz* are used for deep organs, and higher frequencies are used for superficial organs.

Piezoelectric materials used for the ultrasonic transducers are: PZT ceramics, polymer PVDF, or composites of PZT and polymer. Use of PZT – polymer composites has the advantage of better sensitivity of PZT and better impedance matching of pure PVDF. The transducer may contain a single piezoelectric element or multiple elements. The basic transducer (Figure 2.10) consists of a piezoelectric material which is concave shaped for focusing. The same transducer is used as a generator and detector. The piezoelectric element is supported by a backing layer which is used for damping. The backing material must have good impedance matching with the piezoelectric material for effective damping. An impedance – matching layer is attached at the head of the transducer for matching with the human tissue. Its thickness must be one fourth of the wavelength of the ultrasonic frequency in the medium for effective transmission [41].
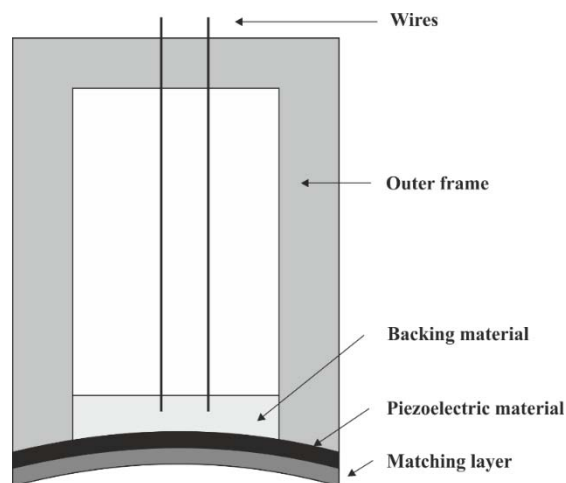

Figure 2.10 Diagram of a basic piezoelectric ultrasonic transducer (single element)

Doppler shift effect, mentioned earlier, is used in the study of blood flow and tissue motion imaging. When the beam produced by a piezoelectric ultrasonic transmitter encounters a blood vessel, it gets backscattered by the particles in the blood, and the scattered ultrasound is detected by a piezoelectric ultrasound receiver which is kept close to the transmitter. The scattered ultrasound will have a shift in frequency proportional to the component of velocity of flow in the direction of the beam. The shift in frequencies of the signal from different locations of the blood vessel or a moving tissue is recorded, and the velocity distribution data is coded and converted to a color image.

Another use of piezoelectric ultrasonic transducers is bone density measurement (for detection of osteoporosis). There are two principles used in this method: measurement of attenuation of ultrasonic wave as it transmits through the bone and measurement of velocity of ultrasonic waves in the bone. In both methods, ultrasonic waves are transmitted through the bone using an ultrasonic transmitter, and the response pulse is detected using an ultrasonic receiver. The basic structure of the ultrasonic transducers is the same as the single element transducer shown in Figure 2.10. The piezoelectric element does not need to be concave, because focusing is not required. The frequency range used normally is 200 to 1000 *kHz*. The thickness of the piezoelectric material is set to have resonance within this frequency range with a broad band output.

In the attenuation measurement method, the parameter measured is called Broadband Ultrasonic Attenuation (BUA). The attenuation of ultrasonic intensity as it enters the bone increases linearly with frequency. The slope of the linear curve of attenuation versus frequency is used to determine the extent of osteoporosis (the slope is higher for a healthy bone than the osteoporotic one). The ratio of the measured BUA to the one of a healthy bone gives a measure of the bone's condition. In the velocity technique, the time elapsed between the entry of the transmitted pulse and the received one is measured, and the velocity of the sound wave is measured. The velocity is higher in the healthy bone than in the osteoporotic bone [40].

2.5 Piezoelectric transducers for measurement of soft tissues (including human skin)

Skin is the most crucial of our organs, and the most sensitive. This is our first communication mode, and the most effective of our protections. In addition, it is one of the largest organs of the body in relation to its surface and its mass: for adults, about 2 m^2 and 5 kg. Long being neglected, skin is experiencing a revival of interests since the 80's. Both in terms of medical, surgical, pharmaceutical and cosmetic applications, the skin raises today the interest of many researchers, particularly in the following areas:

- medical research for the treatment and detection of dermatological diseases and cancer;
- the surgical research, whether in a corrective or cosmetic purpose, which requires better understanding of the mechanical behavior;
- pharmacological research to develop new methods of treatment administration;
- the dermo-cosmetic research in order to better focus the effect of the developed anti-aging products[37].

Below few examples of piezoelectric transducers (existing or being under-research) are considered, that are aimed to detect the mechanical properties of tissues, mainly for abnormal states recognition (early cancer detection) and tactile human – machine interfaces.

A spring loaded tactile sensor with displacement sensing has been reported as suitable for non-invasive assessment of physical properties, stiffness and elasticity, of human skin in vivo. The instrument was able to detect changes in stiffness and elastic related properties of human skin, related to age, day-to-day variations and application of cosmetics. The tactile sensor consisted of a piezoelectric vibrator with a vibration pickup, and electronics connected to a PC. The change in frequency when the sensor is attached to an object was measured. Integrated displacement sensor showed the compression of the spring loading the sensor element against the object during measurement. For a fixed contact pressure, a change of frequency for the measured acoustic impedance of the object can be associated with the stiffness of soft tissue. The experimental results were obtained on silicone gum and on healthy women skin [45].

The most common example of piezoelectric transducer for measurement of stiffness variations is an element in a feedback system. It has been used to detect various pathophysiological conditions, especially caused by prostate cancer. Some prostate tumors are regarded as stiffer than the surrounding normal tissue, and therefore it is desired to reliably measure the prostate tissue stiffness. A piezoelectric transducer element in a feedback system is set to vibrate at its resonance frequency. When the sensor element contacts an object, a change in the resonance frequency is observed. This feature has been utilized in sensor systems to describe physical properties of different objects. The purpose of the feedback circuit is to ensure that the driving frequency of the supply voltage is the same as the resonance frequency of the system. A zero phase shift condition for the sensor system gives a change in resonance frequency, when the sensor is put in contact with an object. The change of the resonance frequency is related to the acoustic impedance of the object [63].
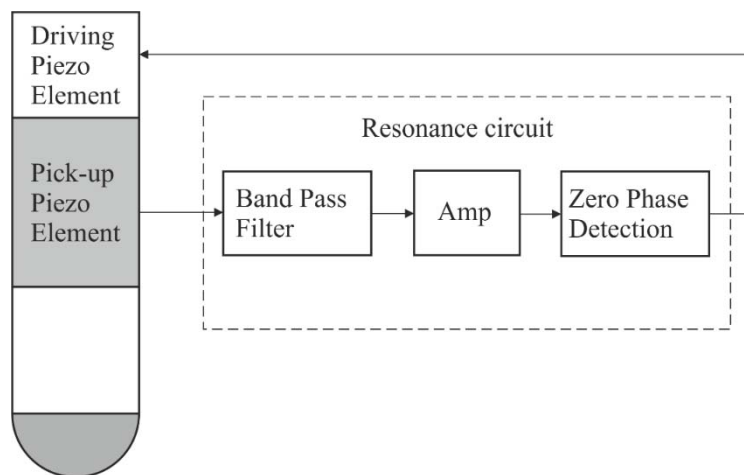

Figure 2.11 Diagram of the resonance sensor working in the feedback system [45],[63],[17]

Physical and biological markers of cancer cells are useful information for detection of cancers in the human body. Some of the potential physical markers are the mechanical properties of bio cells such as elasticity and viscosity. The acoustic attenuation was also reported as one of the major physical markers. Recently, PVDF ultrasonic transducer measuring frequency – dependent attenuation of bio cells, was verified. The system consisted of a transmitter generating an ultrasonic wave and a receiver which converted the attenuated wave into electrical signal. PVDF polymer has been used due to its low acoustic impedance, which is similar to human body. Thanks to this, the transmission of acoustic power is improved by impedance matching with that of medium [36].

Another example of piezoelectric transducer used for detecting prostate cancer and hypertrophy is a palpation (tactile) sensor developed in Japan [42]. Piezoelectric material used is PVDF film placed on the surface of a matrix rubber base. The sensor is pressed against the prostate gland and supplied with sinusoidal voltage, with constant amplitude. The voltage signal from the PVDF film is integrated over sampling period and used to evaluate the stiffness of the pressed prostate gland. The output level is dependent on the relative stiffness of the sensor base rubber to the stiffness of the measured object.

An active muscle stiffness sensor (aMSS) that measures muscle activation using a piezoelectric resonance probe was recently developed. The main purpose of this sensor was estimation of human's motion intension, which is a major issue in human – robot interfaces. The analysis methods were based on a frequency shift and amplitude change. The aMSS measured muscle contraction based on the changes in the resonance signal, which were generated from the PZT. The aMSS consisted of two main parts: the resonating PZT probe and the resonance circuit. The probe was designed by combining a driving PZT and a pickup PZT. The driving PZT induced mechanical oscillation, and the pickup PZT measured the oscillation. The contact tip was designed by considering the contact area between the sensor and the skin [17].

For the transducer which is the research goal of this thesis, a different approach is used than for the devices mentioned above, i.e. using mostly combinations of transmitter and receiver piezoelectric transducers working in feedback system. Its development is based on the basic properties of human skin – a highly complex, multilayer and non – homogeneous structure. Those features presented in the literature, will be shortly described in next sections. The main task of the considered (to be developed) transducer is the preliminary evaluation of mechanical properties of soft tissues. It can be taken as an introduction assessment of the skin's aging.

2.5.1 Basic properties of human skin

The anatomy of human skin shows a complex multi-layer structure which consists of the epidermis, dermis and hypodermis. Each skin layer by its unique physical nature, components and organization contributes to the complexity of its mechanical properties. The basic cross-section of the human skin is shown in the Figure 2.12.
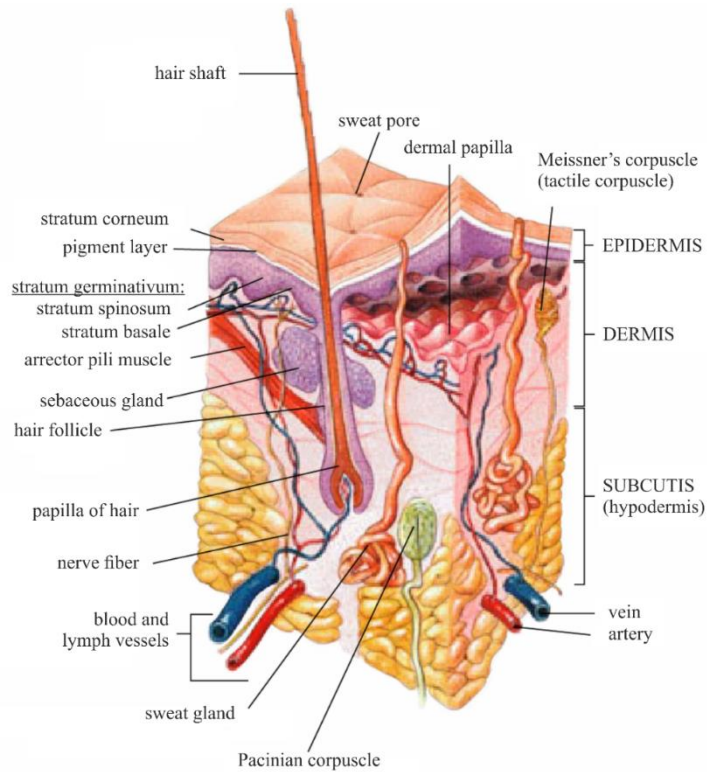
Figure 2.12 Cross-section of the human skin [72]

- **The epidermis**

The epidermis, superficial layer of the skin is very thin, about 0.10 *mm* thickness. This is the tissue's external protection against external penetration (bacteria, chemicals). Its role is to protect the body of water loss and various external aggressions (UV, pollution, chemical factors). This property, called barrier function, is mainly provided by the stratum corneum.

- **The dermis**

The dermis is the support tissue, the nourishment of our skin. It plays a key role in thermoregulation, and by its high vascularity, in wound healing. The strength and firmness of the skin is delivered through collagen fibers located in dermis layer. The layer's thickness is in the order of $1 - 1.3$ *mm*.

- **The hypodermis**

The hypodermis is adipose, greasy cushion of variable thickness depending on region of the body and sex. It models the body and gives it its shape. The hypodermis stores lipids as triglycerides and provides fatty acids in case of energy demand. It plays an important role in

the thermoregulation because of the insulating nature of the fat, it also plays a role as an energy reserve and protects the body from shocks [37].

2.5.2 Mechanical properties of human skin

Skin, due to its composition, a superposition of several layers, presents a complex mechanical behavior. The skin is non-homogeneous and anisotropic throughout its structure. Those features contribute to the fact that the mechanical properties of the skin (Young's modulus, stiffness, viscosity) are highly dependent on magnitude and type of forces applied (torsion, compression, tension, suction). Skin exhibits elastic behavior under low load, moving towards a visco-elastic behavior under higher loads [19].

The most interesting part is the principal mechanical function of the skin. Thanks to its composition (collagen, elastin, GAGs and water), the dermis plays the key role in the shaping of mechanical properties. It gives the skin its deformability, elasticity, flexibility but also resistance and damping to external shocks. The skin's micro relief effects also play a crucial role in the mechanical behavior of the skin. Lines of Langer determine the stretching and folding axes, while the micro – depression network (MDN) is a reserve for the skin's expansion. Each element of the skin responds to mechanical stresses, contributing to a complex mechanical behavior. However, in biomechanical analysis, the skin is often considered as a single-layer material [73].

The mechanical behavior of the skin is largely dependent on age, body region and sex. Skin aging is inevitable, many of microbiological changes in the body are the cause (decrease in the fibroblast metabolism, decreased synthesis of extracellular matrix, decreased procollagen synthesis and increased partial degradation of collagen, etc.) These alterations are resulting in the loss of elasticity, viscosity, hydration and skin scarring. The study of the mechanical properties of the skin is aimed to characterize and quantify these alterations [37].

Considering the mechanical description of the skin, these parameters are the most important: stress, the deformation, and the Young's modulus (representation of the constant of proportionality between stress and deformation shown by Hooke's law). The stress is defined by the ratio between resulting force and the surface, on which the force is acting. It is homogenous to pressure:

$$\sigma = \frac{dF}{dA} \tag{2.15}$$

where: σ – stress [N/m^2], F – resultant force, A – surface [m^2]

The deformation is linear expansion defined by ratio of elongation and initial length of the body.

$$\varepsilon = \frac{dL}{L} \tag{2.16}$$

where: ε – deformation [%], dL – elongation [m], L – initial length [m]

The Young modulus represents the force necessary to produce 100 % of elongation of 1 cm^2 surface of the body. It describes the constant of proportionality between stress and deformation shown by Hooke's law for elastic body:

$$E = \frac{\sigma}{\varepsilon} \tag{2.17}$$

The theory of elasticity establishes a relationship between stress and strain that is independent of time. It cannot account for the properties of an assembly of macromolecules whose characteristics change over time under the influence of forces applied to them. A heterogeneous structure of macromolecules has a memory, or hysteresis, which means, that the stress state and deformation at an instant t_i is dependent on sample history for the previous period t_{i-1}. It then becomes necessary to introduce the time variable in the equation of state of a viscoelastic body. The skin, which is an anisotropic material, has the characteristics of a viscoelastic body.

2.5.3 Methods for evaluation of skin's mechanical properties

In recent years, many non-invasive techniques have been developed to understand and characterize in vivo skin mechanical properties. The most commonly used techniques are based on the static measurements of torsion, suction and extensibility of the skin. However, the data are mainly semi-quantitative and often distorted by the experimental conditions. In the past decades, a few authors have been using the indentation techniques in order to improve measurements of the thin layer material properties, and to minimize the disturbance due to the experimental conditions. In addition to the already existing systems, based on a static

40

characterization, the dynamic methods can be implemented. Those methods are suitable for determining the elasticity, viscosity and adhesiveness of the tested sample [8], [10], [9].

Skin deformations depend on the type of test used. Depending on the type of stress and the device used, the obtained parameters values can be different. The main mechanical examinations currently used for the characterization of the human skin are:

- extensometry (elasticity, anisotropy measurement);
- levarometry (distensibility comparison);
- suction test (Young modulus E);
- torsion test (shear modulus G, Young modulus E);
- ballistometry (viscosity, Young modulus E);
- static and dynamic indentation (elasticity, viscosity and stickiness).

In this thesis the measurement method is based on the indentation principle of skin characterization. This is a supplementary trial for methods of suction and torsion. It measures the compressibility of the tissue and therefore its resistance against external aggression. This technique is based on registering the normal component of force applied on the surface of the material as a function of the displacement imposed by the rigid indenter (Figure 2.13).
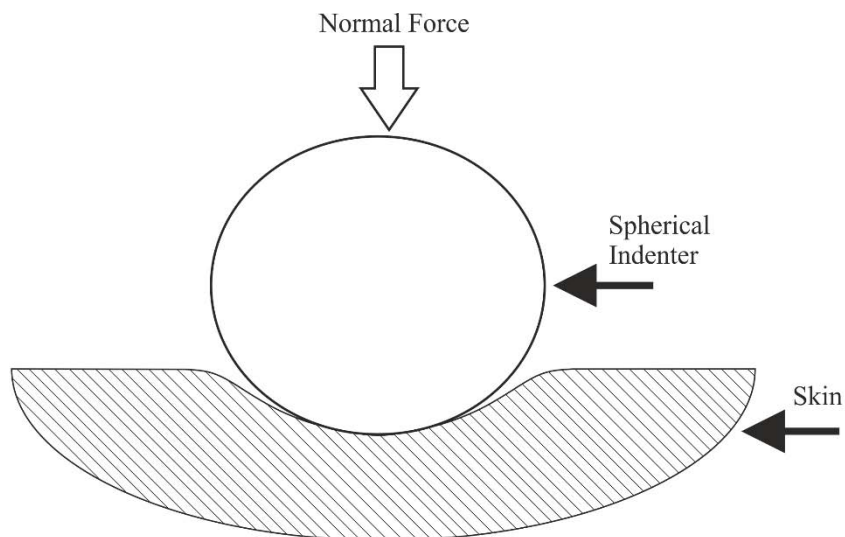

Figure 2.13 Schematic explanation of the indentation method.

The dynamic indentation is an evolution of the trial described above. This method consists of applying a variable force (sinusoidal in general) to the indenter and analyzing the skin's response to this constraint. Using this, you can access the same characteristics as with conventional indentation but with loads of variable frequency. One advantage of such technique is that one can obtain the Young's modulus for a given frequency of stimulation and to distinguish the viscous contribution and the elastic contribution [37].

Apart from choosing the right method to characterize the properties of the skin, it is crucial to use the stimulus in the appropriate force level and depth of penetration. Moreover, the frequency of the stimulation should be in the range perceivable by the skin receptors. The stimulus outside those boundaries might modify measured mechanical properties and as a result change the characterization of the skin. The appropriate values of the stimuli were taken from the characteristics of indentation tests made by team of Laboratoire de Tribologie et Dynamique des Systèmes, (LTDS) from École Centrale de Lyon [8].

2.6 Conclusions

The main focus of this chapter was a brief introduction to piezoelectric phenomenon, including its history, description of existing materials, manufacturing process as well as basic physical structure. The constitutive relations for a piezoelectric material, binding elastic and electric quantities, were presented in the general tensor form. That was later simplified to a matrix form thanks to the crystal symmetry of piezoelectric materials and choice of reference axes. The chosen independent variables were stress T and electric filed E. This was the starting point to present basic coupling modes and coupling coefficients of piezoelectric ceramics. Various types of piezoelectric transducers are available, thanks to the adaptation of these elementary couplings, either used independently or in combination.

Further on, the physical limitations of piezoelectric materials were presented. This section comprised: description of Polarization – Electric field hysteresis loop and Strain – Electric Field "butterfly" curve with selected work area, temperature considerations and mechanical stress limits. At the end of this section, limitations concerning piezoelectric transducer's power were addressed, stressing the fact that the useful area of operation is the combined result of all the above physical limits.

The second part of this chapter was devoted to chosen applications of piezoelectric materials in the fields of medicine and bioengineering. Various types of piezoelectric transducers were presented including: touch sensors, vibration sensors, pressure and sound sensors. Applications ranged from: minimal invasive surgery, pacemaker control, monitoring of patient's activity, blood pressure monitor and hearth beat monitor. Valve actuators were described, applied in precision micro pumps used for insulin delivery. Last, but not least, the largest area of applications was presented: the generation and detection of ultrasonic waves, known as ultrasound. Ultrasonic piezoelectric transducers are used for local drug delivery, ablation of cancer cells, as aid in bone healing and growth process in terms of ultrasonic generation. Medical imaging and bone density measurement are main examples of ultrasound detection.

Separate sections were devoted to present the applications of piezoelectric transducers for the measurement of soft tissues, including human skin. In most cases, those transducers worked in resonance mode in the feedback system. The mechanical properties were extracted basing on the shift of the frequency of the system in contact with the tested material. Serving the role of a theoretical background, the basic properties of the human skin were discussed. This included the main functions, the constitution, as well as elementary parameters which could describe the state of the skin. Finally, the methods for mechanical description of the skin were presented. In the next chapter, those carried out considerations will be used as a base for formulation the requirements for the considered concept of the transducer.

3 A CONCEPT OF PIEZOELECTRIC RESONANT TRANSDUCER

This chapter presents the basic concept of the developed piezoelectric resonant transducer. It begins with a description of requirements which were formulated based on the methods of extracting mechanical properties of soft tissues, in particular indentation method. Further on, the choice of resonant piezoelectric transducer is justified and the proposed bending mode transducer is described in details. Finally, two chosen structures (geometries) of resonant bending transducer are discussed, and then a prototype for each configuration is then presented.

3.1 General requirements

A new concept of transducer, which is the subject of the thesis has to fulfill the requirements based on properties of the skin that have been discussed in the previous chapter. The Figure 3.1 represents the general characteristics which the developed transducer should answer.
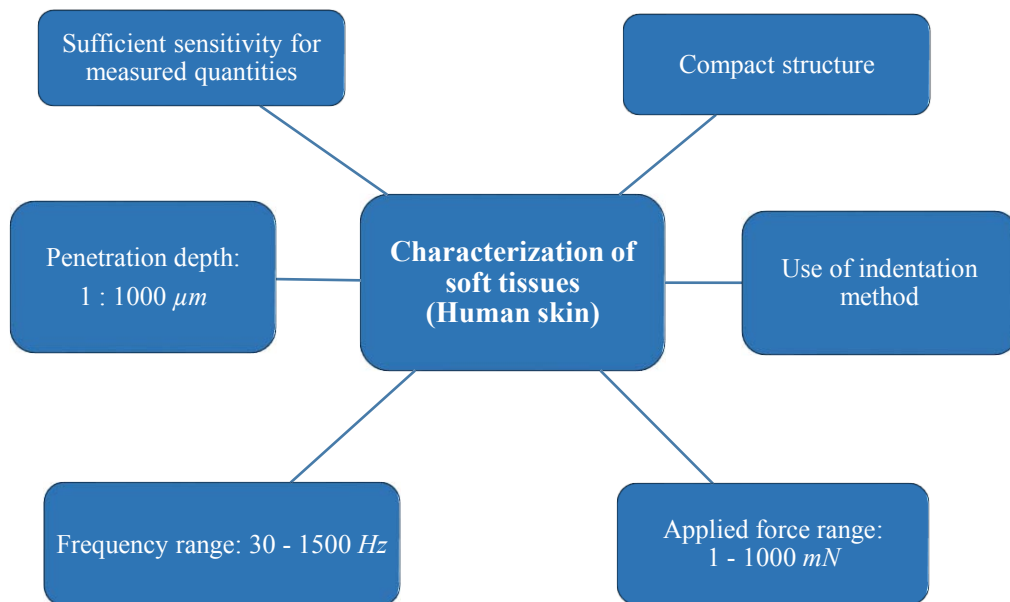

Figure 3.1 General requirements for the developed piezoelectric transducer

The skin has a rich innervation, which amount varies greatly from one territory to another. The face and extremities of the body (e.g. fingers: 2500 receivers / cm^2) are particularly

innervated. The differences in the amount of receptors based on skin areas lead to large differences in the individual thresholds based on territories studied. The sensitivity threshold to mechanical stimulation of the skin corresponds to a depression of 6 microns and varies widely depending on the location of the stimulus. The lowest thresholds are measured at the fingertips. The spatial discrimination threshold is also very variable depending on the location of the stimulus: the lowest thresholds are located at the tip of the tongue and fingertips ($1 - 3$ *mm*); the back is the region where the spatial discrimination is the highest ($50 - 100$ *mm*).

Within the mechanical sensitivity of skin, there can be distinguished three main qualities: sensitivity to pressure, sensitivity to vibration and touch. These qualities are related to the presence of different sensory receptors throughout the skin thickness (free nerve endings, Ruffini endings, Merkel's discs, Meissner's corpuscles and Pacinian corpuscles). From those five types of receptors the Pacinian corpuscles have the most rapid adaptation rate, and therefore are sensitive to vibrations of high frequency. The sensitivity of these receptors is optimal for skin vibration frequencies of 300 *Hz*, but they respond in a frequency range of 30 to 1500 *Hz*. The other skin receptors are sensitive to pressure and touch of lower frequency [39].

The normal force applied onto the tissue's surface should not exceed 1 *N*. The depth of skin's penetration should be in the range of 1 to 1000 *μm*, as the skin characterization concerns only the first millimeter of skin tissue. As described above, sensitivity to vibration responds to pressure changes in a frequency range of 30 to 1500 *Hz*. These properties are related to the presence of different sensory receptors in the skin's thickness.

3.2 Transducer for the characterization of soft tissues

The technical requirements for the developed transducer were specified based on the range of forces, indentation depths and the frequency applicable on the surface of the human skin. As a characterization technique the dynamic indentation method was chosen. It is suitable for determining the elasticity, viscosity and adhesiveness of the tested tissue [9]. The decision to utilize a resonant piezoelectric transducer was made considering the fact, that such a transducer fulfils most of the requirements for the characterization of the human skin. The piezoelectric transducers are well suited to generate high frequency microscopic displacements. They can also be used to generate acoustic waves of up to tens of megahertz.

They are small, robust and do not produce electromagnetic interference. The same structure can work (operate) as a sensor or an actuator, leading to a higher level of integration [43], [28], [58].

Considering the indentation of relatively soft tissues, actuators operating in a bending mode are often the best choice – thanks to their sensitivity. Piezoelectric devices using bending mode have been proposed for the range of sensor applications including: a stiffness measurement, as the pressure and the temperature sensors or as a dilatometers. Specially fabricated piezoelectric bimorph structures have also been used as sensors for atomic force microscopes (AFM), which can reach a femto – Newton level of sensitivity [57].

Prior to the research work of this thesis, two different prototypes were developed at Laboratoire Plasma Et Conversion D'energie (LAPLACE) in Toulouse, France to measure the mechanical properties of materials. The first structure used a Langevin type of piezoelectric actuator. The device shown in the Figure 3.2 contains two piezoelectric ceramics arrangements (transmitter and receiver; polarization is indicated by black arrows) separated by aluminum counter-masses. The primary phase (transmitter) supplied by 46 *V*, performed the role of an actuator. The secondary phase (receiver) performed as a sensor.
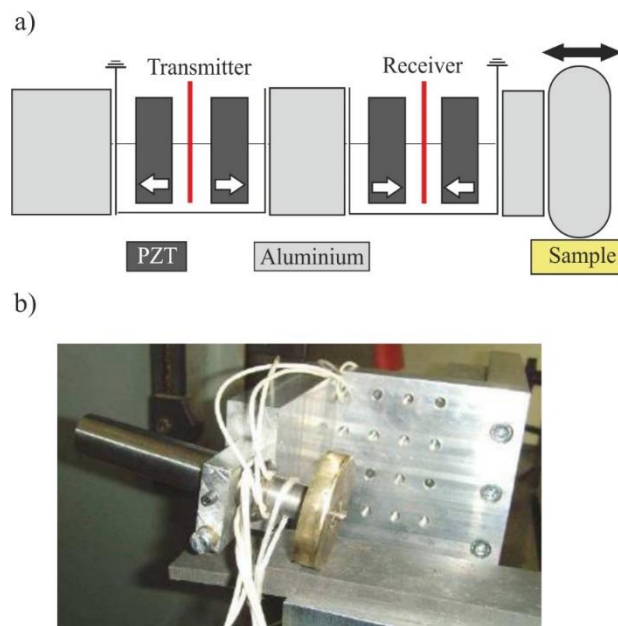

Figure 3.2 a) Schematic view of the Langevin transducer b) prototype of the Langevin transducer

Such an electromechanical arrangement (structure), through the coupling of the piezoelectric ceramic, allowed a tangential excitation at the resonance of the indenter in contact with the sample to be characterized. The contact phase was performed manually, by suspending load masses close to the indenter. The loads applied to the contact materials ranged from 0 to 11 *N*. The above structure was analyzed with aluminum (dry / lubricated), steel (dry / lubricated), polyethylene and silicone by means of acoustic impedance tests and laser vibrometry. The results has showed that the structure exhibited no sensitivity in contact with softer materials such as silicone and high-density polyethylene (HDPE). In addition, such structure provided an excessive tangential contraction of the soft tissues. For skin tissue, such contraction would mean a significant change of the mechanical properties by improper measurement conditions [1].

Another piezoelectric transducer was developed more recently in LAPLACE than the one discussed above. It is consisted of a disc shaped PZT piezoelectric ceramic, working in transversal mode, that is glued to a brass base, acting as an elastic layer. An indentation sphere was attached to the end of the elastic layer. The contact area, between the sphere and the tissue to be characterized, was very low due to the small diameter (4 *mm*) of the sphere. The transducer was based on the principle of piezoelectric bending device, which will be explained in more detail in the following sections. This structure had the possibility of normal and tangential mode of indentation of tissues in contact with the spherical indenter (depending on the mounting of the transducer). In general, this transducer had a good flexibility and therefore its sensitivity to contact was adequate. By means of acoustic impedance measurement the stiffness of polymer samples was assessed. The 3D model of the transducer in question, and the results of characterization of polymer samples are shown in the Figure 3.3.
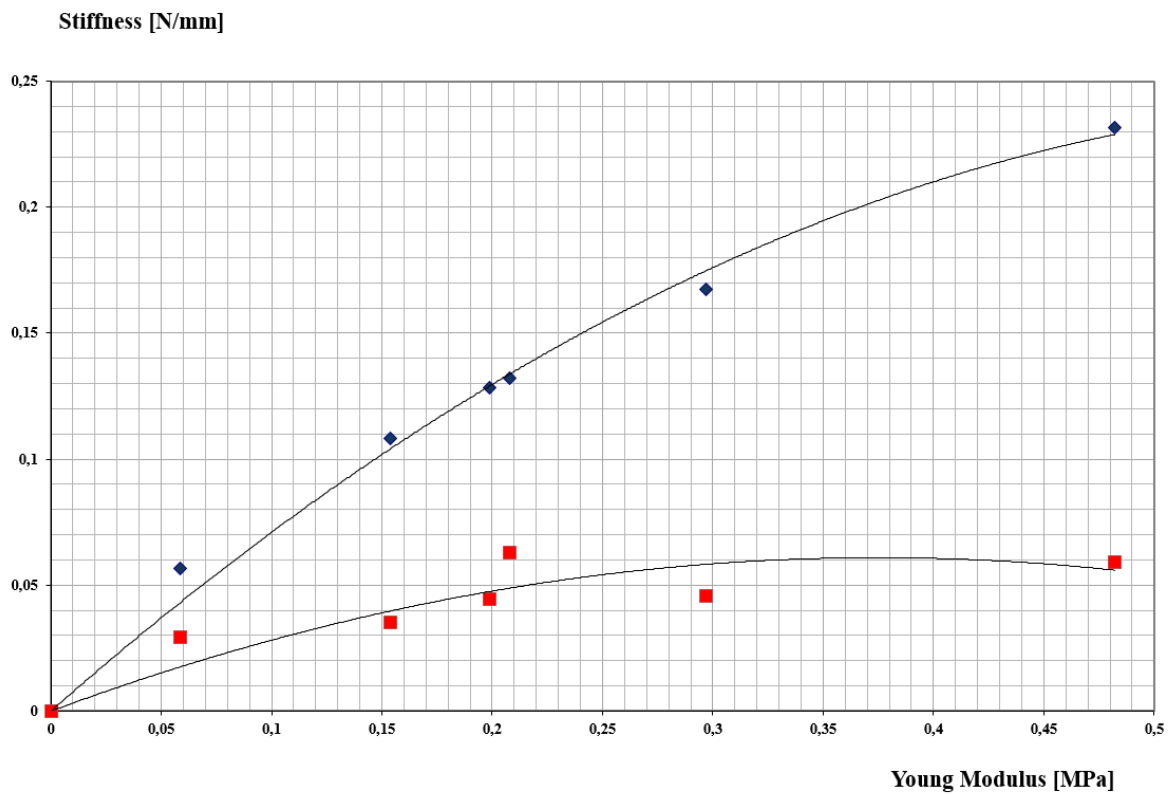
a)

b)

Stiffness [N/mm]

Young Modulus [MPa]
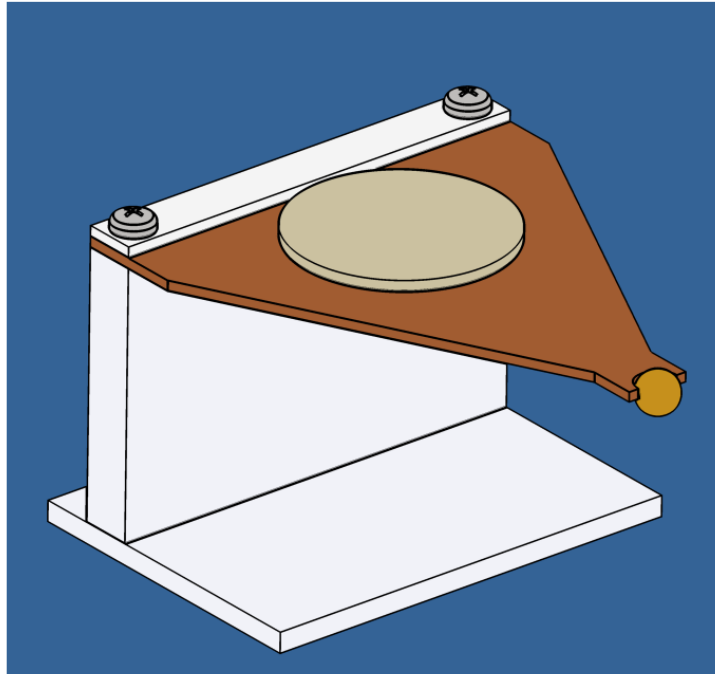
Figure 3.3 Piezoelectric resonant transducer working in bending mode: a) 3 D Model of the transducer mounted on its stand, b) results of normal indentation of polymers obtained by the prototype transducer: theoretical stiffness of the material (blue) and experimental results (red) [1]

3.3 Structures of piezoelectric bending transducers

The longitudinal deformation of a piezoelectric material can be used for the realization of linear actuators (stack actuators), utilizing the longitudinal coupling mode. This type of transducers is characterized by small deflections and high forces. Those small length deformations can be transformed mechanically, by connecting with another elastic (non-piezoelectric) material, as in the case of bending piezoelectric transducers. Concerning the framework of this thesis, three main types of bending transducers can be highlighted, depending on the configuration of active piezoelectric material and the passive, i.e., elastic one.

3.3.1 Unimorph structure

The most basic structure of piezoelectric bending transducer is a unimorph (sometimes also called monomorph). The unimorph structure consists of one active layer and one passive, elastic layer bonded together. The active layer is constructed using PZT ceramics or PVDF polymers with electrodes arranged on two opposite surfaces. The PZT ceramics are usually working in transverse coupling mode (d_{31}), less frequently in longitudinal (d_{33}) mode. The passive layer, also known as elastic layer, is made of material without piezoelectric properties, most often: steel, aluminum, brass, or various types of polymers. The side view of unimorph transducer is shown in Figure 3.4. When the voltage is supplied to the electrodes of the active layer, then the piezoelectric material attempts to react to the electrical signal, while being constrained at the bonded surface. The net result is deflection or bending. Conversely, flexural excitation of such a device will result in the generation of electrical energy within the active layer. In [23] this type of bending transducer is referred to as heterogeneous bimorph structure.
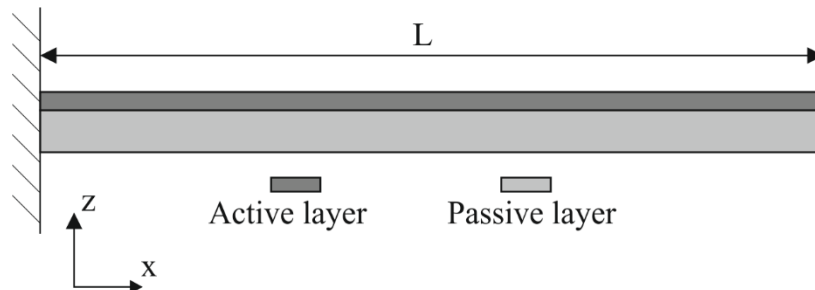

Figure 3.4 Profile of asymmetric unimorph bending transducer

3.3.2 Bimorph structure

The bimorph structure of bending piezoelectric transducer consists of two active layers, directly bonded together or separated by a passive layer. The general principle of work is the same as for unimorph transducers. The side view of a bimorph transducer is shown in Figure 3.5.
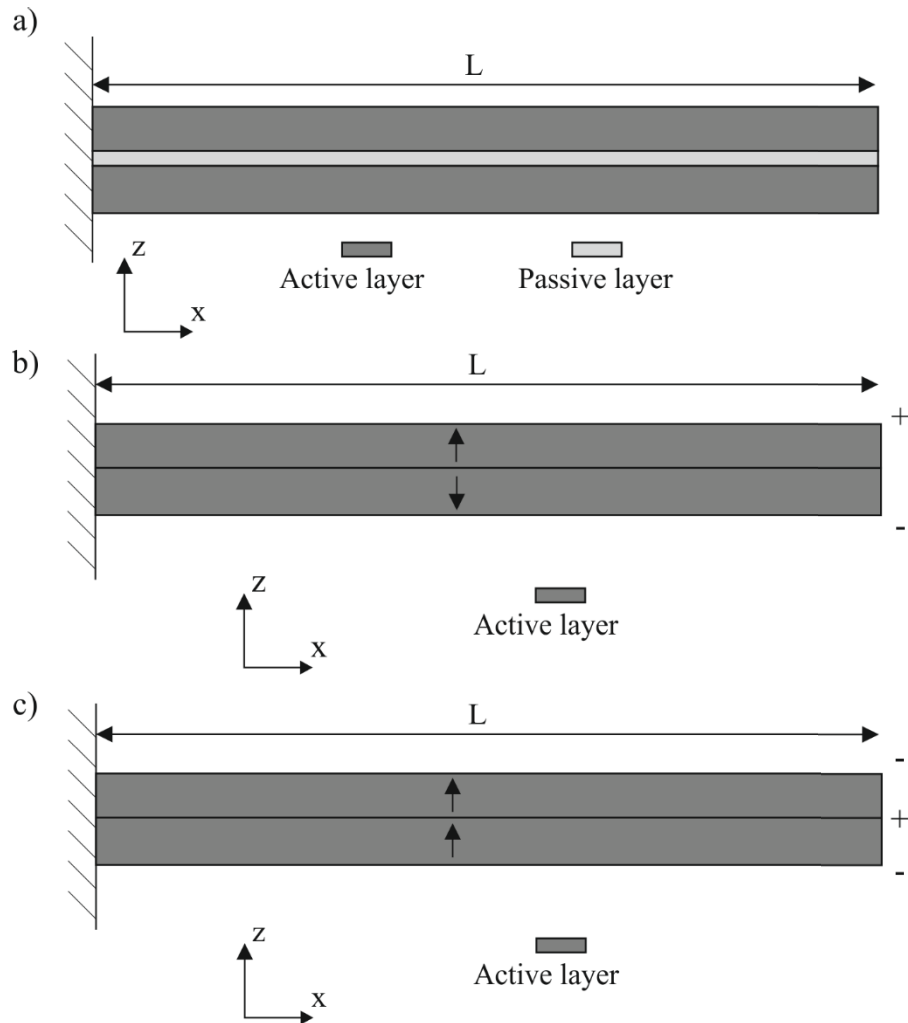

Figure 3.5 Profile of symmetric bimorph bending transducer: a) configuration with center passive layer, b) active layers polled and electrodes set to series operation, c) active layers polled and electrodes set to parallel operation

In the case of a single non-attached piezoelectric element, expansion and contraction are unrestricted in any direction. However, if two elements are joined along one surface where one of the two is in a condition of expansion, while the other tends to contract, motion along this surface will be inhibited. This is the case of piezoelectric bimorph. When a piezoelectric

bimorph has been joined in such a way that under an applied electric field one layer expands, while the other contracts, the motional restriction along the joined surface generate forces and moments which result in the curling of the bimorph.

The simplest example of a piezoelectric bender is the antiparallel bimorph (series connection of active layers). In this structure, the active layers are joined so that their polarizations are antiparallel one to another, and the electric field is applied across the entire beam. A more complex configuration requires that the polarizations be in parallel, with an electrode placed between the two elements, as well as along the upper and lower surfaces (parallel connection). Therefore, each element feels the effect of its own electric field, and the bending moments generated at the joined surface are larger than in the antiparallel configuration, for any given applied electric field.

Piezoelectric bimorph transducers are frequently used as piezoelectric energy harvesters. For this application, parallel configurations are rarely seen in the literature. Due to the very low thickness and fragile nature of piezoceramics, it is easier to electrode the top and bottom surfaces of the bimorph, as opposed to electroding the top and bottom surfaces in addition to the center surface [33].

3.3.3 Multimorph structure

Multimorph piezoelectric transducers are based on expansion of the ideas present in unimorph and bimorph transducers to multiple levels of active and passive layers, forming one structure. This type of actuator is used in cases where large displacements and low applied voltage are needed. However, the multimorph shows a small resultant force and low natural frequency. When a PZT actuator consists of multimorph layers, it can enlarge both the generated force and the resonance frequency, even though applied voltage and manufacturing cost are increased. A multimorph is usually bonded to the top and bottom surfaces of the structures and is driven by voltages of the opposite polarity. Therefore, when one is expanded, the other is contracted. Figure 3.6 shows multimorph bending transducer consisting of active

layers only, with a symmetrical structure in the x-direction. The case of passive layer existing between two active layers is also common.
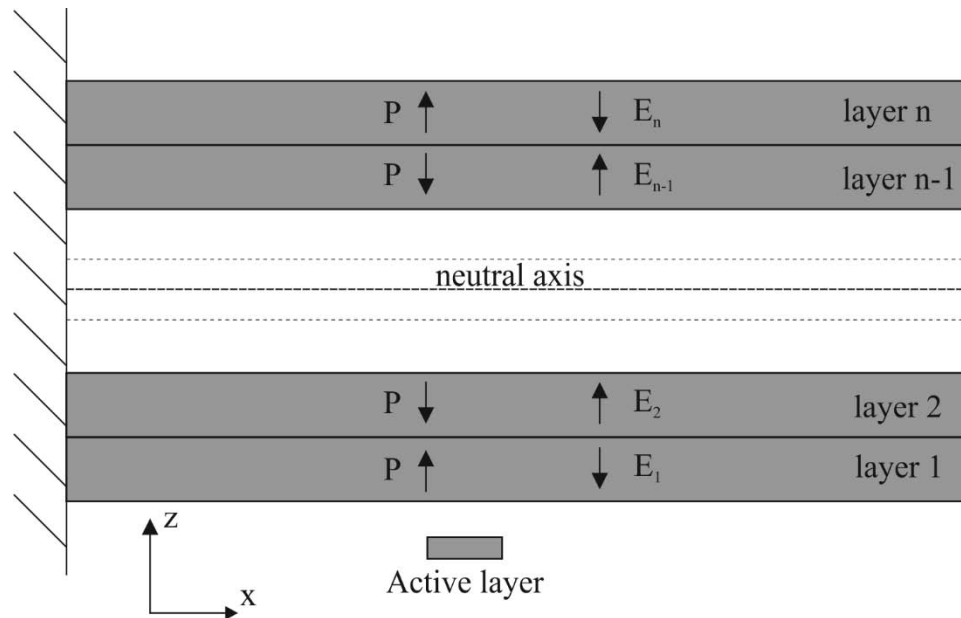

Figure 3.6 Profile of symmetric multimorph bending transducer - arrows indicate example of polarization direction and the electric field direction applied to active layer

3.4 Chosen geometry of the transducer

For the reasons described in previous sections a piezoelectric unimorph structure has been chosen. In general, this structure has a good flexibility (a bending mode of operation) and thus exhibits appropriate level of sensitivity to measured quantities of soft tissues. Moreover it is characterized by relatively simple electromechanical arrangement and compact dimensions.

Unimorph piezoelectric transducer, as has been described in previous sections, consists of two basic layers. The piezoelectric layer, working in d_{31} coupling mode, is bonded to a passive, elastic layer (as described in section 3.3.1). When the voltage is applied across the thickness of the piezoelectric layer, longitudinal and transverse strain appear. The elastic layer opposes the transverse strain and the asymmetry of the whole structure leads to a bending deformation. A basic rectangular unimorph device under deformation is shown in Figure 3.7. In next two paragraphs two variations in unimorph geometry will be presented. Furthermore, these two structures will be analyzed in the following chapters in the frame of analytical approach, simulation and experimental analysis.
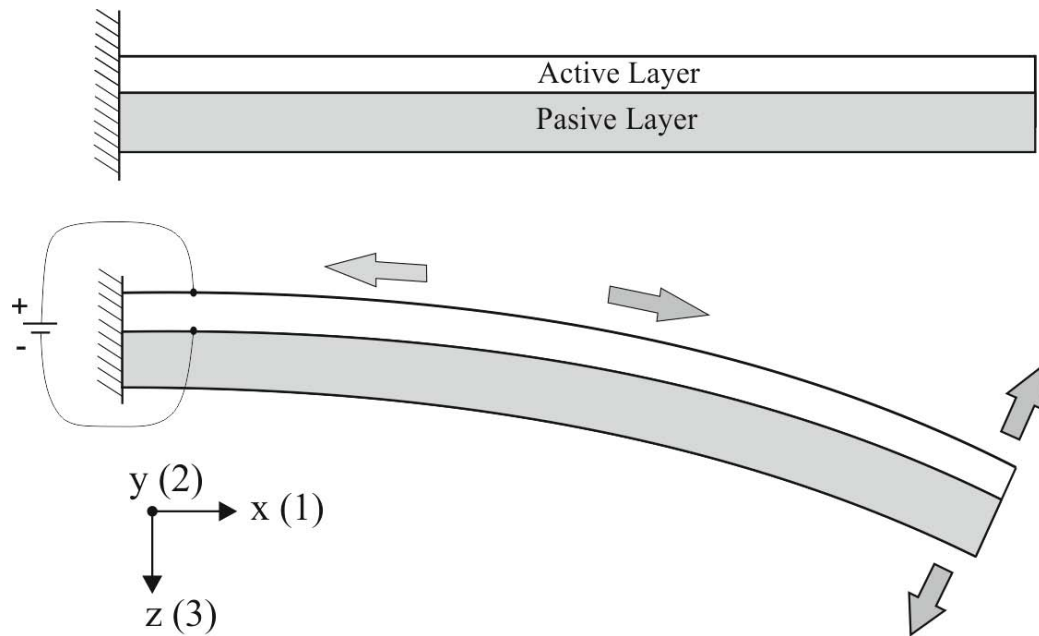
Figure 3.7 Operating principle of piezoelectric unimorph

3.4.1 Unimorph transducer - geometry "I"

The first iteration of the piezoelectric bending transducer, proposed for the characterization of the soft tissues, is an example of unimorph structure. The classic two-layer structure consists of active layer made of hard doped PZT ceramic, which is polled in thickness (3) direction, and passive layer constructed from brass. Two layers are glued by epoxy-resin glue (the details concerning material properties will be presented in the next paragraphs). This unimorph geometry is shown in the Figure 3.8. The transducer is working in the clamped-free condition, which means that one side of the unimorph is blocked (the movement in every direction is constrained by the base of the transducer and a pre-stress plate), and the other side of the bender is able to move freely. The active length of the unimorph is $l_1 = 0.1$ m, and width $l_2 = 0.012$ m, with the thickness of the active layer of 0.002 m.

The indenter is an important addition to the unimorph geometry, as it acts as a probe, which is directly in contact with tested soft tissue. By this probe piezoelectric unimorph transmits the deformations, forces and vibrations to the tested sample. Shaped as a half-sphere, it also enables the use of classic contact theory in addition to indentation method, and electromechanical impedance approach to characterize the tested material sample.
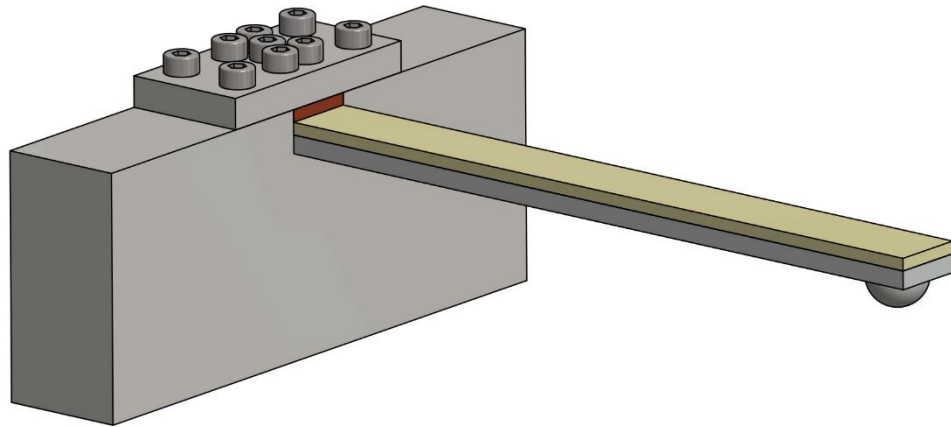
Figure 3.8 Unimorph transducer – geometry "I". The size is not scaled

3.4.2 Unimorph transducer – geometry "II"

To better satisfy the requirements, explained in the previous sections, some major changes were implemented in the geometry "I" of the piezoelectric bending transducer. The new prototype is shown in the Figure 3.9.
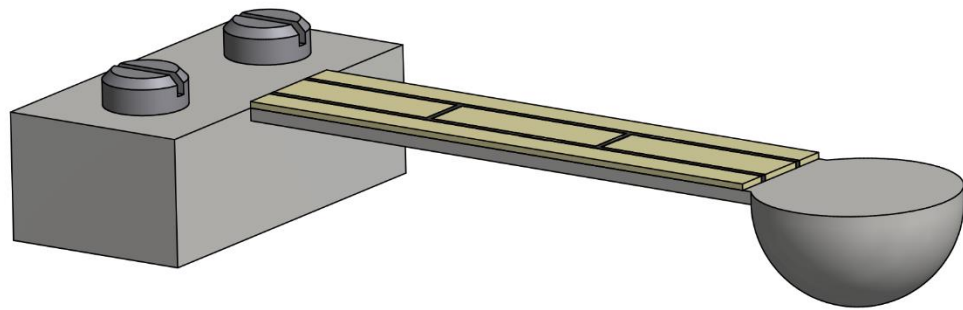
Figure 3.9 Unimorph transducer – geometry "II". The size is not scaled

First, to better fulfill the compact dimensions condition, the new structure is 40 % smaller than the first transducer. The total active length of the new transducer is only 60 *mm*, width – 10 *mm* for the piezoelectric ceramics, and only 1.5 *mm* thick. On the other hand, the indentation device – a rigid half-sphere – is larger, with the diameter of 16 *mm*, which contributes to a larger contact area and a higher sensitivity for measured quantities. The passive layer of the transducer "II" is integrated with the base on the clamped end of the transducer, and also with

the indentation half-sphere at the free end, which leads to simplification of the structure. Material for the active layer had been changed to Noliac NCE-40 ceramic, due to its better electro-mechanical coupling and lower dielectric losses. Also, the area for the electrodes has been re-arranged. Thanks to sectorization of the ceramics there are five areas dedicated to sensing and actuation at a desired resonance frequency (Figure 3.10). The middle three are dedicated to sensing/actuation of first and the third resonant mode, while the other two are dedicated for the second resonant mode.
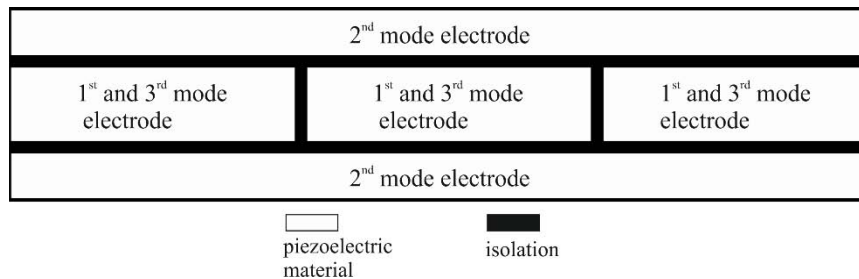
2nd mode electrode		
1st and 3rd mode electrode	1st and 3rd mode electrode	1st and 3rd mode electrode
2nd mode electrode		

piezoelectric material   isolation

Figure 3.10 Diagram of the sectorization of the active, piezoelectric layer

3.5 Prototype of the unimorph transducer "I"

The prototype of the unimorph transducer, considered in this section, was originally developed and studied by Valérie Monturet in her thesis [65]. The research work was carried out at LAPLACE Laboratory in Toulouse. It concerned the development and implementation of a new methodology for optimal design of piezoelectric actuators. The research work was based on the example of unimorph structure working as a vibrator in the magnetometer.

3.5.1 Choice of the materials

The active piezoelectric layer of the unimorph transducer was constructed using "hard-doped" PZT ceramics P1-89, due to the low dielectric loss factor and higher quality coefficient Q, while compared to "soft" piezoelectric ceramics. It is working in transversal mode, meaning it's polarized in the 3rd direction, and the active layer elongates in 1st direction, when supplied with voltage across its thickness. The passive elastic layer was made of brass. Those two layers were glued by two-component adhesive (epoxy-resin E505 glue form Epotecny). The indentation half-sphere was made of 100C6 type steel. The main physical properties of those materials are shown in the Table 3.1.

Table 3.1 Chosen properties of materials used in the prototype unimorph transducer "I"

Property	P1 – 89 (PZT ceramic)	Brass	100C6 Steel
Density $[kg \cdot m^{-3}]$	7650	8450	7800
Young modulus $[10^{10} \cdot N \cdot m^{-2}]$	9.38	10.5	21.0
Poisson coefficient ν $[-]$	0.31	0.3	0.3
Relative dielectric constant $\varepsilon_{33}^{S}[-]$	1142	-	-
Charge constants d $[10^{-12} \cdot C \cdot N^{-1}]$	$d_{31} = -108$ $d_{33} = 240$ $d_{15} = 280$	-	-
Elastic Compliances S^{E} $[10^{-12} \cdot m^{2} \cdot N^{-1}]$	$S_{11}^{E} = 10.66$ $S_{33}^{E} = 13.25$	-	-
Dielectric loss factor $tan\delta$ $[10^{-4}]$	30	-	-

3.5.2 Assembly process

The prototype unimorph transducer "I" consists of a brass, passive layer and active layer made of P1-89 PZT ceramics. The rigid hemispherical 100C6 type steel is glued to the free end of the unimorph transducer and acts as the indentation device. The active length of the unimorph is $l_1 = 0.1$ m, and width $l_2 = 0.012$ m. The thickness of piezoceramic layer is $h_a = 0.002$ m, where the passive layer of brass is $h_s = 0.003$ m thick. The indentation sphere has a radius of $r = 0.005$ m. The technical drawing of the prototype unimorph transducer "I" is shown in Appendix A4.

The assembling of the two layers is achieved by gluing with epoxy-resin adhesive. This type of glue is especially resistant to shear stress. Moreover, the glue used was non-conductive,

which means that the electric contact had to be obtained by the applied pressure during the curing process, and additionally by the roughness of surfaces and by low thickness of the glue layer (in the *μm* range). The prototype unimorph was connected to a voltage source by the steel base (ground potential) and the upper electrode of active layer (high potential). The complete structure of the transducer attached to steel base (with intermediate, pre-stress, copper plate) is shown in Figure 3.11.
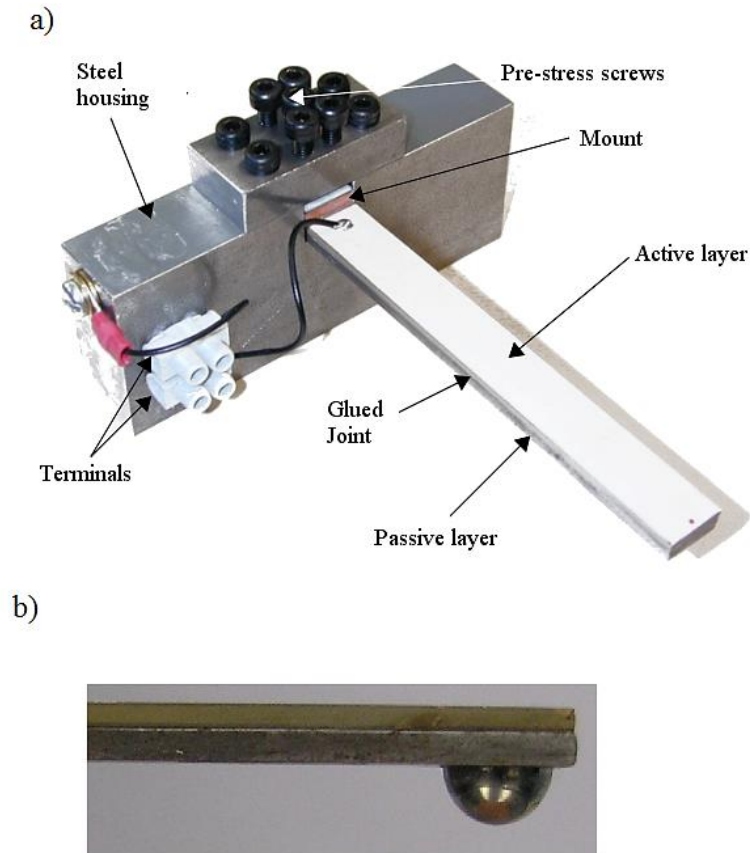

Figure 3.11 Prototype of unimorph transducer: a) the original design [65] without hemisphere, b) the rigid hemisphere (indentation device) glued to the free end of the transducer

3.6 Prototype of the unimorph transducer "II"

3.6.1 Choice of the materials

The active layer of second prototype was constructed using piezoelectric ceramic NCE-40 manufactured by Noliac. It is "hard" lead zirconate titanate material, belonging to the Navy Type I standard of piezoelectric materials. It was developed for general power applications. Having high electromechanical coupling, high piezoelectric charge constant, and low dielectric

loss under high electric driving fields, it is suitable for broadband of electro-mechanical and electro-acoustic devices. On the other hand, the P1-89 ceramics belonged to the Navy Type III standard, which provided the maximum stability under temperature, electric field, and stress. It was designed for high power acoustic projectors, ultrasonic welders, bonders, hand-held medical, dental devices, and deep water applications [13]. The ceramic is polarized in the thickness (3rd) direction. The passive, elastic layer is CNC milled from block of aluminum. It integrates the passive layer with the indentation hemisphere and the base, for the sake of simpler structure of the transducer. Passive and active layers are glued by epoxy-resin E505 glue form Epotecny. The basic properties of those materials are in the Table 3.2.

Table 3.2 Chosen properties of materials used in the prototype unimorph transducer "II"

Property	NCE-40 (PZT ceramic)	Aluminum
Density [$kg \cdot m^{-3}$]	7750	2770
Young modulus [$10^{10} \cdot N \cdot m^{-2}$]	7.69	7.10
Poisson coefficient ν [$-$]	0.31	0.33
Relative dielectric constant ε_{33}^T [$-$]	1250	-
Charge constants d [$10^{-12} \cdot C \cdot N^{-1}$]	$d_{31} = -140$ $d_{33} = 320$ $d_{15} = 500$	-
Elastic Compliances S^E [$10^{-12} \cdot m^2 \cdot N^{-1}$]	$S_{11}^E = 13$ $S_{33}^E = 17$	-
Dielectric loss factor $tan\delta$ [10^{-4}]	25	-

3.6.2 Assembly process

The first stage of the assembling was verification of polarization level of NCE-40 ceramics. The d_{33} piezoelectric constant was measured on the wide-range d_{33} tester from APC and compared with material data supplied by the manufacturer of ceramics. A ceramic during test is shown in Figure 3.12.
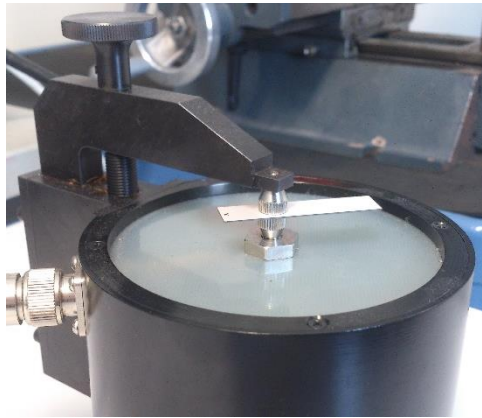

Figure 3.12 View of d_{33} coefficient tester

After that, the ceramic was sectorized, based on the scheme presented in 3.4.2. PC-controlled laser system was used for this task. The depth, which should be enough for an electrical separation of the sectors, was examined under the microscope (Figure 3.13).

Figure 3.13 Sectorization process: upper right – laser cutting system; upper left – inspection of the depth of the cut; lower – sectorized ceramic

The following stage, included milling of the passive layer with the base and the indentation device on a CNC machine to dimensions specified in previous paragraphs. The main goal here, was the miniaturization without lowering of the electromechanical performance of the transducer (Figure 3.14). Overall, 40% smaller dimensions were achieved, compared to the first prototype.

Figure 3.14 The passive layer of prototype unimorph transducer "II". The actual passive layer is integrated with the base and the indentation half-sphere for the sake of simpler structure

The active layer consisting of NCE-40 sectorized ceramic had to be glued to the passive layer. Two component epoxy-resin adhesive was used. To ensure the best bonding condition the process lasted 90 minutes in temperature of 60 ℃. Evenly distributed pressure was applied to the glued pieces by the apparatus shown in Figure 3.15. This enabled the electrical contact between the PZT ceramic and the passive layer (with thin layer of glue).

Figure 3.15 Application of evenly distributed pressure during the gluing process of the active and passive layers

The completed transducer with wire leads soldered to the sectors of the active layer is presented in Figure 3.16. This prototype was assembled in two variants: with active layer sectorized and without the sectors, which is the case of Figure 3.17 (Appendix A5).
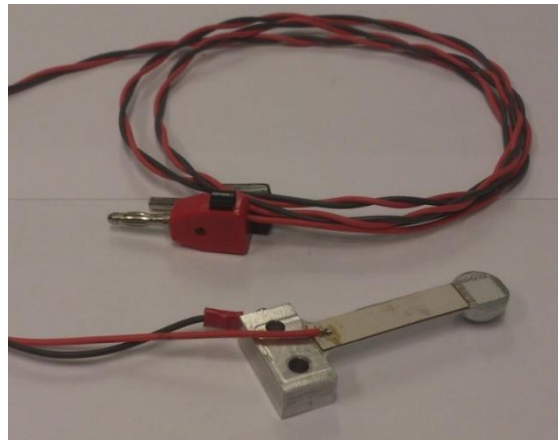

Figure 3.16 Completed prototype unimorph transducer "II"

Figure 3.17 Complete prototype unimorph transducer "II" (variant without sectorized active layer)

3.7 Conclusions

The aim of this chapter was to describe the concept and prototype development of the transducer for characterization of the mechanical properties of soft tissue, in particular human skin. The general requirements, formulated on the basis of human skin's properties, have served as a starting point for the presented considerations. The choice of piezoelectric bending transducer in a form of unimorph structure was justified. Further on, two geometries of such transducer were presented, and its two prototype developments were described. In the next chapter those two prototype transducers will be studied using analytical approach, including static calculations of deformations, equivalent circuit representation, and an assessment of contact conditions.

4 ANALYTICAL APPROACH TO STUDY THE UNIMORPH TRANSDUCER

In this chapter an analytical approach to study the unimorph transducer is presented. First, using the approach published in [20], a set of equations and boundary conditions for multimorph transducer with bounding layers and electrodes is derived. Next the case study is simplified to an unimorph transducer with one elastic, one piezoelectric and electrode layer. The study of the unimorph transducer has the following steps: static calculations of tip deflection, dynamic description in terms of equivalent circuits, and finally, an assessment of the contact conditions based on the Hertz theory.

4.1 Static analysis

4.1.1 General equations

A multi-layered actuator with all layers connected in series is considered. The piezoelectric layer and bonding layer are placed alternately. There are $n + 1$ elastic layers (including two electrodes and $n - 1$ bonding layers), and n piezoelectric layers. Actually, the actuator will become a multi-layered pure piezoelectric actuator if the thickness of each elastic layer is zero. Between the upper and lower surfaces of the actuator there is an external electrical potential V_0. The thickness of the elastic layer k is determined by (h_{2k-1} - h_{2k-2}) and the thickness of the piezoelectric layer k is determined by (h_{2k} - h_{2k-1}) as shown in Figure 4.1.
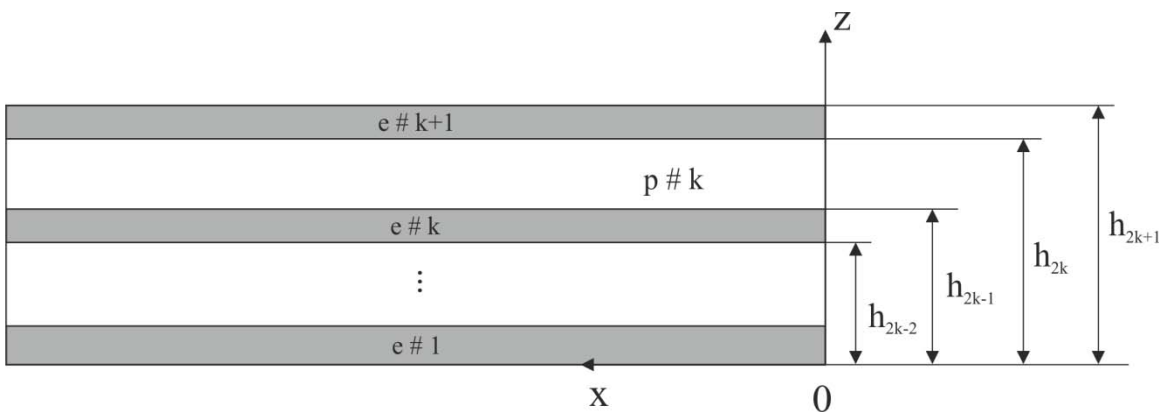

Figure 4.1 2D geometric model of multimorph consisting of $k+1$ elastic layers and k piezoelectric layers

In Cartesian coordinate system (x-0-z) the constitutive equations for transversely isotropic elastic materials (4.1) and piezoelectric materials (4.2), under the condition of plane deformation, can be written as follows:

$$\begin{cases} \varepsilon_x = S_{11Ek}\sigma_x + S_{13Ek}\sigma_z \\ \varepsilon_z = S_{13Ek}\sigma_x + S_{33Ek}\sigma_z \\ \quad \gamma_{xz} = S_{44Ek}\tau_{xz} \end{cases} \tag{4.1}$$

$$\begin{cases} \varepsilon_x = S_{11Pk}\sigma_x + S_{13Pk}\sigma_z + g_{31k}D_z \\ \varepsilon_z = S_{13Pk}\sigma_x + S_{33Pk}\sigma_z + g_{33k}D_z \\ \quad \gamma_{xz} = S_{44Pk}\tau_{xz} + g_{15k}D_x \\ \quad E_x = -g_{15k}\tau_{xz} + \beta_{11k}D_x \\ E_z = -g_{31k}\sigma_x - g_{33k}\sigma_z + \beta_{33k}D_z \end{cases} \tag{4.2}$$

where: $\varepsilon_{ij}, \sigma_{ij}, D_i, E_i$ – components of strain, stress, induction and electric field, respectively; S_{ijEk}, S_{ijPk} are the coefficients of the elastic compliance for elastic and piezoelectric layers, respectively; g_{ij}, β_{ij} are piezoelectric and dielectric impermeability for piezoelectric layers.

The strain components for both elastic and piezoelectric materials can be expressed by the displacement components (*u* and *w*):

$$\varepsilon_x = \frac{\partial u}{\partial x}, \varepsilon_z = \frac{\partial w}{\partial z}, \gamma_{xz} = \frac{\partial u}{\partial z} + \frac{\partial w}{\partial x} \tag{4.3}$$

For piezoelectric materials, the electric field and the electric potential φ are linked by:

$$E_x = -\frac{\partial \varphi}{\partial x}, E_z = -\frac{\partial \varphi}{\partial z} \tag{4.4}$$

Without consideration of body force, the static equilibrium equations for both elastic and piezoelectric materials can be described as:

$$\frac{\partial \sigma_x}{\partial x} + \frac{\partial \tau_{xz}}{\partial z} = 0, \qquad \frac{\partial \tau_{xz}}{\partial x} + \frac{\partial \sigma_z}{\partial z} = 0 \tag{4.5}$$

Without consideration of body charge, the induction components in the piezoelectric materials should satisfy the following equation:

$$\frac{\partial D_x}{\partial x} + \frac{\partial D_z}{\partial z} = 0 \tag{4.6}$$

If the displacement and the electric potential are to be obtained from (4.3) and (4.4), the components of strain and electric field must satisfy the following equations:

$$\frac{\partial^2 \varepsilon_x}{\partial z^2} + \frac{\partial^2 \varepsilon_z}{\partial x^2} = \frac{\partial^2 \gamma_{xz}}{\partial x \partial z}, \qquad \frac{\partial E_x}{\partial z} - \frac{\partial E_z}{\partial x} = 0 \tag{4.7}$$

These equations will be solved in the following paragraphs, taking into the considerations the boundary conditions of a multimorph transducer and finally the unimorph transducer.

4.1.2 Analytical model of multimorph transducer

To solve the equations presented above, the Airy stress function method is used. Introducing the stress function $\tilde{\varphi}$ and the induction function ψ, the stress and induction components are expressed as:

$$\sigma_x = \frac{\partial^2 \tilde{\varphi}}{\partial z^2}, \qquad \sigma_z = \frac{\partial^2 \tilde{\varphi}}{\partial x^2}, \qquad \tau_{xz} = -\frac{\partial^2 \tilde{\varphi}}{\partial x \partial z}$$

$$D_x = \frac{\partial \psi}{\partial z}, \qquad D_z = -\frac{\partial \psi}{\partial x} \tag{4.8}$$

The stress function $\tilde{\varphi}_{Ek}$, $\tilde{\varphi}_{Pk}$ and induction function ψ_k of elastic and piezoelectric layer k, respectively, are assumed as:

$$\tilde{\varphi}_{Ek} = -a_{Ek} z^3 + b_{Ek} z^2$$

$$\tilde{\varphi}_{Pk} = -a_{Pk} z^3 + b_{Pk} z^2, \quad \psi_k = l_k x \tag{4.9}$$

where: a_{Ek}, b_{Ek}, a_{Pk}, b_{Pk} and l_k are constants to be calculated.

The components of stress and induction in k elastic and piezo layer, respectively, can be expressed as:

$$\begin{cases} \sigma_x = -6a_{Ek} z + 2b_{Ek} \\ \quad \sigma_z = \tau_{xz} = 0 \end{cases}$$

$$\begin{cases} \sigma_x = -6a_{Pk} z + 2b_{Pk} \\ \quad \sigma_z = \tau_{xz} = 0 \\ \qquad D_x = 0 \\ \qquad D_z = -l_k \end{cases} \tag{4.10}$$

Using equations (4.1), (4.2) and (4.3), (4.4), the displacement and electrical potential in elastic layer k and piezoelectric layer k, respectively, can be described as:

$$\begin{cases} u = -6a_{Ek}S_{11Ek}xz + 2b_{Ek}S_{11Ek}x + \omega_{Ek}z + u_{Ek} \\ w = -3a_{Ek}S_{13Ek}z^2 + 2b_{Ek}S_{13Ek}z + 3a_{Ek}S_{11Ek}x^2 - \omega_{Ek}x + w_{ek} \end{cases} \quad (4.11)$$

$$\begin{cases} u = -6a_{Pk}S_{11Pk}xz + 2b_{Pk}S_{11Pk}x - g_{31k}l_{Pk}x + \omega_{Pk}z + u_{Pk} \\ w = -3a_{Pk}S_{13Pk}z^2 + 2b_{Pk}S_{13Pk}z - g_{33k}l_{Pk}z + 3a_{Pk}S_{11Pk}x^2 - \omega_{Pk}x + w_{Pk} \\ \varphi = -3a_{Pk}g_{31k}z^2 + 2b_{Pk}g_{31k}z + \beta_{33k}l_{Pk}z + \varphi_k \end{cases} \quad (4.12)$$

where: $a_{Pk}, a_{Ek}, b_{Pk}, b_{Ek}, l_{Pk}, \omega_{Pk}, \omega_{Ek}, u_{Pk}, u_{Ek}, w_{Pk}, w_{Ek}, \varphi_k$ are constants calculated with help of geometrical and electrical boundary conditions. The following boundary conditions are automatically satisfied.

$$D_x = 0 \text{ at } x = 0, L$$
$$\tau_{xz} = 0 \text{ at } x = L \quad (4.13)$$
$$\sigma_z = 0, \ \tau_{xz} = 0 \ \text{ at } z = 0 \ \text{ and } z = h_{2n} + 1$$

The continuous conditions of induction in z-direction at the interfaces gives:

$$l_1 = l_2 = \cdots = l_n = l \quad (4.14)$$

The displacement u and w should be continuous at the interfaces:

$$\begin{cases} u(x, h_{i-}) = u(x, h_{i+}) \\ w(x, h_{i-}) = w(x, h_{i+}) \end{cases} for \ (1 \leq i \leq 2n) \quad (4.15)$$

That leads to the following equations for $1 \leq k \leq n$:

$$\begin{cases} u(x, h_{2k-1}) = -6a_{Ek}S_{11Ek}xh_{2k-1} + 2b_{Ek}S_{11Ek}x + \omega_{Ek}h_{2k-1} + u_{Ek} \\ \quad = -6a_{Pk}S_{11Pk}xh_{2k-1} + 2b_{Pk}S_{11Pk}x - g_{31k}lx + \omega_{Pk}h_{2k-1} + u_{Pk} \\ u(x, h_{2k}) = -6a_{E,k+1}S_{11E,k+1}xh_{2k} + 2b_{E,k+1}S_{11E,k+1}x + \omega_{E,k+1}h_{2k} + \\ u_{E,k+1} = -6a_{Pk}S_{11Pk}xh_{2k} + 2b_{Pk}S_{11Pk}x - g_{31k}lx + \omega_{Pk}h_{2k} + u_{Pk} \\ w(x, h_{2k-1}) = -3a_{Ek}S_{13Ek}h_{2k-1}^2 + 2b_{Ek}S_{13Ek}h_{2k-1} + 3a_{Ek}S_{11Ek}x^2 + \\ -\omega_{Ek}x + w_{ek} = -3a_{Pk}S_{13Pk}h_{2k-1}^2 + 2b_{Pk}S_{13Pk}h_{2k-1} - g_{33k}lh_{2k-1} + \\ \quad\quad 3a_{Pk}S_{11Pk}x^2 - \omega_{Pk}x + w_{Pk} \\ w(x, h_{2k}) = -3a_{E,k+1}S_{13E,k+1}h_{2k}^2 + 2b_{E,k+1}S_{13E,k+1}h_{2k} + \\ 3a_{E,k+1}S_{11E,k+1}x^2 - \omega_{E,k+1}x + w_{E,k+1} = -3a_{Pk}S_{13Pk}h_{2k}^2 + \\ 2b_{Pk}S_{13Pk}h_{2k} - g_{33k}lh_{2k} - g_{33k}lh_{2k} + 3a_{Pk}S_{11Pk}x^2 - \omega_{Pk}x + w_{Pk} \end{cases} \quad (4.16)$$

Besides the point of $\omega_{Ek} = \omega_{Pk} = \omega_0, u_{Ek} = u_{Pk} = u_0$ the above equations are satisfied only if:

$$a_{Pk}S_{11Pk} = a_{Ek}S_{11Ek} = a_{P1}S_{11P1} \tag{4.17}$$

$$2b_{Ek}S_{11Ek} = 2b_{P1}S_{11P1} - g_{311}l \tag{4.18}$$

$$2b_{Pk}S_{11Pk} = 2b_{P1}S_{11P1} + (g_{31k} - g_{311})l \tag{4.19}$$

$$-3a_{Ek}S_{13Ek}h_{2k-1}^2 + 2b_{Ek}S_{13Ek}h_{2k-1} + w_{Ek}$$
$$= -3a_{Pk}S_{13Pk}h_{2k-1}^2 + 2b_{Pk}S_{13Pk}h_{2k-1} - g_{33k}lh_{2k-1} + w_{Pk} \tag{4.20}$$

$$-3a_{E,k+1}S_{13E,k+1}h_{2k}^2 + 2b_{E,k+1}S_{13E,k+1}h_{2k} + w_{E,k+1}$$
$$= -3a_{Pk}S_{13Pk}h_{2k}^2 + 2b_{Pk}S_{13Pk}h_{2k} - g_{33k}lh_{2k} + w_{Pk} \tag{4.21}$$

The boundary conditions at the upper and lower surfaces, as well as the conditions at the interfaces of the elastic layer between two neighbor piezoelectric layers for electrical potential, can be expressed as:

$$\begin{cases} \varphi(x,0) = 0 \\ \varphi(x,h_{2i-2}) = \varphi(x,h_{2i-1}) \quad (i = 1,2,3,\dots,n) \\ \varphi(x,h_{2n}) = V_0 \end{cases} \tag{4.22}$$

To simplify, the following expression is introduced:

$$H_{Ej,k} = \frac{h_{2k-1}^j - h_{2k-2}^j}{S_{11Ek}} \quad for \ (k = 1,2,\dots,n, n+1; j = 1,2,3)$$

$$H_{Pj,k} = \frac{h_{2k}^j - h_{2k-1}^j}{S_{11Pk}} \quad for \ (k = 1,2,\dots,n; \ j = 1,2,3) \tag{4.23}$$

From equations (4.12), (4.17) to (4.19) and (4.22) the following expression can be deduced:

$$k_{11}a_{P1} + k_{12}b_{P1} + k_{13}l = V_0 \tag{4.24}$$

where:

$$\begin{cases} k_{11} = -3\sum_{k=1}^n H_{P2,k}g_{31k}S_{11P1}, \ k_{12} = 2\sum_{k=1}^n H_{P1,k}g_{31k}S_{11P1} \\ k_{13} = \sum_{k=1}^n \left(\frac{g_{31k} - g_{331}}{S_{11Pk}} g_{31k} + \beta_{33k} \right)(h_{2k} - h_{2k-1}) \end{cases} \tag{4.25}$$

66

For the free end of transducer the mechanical boundary conditions are formulated thanks to Saint-Venant's principle as:

$$\begin{cases} \displaystyle\sum_{k=1}^{n} \int_{h_{2k-1}}^{h_{2k}} (-6a_{Pk}z + 2b_{Pk})dz + \sum_{k=1}^{n+1} \int_{h_{2k-2}}^{h_{2k-1}} (-6a_{Ek}z + 2b_{Ek})dz = N_0 \\ \displaystyle\sum_{k=1}^{n} \int_{h_{2k-1}}^{h_{2k}} (-6a_{Pk}z + 2b_{Pk})zdz + \sum_{k=1}^{n+1} \int_{h_{2k-2}}^{h_{2k-1}} (-6a_{Ek}z + 2b_{Ek})zdz = M_0 \end{cases} \tag{4.26}$$

Substituting equations (4.17) to (4.19) into (4.26), the following equations can be obtained:

$$\begin{cases} k_{21}a_{P1} + k_{22}b_{P1} + k_{23}l = N_0 \\ k_{31}a_{P1} + k_{32}b_{P1} + k_{33}l = M_0 \end{cases} \tag{4.27}$$

where:

$$\begin{cases} k_{21} = -3\left(\displaystyle\sum_{k=1}^{n+1} H_{E2,k} + \sum_{k=1}^{n} H_{P2,k}\right)S_{11P1} \\ k_{22} = 2\left(\displaystyle\sum_{k=1}^{n+1} H_{E1,k} + \sum_{k=1}^{n} H_{P1,k}\right)S_{11P1} \\ k_{23} = -\displaystyle\sum_{k=1}^{n+1} H_{E1,k}g_{311} + \sum_{k=1}^{n} H_{P1,k}(g_{31k} - g_{311}) \\ k_{31} = -2\left(\displaystyle\sum_{k=1}^{n+1} H_{E3,k} + \sum_{k=1}^{n} H_{P3,k}\right)S_{11P1} \\ k_{32} = \left(\displaystyle\sum_{k=1}^{n+1} H_{E2,k} + \sum_{k=1}^{n} H_{P2,k}\right)S_{11P1} \\ k_{33} = -\frac{1}{2}\displaystyle\sum_{k=1}^{n+1} H_{E2,k}g_{311} + \frac{1}{2}\sum_{k=1}^{n} H_{P2,k}(g_{31k} - g_{311}) \end{cases} \tag{4.28}$$

From equations (4.24) and (4.27) the parameters a_{P1}, b_{P1} and l can be determined.

$$\begin{pmatrix} a_{P1} \\ b_{P1} \\ l \end{pmatrix} = \begin{pmatrix} k_{11} & k_{12} & k_{13} \\ k_{21} & k_{22} & k_{23} \\ k_{31} & k_{32} & k_{33} \end{pmatrix}^{-1} \begin{pmatrix} V_0 \\ N_0 \\ M_0 \end{pmatrix} = \boldsymbol{K}^{-1} \begin{pmatrix} V_0 \\ N_0 \\ M_0 \end{pmatrix} \tag{4.29}$$

The parameters a_{Ek}, a_{Pk}, b_{Ek}, b_{Pk} can be calculated as:

$$a_{Ek} = \frac{S_{11P1}}{S_{11Ek}} a_{P1} \tag{4.30}$$

$$a_{Pk} = \frac{S_{11P1}}{S_{11Pk}} a_{P1} \tag{4.31}$$

$$b_{Ek} = \frac{S_{11P1}}{S_{11Ek}} b_{P1} - \frac{g_{311}}{2S_{11Ek}} l \tag{4.32}$$

$$b_{Pk} = \frac{S_{11P1}}{S_{11Pk}} b_{P1} - \frac{g_{31k} - g_{311}}{2S_{11Pk}} l \tag{4.33}$$

To calculate the rest of the parameters, the following geometrical restraint conditions are used:

$$u(L, h_{2I-1}) = 0, w(L, h_{2I-1}) = 0, \frac{\partial w(L, h_{2I-1})}{\partial x} = 0 \quad I \in \{1, 2, 3, \dots, n\} \tag{4.34}$$

That leads to:

$$\begin{cases} -6a_{EI}S_{11EI}Lh_{2I-1} + 2b_{EI}S_{11EI}L + \omega_0 h_{2I-1} + u_0 = 0 \\ -3a_{EI}S_{13EI}h_{2I-1}^2 + 2b_{EI}S_{13EI}h_{2I-1} + 3a_{EI}S_{11EI}L^2 - \omega_0 L + w_{EI} = 0 \\ 6a_{EI}S_{11EI}L - \omega_0 = 0 \end{cases} \tag{4.35}$$

The parameters u_0, ω_0 and w_{EI} can be expressed by substituting equations (4.30) to (4.33) into above equation and letting $\lambda_{EI} = \frac{S_{13EI}}{S_{11EI}}$:

$$\begin{cases} u_0 = -2S_{11P1}Lb_{P1} + g_{311}Ll \\ \omega_0 = 6S_{11P1}La_{P1} \\ W_{EI} = 3(\lambda_{EI}h_{2I-1}^2 + L^2)S_{11P1}a_{P1} - 2\lambda_{EI}S_{11P1}h_{2I-1}b_{P1} + \lambda_{EI}g_{311}h_{2I-1}l \end{cases} \tag{4.36}$$

The rest of the unknowns can be determined from (4.20) and (4.21).

$$
\begin{cases}
w_{Ek} = W_{EI} + 3\big(H_{2,k-1} - H_{2,I-1}\big)a_{P1} + 2\big(H_{1,k-1} - H_{1,I-1}\big)b_{P1} + \\
\qquad\qquad \big(\widetilde{H}_{1,k-1} - \widetilde{H}_{1,I-1}\big)l \\
w_{Pk} = w_{Ek} + 3(\lambda_{Pk} - \lambda_{Ek})h_{2k-1}^2 S_{11P1} a_{P1} - 2(\lambda_{Pk} - \lambda_{Ek})h_{2k-1}S_{11P1}b_{P1} \\
\qquad\qquad -[\lambda_{Pk}(g_{31k} - g_{311}) + \lambda_{Ek}g_{311} - g_{33k}]h_{2k-1}^l \\
\varphi_k = 3S_{11P1}(\lambda_{gk}h_{2k-1}^2 - \displaystyle\sum_{i=1}^{k-1} g_{31i}H_{P2,i})a_{P1} - 2S_{11P1}(\lambda_{gk}h_{2k-1} \\
\qquad\qquad - \displaystyle\sum_{i=1}^{k-1} g_{31i}H_{P1,i})b_{P1} + \widehat{H}_{1,k}l
\end{cases}
\tag{4.37}
$$

where:

$$
\begin{cases}
H_{1,k} = \displaystyle\sum_{i=1}^{k}\big[\lambda_{Pi}(h_{2i} - h_{2i-1}) - \lambda_{E,i+1}h_{2i} + \lambda_{Ei}h_{2i-1}\big]S_{11P1} \\
\widetilde{H}_{1,k} = \displaystyle\sum_{i=1}^{k}\{(h_{2i} - h_{2i-1})[\lambda_{Pi}(g_{31i} - g_{331}) - g_{33k}] + \lambda_{E,i+1}h_{2i}g_{311} \\
\qquad\qquad - \lambda_{Ei}h_{2i-1}g_{311}\} \\
\widehat{H}_{1,k} = \displaystyle\sum_{i=1}^{k-1}\big[g_{31i}(g_{31i} - g_{311})H_{P1,i} + \beta_{33k}(h_{2i} - h_{2i-1})\big] \\
\qquad\qquad -[\lambda_{gk}(g_{31k} - g_{311}) + \beta_{33k}]h_{2k-1} \\
H_{2,k} = \displaystyle\sum_{i=1}^{k}\big[-\lambda_{Pi}(h_{2i}^2 - h_{2i-1}^2) + \lambda_{E,i+1}h_{2i}^2 - \lambda_{Ei}h_{2i-1}^2\big]S_{11P1}
\end{cases}
\tag{4.38}
$$

$$
\lambda_{Ek} = \frac{S_{13Ek}}{S_{11Ek}}, \lambda_{Pk} = \frac{S_{13Pk}}{S_{11Pk}}, \lambda_{gk} = \frac{g_{31k}}{S_{11Pk}}
\tag{4.39}
$$

The displacement of the free end of multimorph transducer can be calculated from equation (4.11) as:

$$
\delta = w(0,0) = W_{E1}
\tag{4.40}
$$

4.1.3 Case study - Unimorph transducer

The 2D geometrical model of unimorph is shown in Figure 4.2.
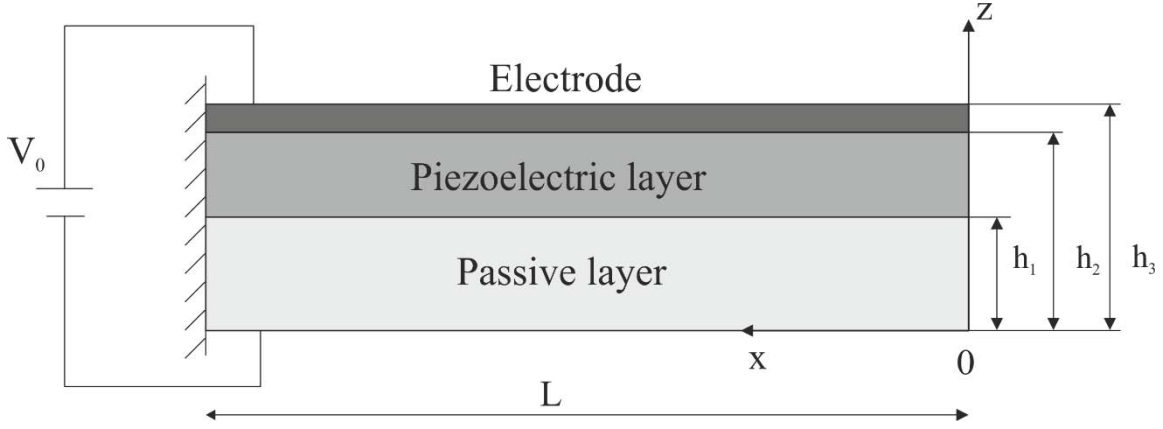
Figure 4.2 2D geometrical model of unimorph transducer

Using the solution obtained in the previous sections, and assuming $n=1$, the equations (4.25) and (4.28) can be simplified to:

$$
\begin{cases}
k_{11} = -3(h_2^2 - h_1^2)g_{311}, \quad k_{12} = 2(h_2 - h_1)g_{311}, \quad k_{13} = (h_2 - h_1)\beta_{331} \\
k_{21} = -3\left(\dfrac{h_1^2}{S_{11E1}} + \dfrac{h_3^2 - h_2^2}{S_{11E2}} + \dfrac{h_2^2 - h_1^2}{S_{11P1}}\right)S_{11P1} \\
k_{22} = 2\left(\dfrac{h_1}{S_{11E1}} + \dfrac{h_3 - h_2}{S_{11E2}} + \dfrac{h_2 - h_1}{S_{11P1}}\right)S_{11P1}, \quad k_{23} = -\left(\dfrac{h_1}{S_{11E1}} + \dfrac{h_3 - h_2}{S_{11E2}}\right)g_{311} \\
k_{31} = -2\left(\dfrac{h_1^3}{S_{11E1}} + \dfrac{h_3^3 - h_2^3}{S_{11E2}} + \dfrac{h_2^3 - h_1^3}{S_{11P1}}\right)S_{11P1}, \quad\quad k_{32} = -\dfrac{k_{21}}{3} \\
\qquad\qquad k_{33} = -\dfrac{1}{2}\left(\dfrac{h_1^2}{S_{11E1}} + \dfrac{h_3^2 - h_2^2}{S_{11E2}}\right)g_{311}
\end{cases}
\quad (4.41)
$$

From equation (4.29) the parameters a_{P1}, b_{P1}, and l can be calculated. Using (4.30) and (4.32) a_{E1}, a_{E2}, b_{E1} and b_{E2} can be written as follows:

$$
\begin{cases}
a_{E1} = \dfrac{S_{11P1}}{S_{11E1}}a_{P1}, \quad b_{E1} = \dfrac{S_{11P1}}{S_{11E1}}b_{P1} - \dfrac{g_{311}}{2S_{11E1}}l \\
a_{E2} = \dfrac{S_{11P1}}{S_{11E2}}a_{P1}, \quad b_{E2} = \dfrac{S_{11P1}}{S_{11E2}}b_{P1} - \dfrac{g_{311}}{2S_{11E2}}l
\end{cases}
\quad (4.42)
$$

Thanks to geometrical restraint conditions: $u(L, h_1) = w(L, h_1) = \dfrac{\partial w(L, h_1)}{\partial x} = 0$ the following equations are obtained:

$$\begin{cases} \omega_0 = 6S_{11P1}La_{P1} \\ u_0 = -2S_{11P1}Lb_{P1} + g_{311}Ll \\ w_{E1} = 3(\lambda_{E1}h_1^2 + L^2)S_{11P1}a_{P1} - 2\lambda_{E1}S_{11P1}h_1b_{P1} + \lambda_{E1}g_{311}h_1l \end{cases} \tag{4.43}$$

Finally, the parameters w_{E2}, w_{P1} and φ_1 are calculated as:

$$\begin{cases} w_{E2} = 3[(\lambda_{E2}h_2^2a_{P1} + L^2)S_{11P1} - (h_2^2 - h_1^2)S_{13P1}]a_{P1} \\ -2[\lambda_{E2}h_2S_{11P1} - (h_2 - h_1)S_{13P1}]b_{P1} + [\lambda_{E2}g_{311}h_2 + g_{331}(h_2 - h_1)]l \\ w_{P1} = 3(L^2S_{11P1} + h_1^2S_{13P1})a_{P1} - 2S_{13P1}h_1b_{P1} + g_{331}h_1l \\ \varphi_1 = 3a_{P1}g_{311}h_1^2 - 2b_{P1}g_{311}h_1 - \beta_{331}lh_1 \end{cases} \tag{4.44}$$

For the purpose of visualization, the static deformation (deflection) at the free end of the unimorph transducer is calculated using the above equations. The effect of change in active length l_1, the thickness of passive layer h_p and the thickness of active layer h_a, on the static deformation is demonstrated. The h_p dimension corresponds to h_1, while h_a is equal to $h_2 - h_1$. The thickness of electrode is equal to $h_3 - h_2 - h_1 = 0.001$ mm.

The passive layer material is brass with Young's modulus $E = 10.5 \cdot 10^{10}$ Pa and Poisson ratio $v = 0.3$. The electrode is made of aluminum with Young's modulus $E = 7 \cdot 10^{10}$ Pa and Poisson ratio $v = 0.35$. The active layer material is P1-89 and PZT-401 ceramics and their material properties are given in Table 5.2. The coefficients S_{ij} for elastic and electrode layer are obtained using expressions $S_{11} = \frac{1}{E}$ and $S_{13} = -\frac{v}{E}$. The piezoelectric and dielectric impermeability g_{ij} and β_{ij} are calculated using expressions $\boldsymbol{g} = \boldsymbol{\beta}^T \cdot \boldsymbol{d}$ and $\boldsymbol{\beta} = 1/\boldsymbol{\varepsilon}$.

The transducer is supplied with voltage $V_0 = 200$ V. The elastic brass layer serves as a bottom electrode. The effect of the mass of the indentation hemisphere is included as additional bending torque M_0 acting on the free end of the transducer. The value of the M_0 is calculated based on the gravitational force generated by the mass of the steel hemisphere.

The results of the analytical calculation are presented in Figure 4.3, Figure 4.4 and Figure 4.5, showing the change in active length l_1, the thickness of passive layer h_p and the thickness of active layer h_a, respectively, and their effect on the static deformation. The change of l_1 parameter is calculated for h_a=1.99 mm and $h_p = 3$ mm. The h_p is calculated for l_1=0.1 m and h_a=1.99 mm. Finally, the h_a contribution is calculated for l_1=0.1 m and $h_p = 3$ mm.
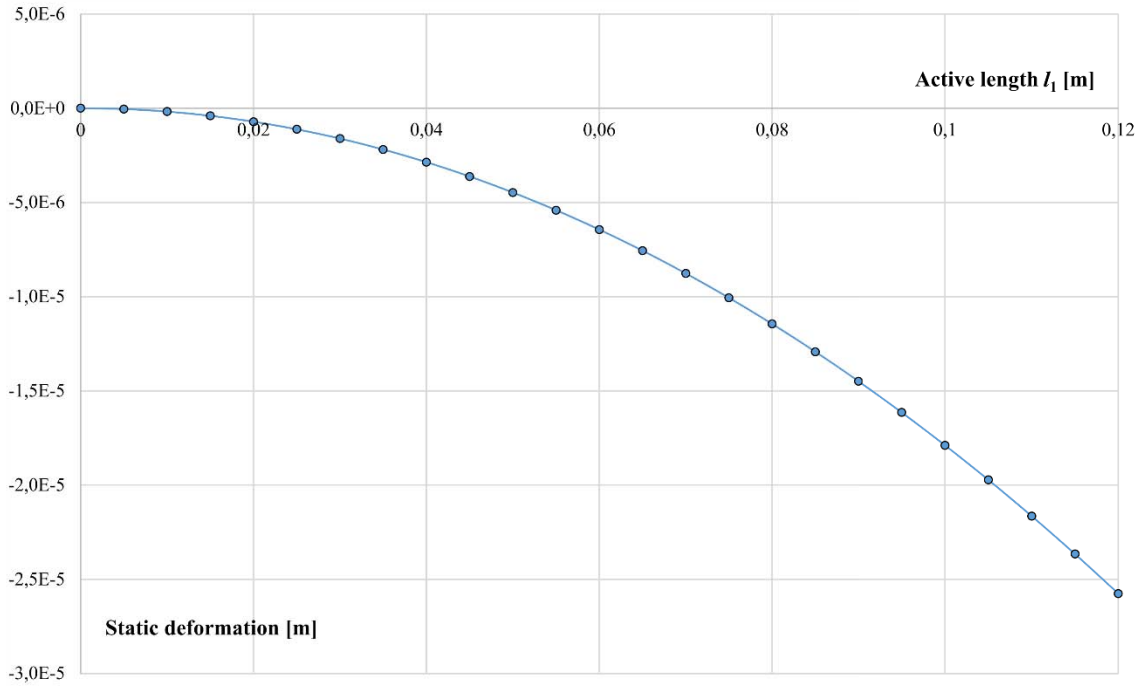
Figure 4.3 Static deformation at the free end of unimorph transducer vs. the active length l_1
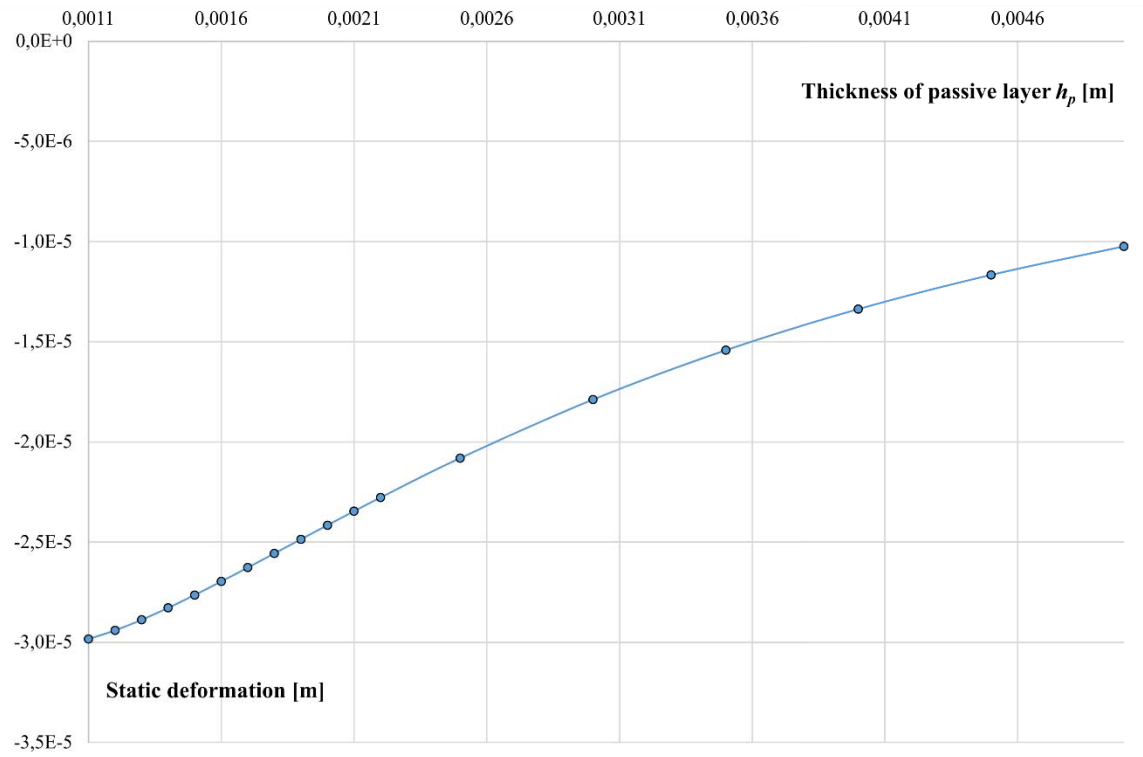

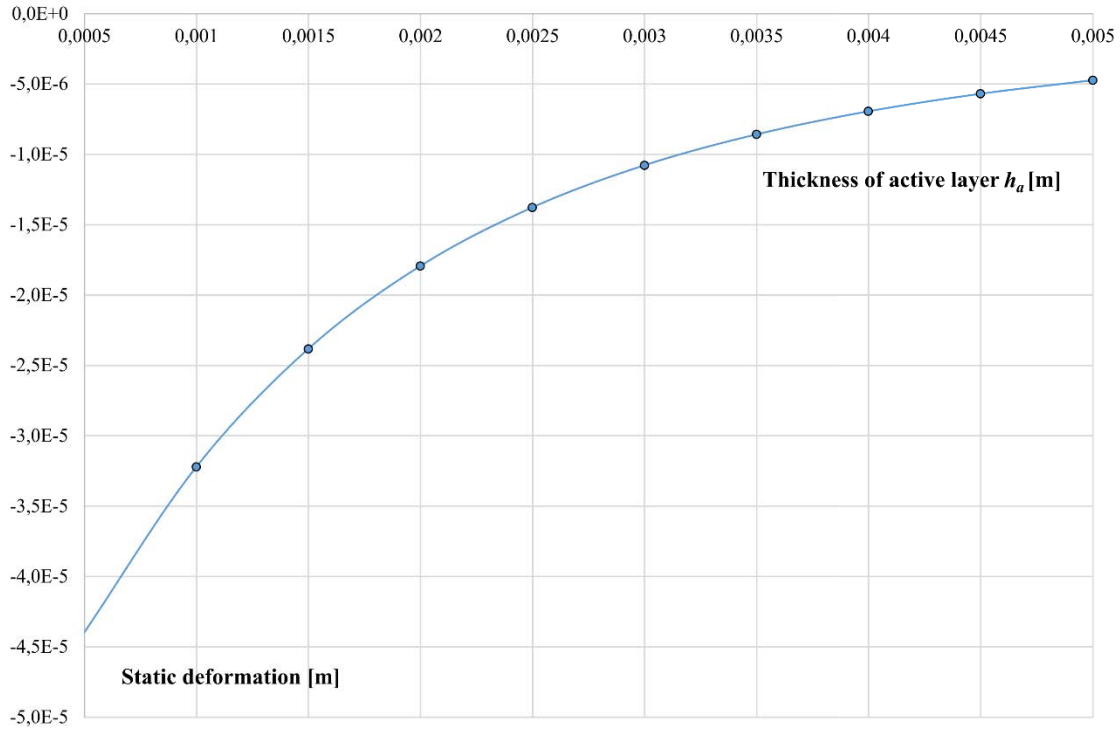Figure 4.4 Static deformation at the free end of unimorph transducer vs. the thickness of passive layer h_p

Figure 4.5 Static deformation at the free end of unimorph transducer vs. the thickness of active layer h_a

4.2 Equivalent circuit representation

The dynamic behavior of unimorph transducer can be described in an unified approach due to analogous relationships between electrical and mechanical quantities describing devices utilizing piezoelectric phenomenon. The theories of electricity and mechanics are based on similar differential equations. This fact becomes evident when using equivalent electrical circuits to model the electro-mechanical systems. The parameters describing electric and mechanical quantities can be treated in a similar way. The electric formulation involves the description of the electric circuits based on voltage and electric current. The mechanical formulation is the same when treated with force and velocity, respectively. Some further analogies are shown in Table 4.1.

Table 4.1 Analogies between electrical and mechanical quantities

Electrical quantities	Mechanical quantities
Voltage V [V]	Force F [N]
Current I [A]	Speed of vibration $\dot{u}$ [$m.s^{-1}$]
Electric charge q [C]	Displacement u [m]
Capacitance C [F]	Elasticity e [$m.N^{-1}$]
Inductance L [H]	Mass m [kg]
Resistance R [Ω]	Damping c [$N.s.m^{-1}$]

Those relations are presented in the unified form in terms of the Mason equivalent circuit, and then simplified to a circuit valid for one resonance frequency of the transducer.

4.2.1 Mason equivalent circuit

As has been noted in previous section, the piezoelectric ceramics exhibit coupled electrical and mechanical properties. W. P. Mason developed an equivalent circuit model, where those properties are coupled only through an ideal transformer [38], [69]. The circuit consists of an electrical port, connected to the center node of the two mechanical (acoustic) ports representing the front and back face of the transducer. On the electrical side of the transformer the voltage is related to the current via $V = ZI$, where Z is an electrical impedance. On the acoustical side of the transformer the force F and the velocity v are related through $F = Z_0 v$, where Z_0 is the specific acoustic impedance.
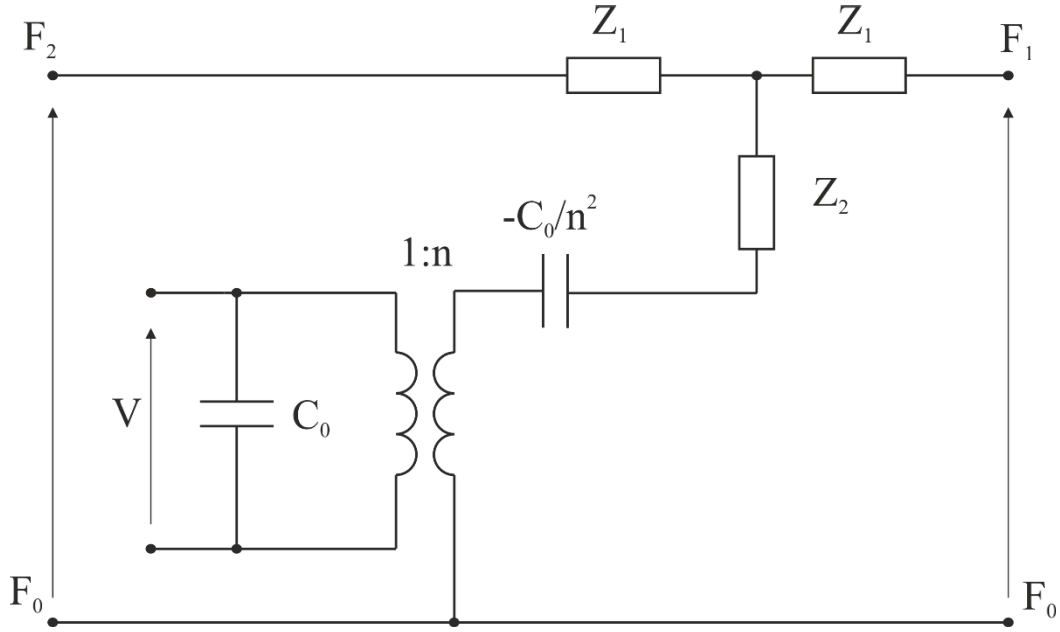
Figure 4.6 Mason's equivalent circuit for a piezoelectric plate

The mechanical impedances of the circuit shown in Figure 4.6 are given by:

$$Z_1 = jZ_0 \tan\left(\frac{\omega l_c}{2v_c}\right) \tag{4.45}$$

$$Z_2 = -\frac{jZ_0}{\sin\left(\frac{\omega l_c}{v_c}\right)} \tag{4.46}$$

where: v_c is the wave propagation velocity in the piezoelectric medium in *m/s*; l_c is the thickness of the piezoelectric ceramic in *m*; $\omega = 2\pi f$ is the angular frequency in *rad/s* and *f*, frequency, given in *Hz*; $Z_0 = \rho v_c A_c$ – is the acoustic impedance of the ceramic in *kg/s*, and A_c is the area of the flat surface of the ceramics in m^2.

The electromechanical transformer ratio *n* is formulated as:

$$n = h_{33} C_0 \tag{4.47}$$

where: $C_0 = (\varepsilon_{33}^S A_c)/l_c$ is the capacitance of the piezoelectric ceramic for zero strain in *F* and h_{33} is the piezoelectric coefficient in *N/C*.

When the piezoelectric plate is unloaded on both of its faces, two acoustic ports of Mason circuit are shorted, i.e. $F_1=F_2=0$. In this case the input electrical impedance of the plate can be obtained:

$$Z = \frac{1}{j\omega C_0}\left[1 - \frac{k_t^2 \tan\left(\frac{\omega l_c}{2v_c}\right)}{\frac{\omega l_c}{2v_c}}\right] \quad\quad (4.48)$$

From the above equation, the resonance and anti-resonance frequency equations can be obtained (in the condition of thickness polling and no external loads present). When Z=0, the resonance frequency equation is:

$$1 - \frac{k_t^2 \tan\left(\frac{\omega l_c}{2v_c}\right)}{\frac{\omega l_c}{2v_c}} = 0 \quad\quad (4.49)$$

When $Z = \infty$, the anti-resonance frequency is calculated from:

$$\tan\left(\frac{\omega l_c}{2v_c}\right) = \infty \quad\quad (4.50)$$

4.2.2 Simplified equivalent circuit

Considering piezoelectric transducer working near its mechanical resonance frequency it is possible to reduce the circuit presented in Figure 4.6 to a series RLC circuit presented in Figure 4.7. Thanks to this representation, it is possible to describe and quantify the material properties of the tested sample, and the actuator itself. The simplified equivalent circuit of the piezoelectric actuator in the resonance mode is shown in the Figure 4.7.

This representation of the electromechanical coupling uses an ideal transformer with the transformation ratio 1/N, establishing a correspondence between electrical variables (voltage V_v, current i_v) and mechanical (force f_v, velocity of vibration $\dot{u}_v$). It consists of two parallel branches around the resonance mode considered.
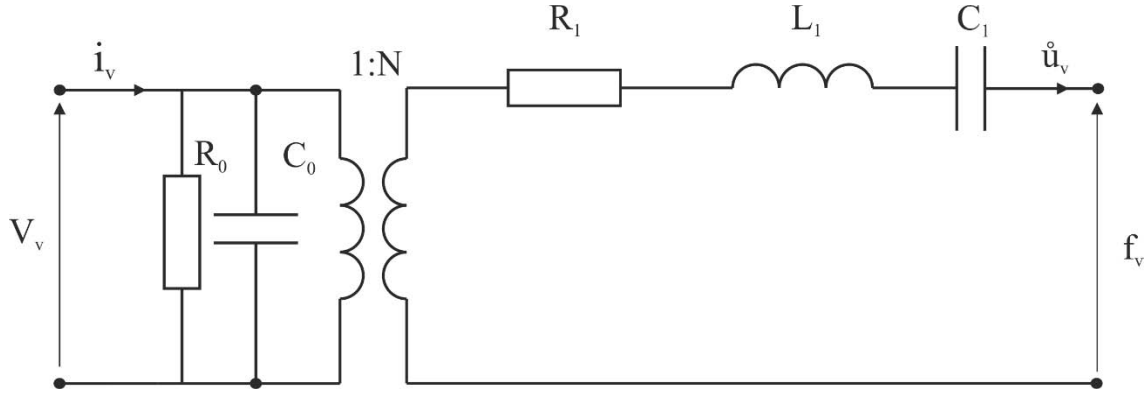
Figure 4.7 Equivalent circuit for piezoelectric transducer working in transversal coupling near the resonance frequency

At the primary side of the transformer, there is a static branch describing purely dielectric properties of the transducer. At base frequency, far from the resonance, electrical impedance of the transducer is directly determined by the elements of this branch. It consists of the C_0 capacity (defined at constant strain) and a resistance R_0 modelling the dielectric losses.

The secondary side of the transformer, called dynamic branch, reflects the elasto-dynamic properties of the medium. The current flowing to the secondary side being analogous to a speed $\dot{u}_V$, the vibrating mass is equivalent to an inductance L_1, capacitance C_1 models elasticity and resistance R_1 - viscous losses. The equivalent diagram shows two oscillating circuits, one corresponding to the series circuit of the dynamic branch and the other to the parallel circuit formed by the combination of the two branches.

Corresponding series (ω_s) and parallel (ω_p) resonance pulsations are thus defined by:

$$\omega_s = 1/\sqrt{L_1 C_1} \tag{4.51}$$

$$\omega_p = 1/\sqrt{L_1(C_1 C_0)/(C_1 + C_0)} \tag{4.52}$$

The admittance of the motional branch R_1, L_1, C_1 in the Nyquist plane is a circle with radius $1/2R_1$ and center in the point ($1/2R_1$, 0), as shown in Figure 4.8.
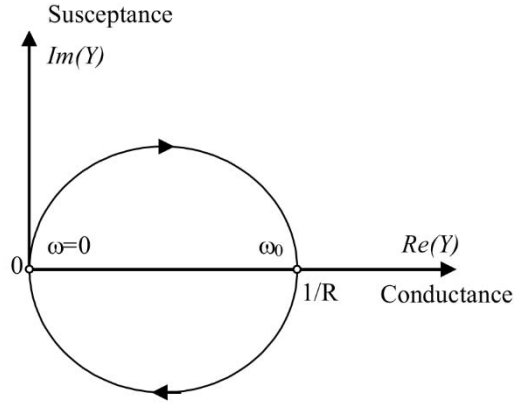
Figure 4.8 Dynamic admittance in the Nyquist plane

Adding the R_0 , then C_0 static branch allows to arrive at the diagram (Figure 4.9) representing the complete equivalent circuit.
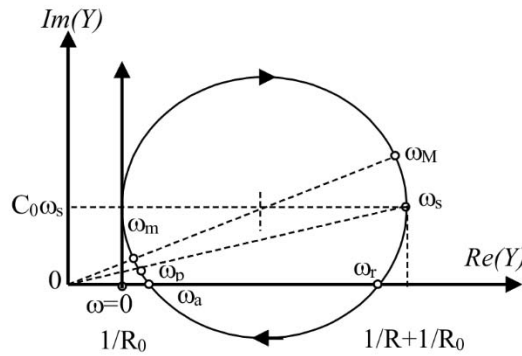
Figure 4.9 Admittance of the equivalent circuit in the Nyquist plane

If the quality factor Q (gain between displacement at resonance and very low frequency) of the dynamic branch is large enough ($Q \gg 10$), the series and parallel pulsations can be written as:

$$\omega_s = \frac{\omega_M + \omega_r}{2} \ and \ \omega_p = \frac{\omega_m + \omega_a}{2} \tag{4.53}$$

where:

$$Q = \frac{L_1 \omega_s}{R_1} = \frac{1}{R_1 C_1 \omega_s} = \frac{1}{R_1}\sqrt{\frac{L_1}{C_1}} \tag{4.54}$$

78

The admittance obtained through the signal or impedance analyzer, enables the calculation of all parameters of the equivalent circuit [35]:

$$R_0 = \frac{1}{Re\left(\underline{Y}(\omega)\right)} \quad for \ \omega \ll \omega_s \tag{4.55}$$

$$\frac{1}{R_1} = Re\left(\underline{Y}(\omega_s)\right) - \frac{1}{R_0} \tag{4.56}$$

$$C_0 = \frac{Im\left(\underline{Y}(\omega_s)\right)}{\omega_s} \tag{4.57}$$

$$C_1 = C_0 \frac{\left(\omega_p^2 - \omega_s^2\right)}{\omega_s^2} \tag{4.58}$$

$$L_1 = \frac{1}{C_0 \cdot \left(\omega_p^2 - \omega_s^2\right)} \tag{4.59}$$

In this thesis, it is essential to quantify the mechanical properties of the actuator (and material to characterize). The equivalent circuit of the transducer in contact with the tested material is shown in Figure 4.10. To do this, it is crucial to calculate the electromechanical transformation ratio $1/N$. Consequently, the dynamic branch can be expressed as follows:

$$s = C_1/N^2 \tag{4.60}$$

$$l = L_1 \cdot N^2 \tag{4.61}$$

$$r = R_1 \cdot N^2 \tag{4.62}$$

$$N = (1/R_1) \cdot (\dot{u}/V)^{-1} \tag{4.63}$$

where: s – compliance, l – vibrating mass and r – dissipation connected with viscosity.
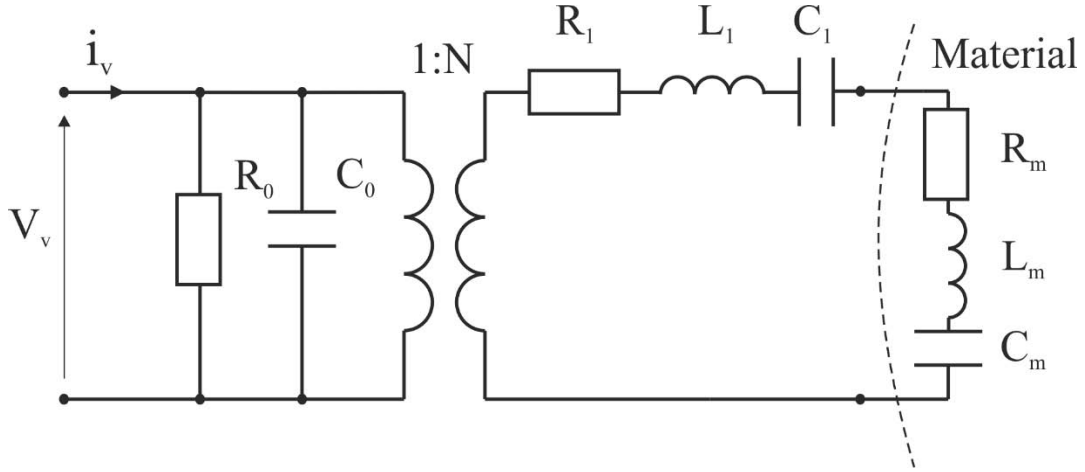
Figure 4.10 Simplified equivalent circuit for piezoelectric resonant actuator in contact with tested material (this circuit is valid only near resonance frequency considered)

Vibrational speed $\dot{u}$ can be obtained by means of laser interferometry for a given supply voltage V and the frequency of mechanical resonance of the actuator. Consequently, to estimate mechanical properties of tested samples it is necessary to compare the simplified circuit parameters for the unloaded piezoelectric actuator and the actuator in contact with the material.

$$\frac{1}{C_M} = \frac{1}{C_{TOT}} - \frac{1}{C_1}$$
(4.64)

where :　　　　C_M – material capacitance,

　　　　　　　C_{TOT} – total capacitance (transducer in contact with the material),

　　　　　　　C_1 – capacitance of the dynamic branch of the transducer.

4.3 Analysis of contact between sphere and surface

Unimorph piezoelectric transducer is equipped with a spherical rigid probe – the indentation device. Such a design grants a way of verification of the contact conditions between the spherical probe and the tested material, based on the classic Hertz contact mechanics theorem. The considerations presented in this section were developed by Heinrich Hertz in the end of nineteenth century. The theory focused on the analysis and behavior of elastic contact ensured by a normal load. It defined the contact area between two solids, pressure and stress distribution in the interior of solids. On the other hand, Hertz theory did not take into account the roughness of surfaces and assumes that one takes a macroscopic scale of the contact. The contact area is denoted by a, relative radius of curvature by R, the radii of each solid are R_1 and

80

R_2 and the significant dimension of solids is l. Taking into account those designations, the laws presented in this sections are valid if the following assumptions are satisfied:

- the surfaces of solids are continuous and non-conforming: $a \ll R$,
- strains are low $a \ll R$,
- each solid is considered as an elastic half-space: $a \ll R_{1,2}$, $a \ll l$,
- the surfaces are frictionless at the interface (contact plane) [26].

Describing the indentation of a flat surface, the radius R_1 can be assumed as infinite which satisfies the $a \ll R_1$ condition. The resulting contact area a is small compared with the dimensions of the tested sample as well as the indenter. The indentation device considered is made of steel. It is used within its elastic limits, therefore satisfy the above requirements. The piezoelectric bending transducer, whose amplified deflections are below 1 *mm*, also satisfies the small strains condition. In the next section, as an effect of normal load, the contact of indentation device (half-sphere) with the test sample (plane) is considered in more details using on the Hertz theory.

4.3.1 Normal force loading

Knowing the normal force acting on an elastic surface, as well as the properties of the spherical indenter, it is possible to assess the Young modulus of the elastic material as well as the stiffness of the contact [64]. The classical problem of the normal contact between a rigid sphere and an elastic half-space is represented symbolically in the Figure 4.11.
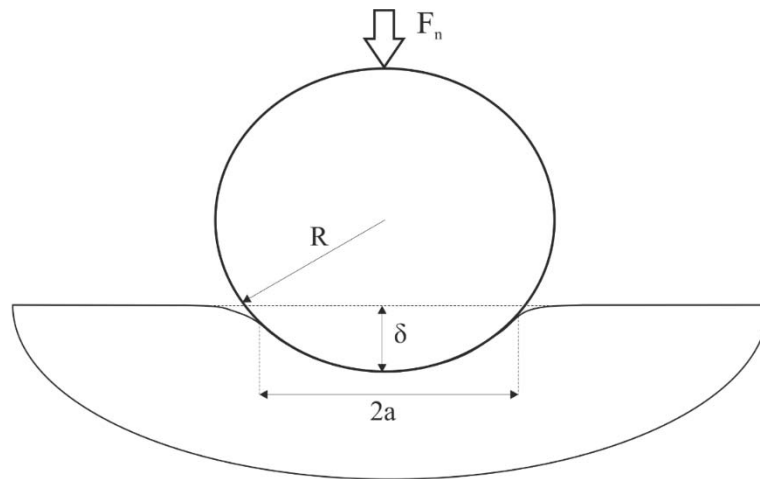
Figure 4.11 Schematic view of rigid sphere in contact with elastic surface, where a – radius of the contact area; δ – penetration depth, R – radius of the sphere; F_n – normal force acting on the sphere

For the hertzian contact of sphere and plane, the contact area is circular, with the radius a described as:

$$a = \sqrt[3]{\frac{3F_n R}{4E^*}} = \frac{\pi p_0 R}{2E^*} \qquad (4.65)$$

The distribution of pressure at contact surface can be described as:

$$p = p_0 \sqrt{1 - \left(\frac{r}{a}\right)^2} \qquad (4.66)$$

The maximum pressure in the center of the contact area p_0 can be expressed as a function of the normal force F_n:

$$p_0 = \sqrt[3]{\frac{6F_n E^{*2}}{\pi^3 R^2}} \qquad (4.67)$$

The penetration depth δ_N is given by:

$$\delta_N = \frac{a^2}{R} = \sqrt[3]{\frac{\frac{9}{16}F_n^2}{RE^{*2}}} \qquad (4.68)$$

where: F_N – normal component of the force applied to the surface; R – radius of the sphere; E^* - reduced Young modulus.

The pressure distribution for a contact between rigid steel sphere and elastic plane is demonstrated in the Figure 4.12. The sphere has a radius $R = 5$ mm. The value of E^* is estimated in the paragraph 4.3.2. The graph in Figure 4.12 was obtained for normal force $F_n = 0.1$ N and 1 N.
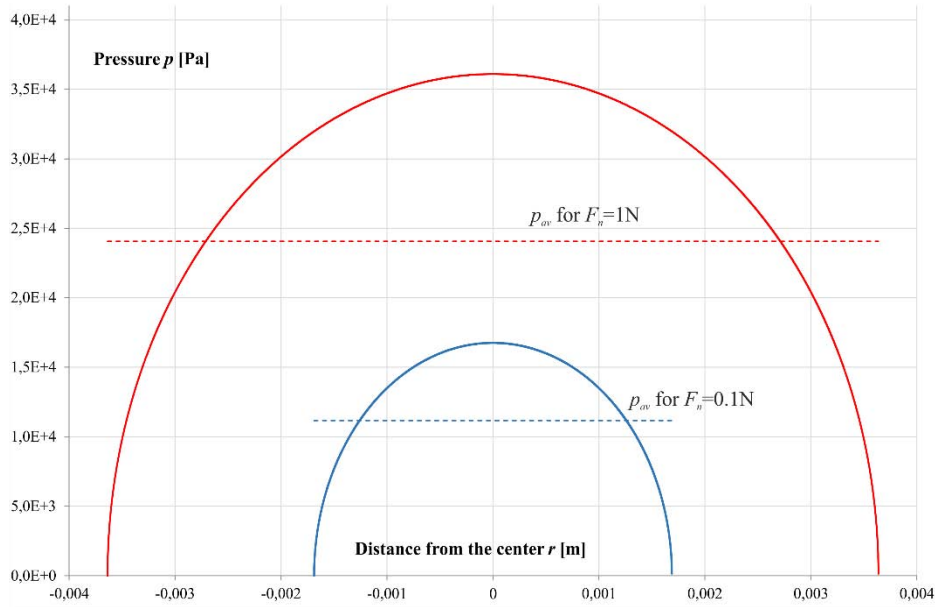
Figure 4.12 Distribution of pressure for sphere/surface contact for two normal forces: 0.1 N (blue trace) and 1 N (red trace); the average pressure levels are marked by dashed lines

From the graph (Figure 4.12) it can be observed that multiplication of normal force F_n by 10 gives approximately two times higher average pressure p_{av} and contact radius a. Furthermore, the surface of the contact is proportional to normal force applied: $S_{contact} \sim F_n$ and the average pressure is varying in accordance to: $p_{av} \sim \sqrt[3]{F_n}$ [32].

Knowing the normal force F_n and the depth of penetration δ, it is possible to calculate the stiffness of the contact. The Young modulus of the material in contact with the transducer can be calculated using a reduced Young's modulus E^* [8]:

$$\frac{1}{E^*} = \frac{1 - v_1^2}{E_1} + \frac{1 + v_2^2}{E_2} \tag{4.69}$$

where: v_1, v_2 – Poisson coefficients of sphere and material, respectively; E_1, E_2 – Young modules of sphere and material, respectively.

4.3.2 Depth of indentation / force relation

A piezoelectric actuator can be considered as an actuator of imposed displacement by its high stress factor, especially considering the relatively low level of mechanical properties of the skin/soft tissue in contact with the transducer.

Thanks to the Hertzian contact theory briefly presented in the previous section, the relationship between applied force and indentation depth can be discussed. From equations (4.68) and (4.69), we can see that the depth of the indentation depends on the radius of the sphere, its material properties, but also on the mechanical properties of the tested materials. To estimate the value of the deformation of the piezoelectric transducer in contact with the material, it is necessary to evaluate the Young's modulus and Poisson's ratio of the human skin. In the literature, the value of Young's modulus of the skin, tested in vivo, varies between 10 *kPa* (during torsion test) to 50 *MPa* (during suction test). With regards to the Poisson's coefficient, some research works report *v* equal to 0.48. This means that the skin is not completely incompressible. Nevertheless, it depends on the subject, and the region of the body [8].
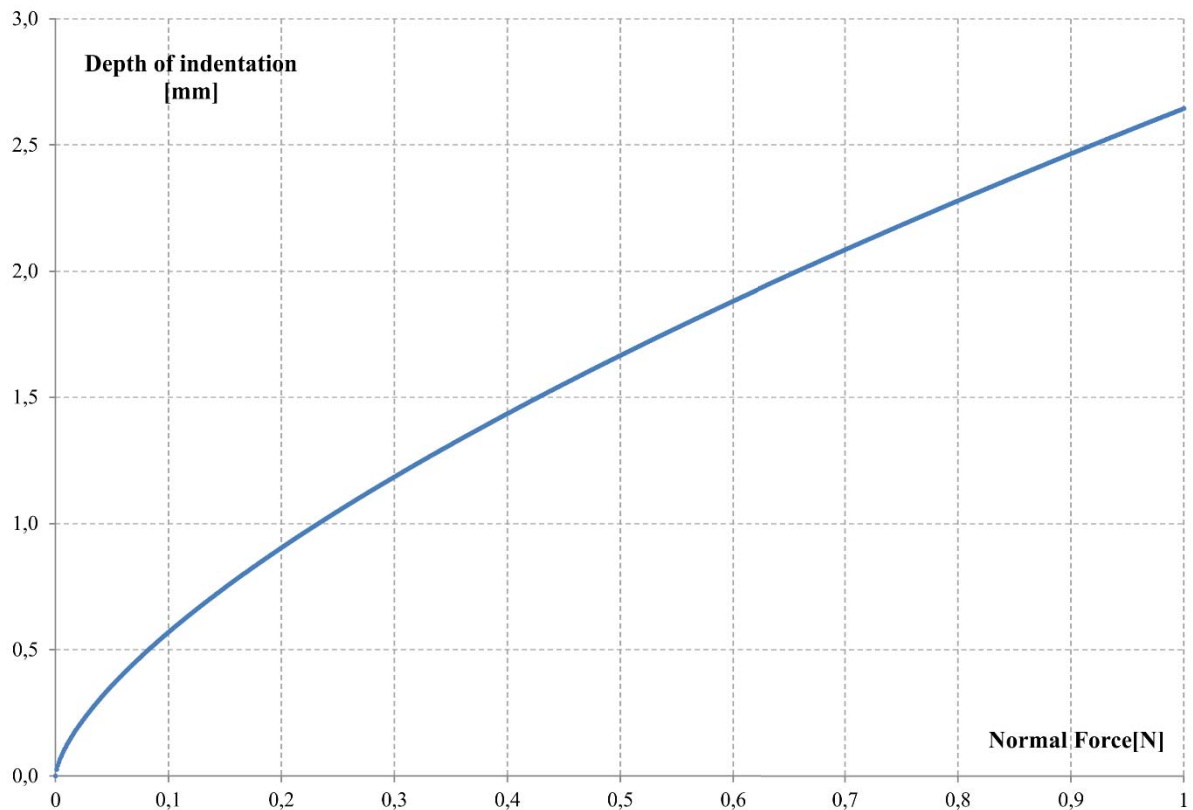
Figure 4.13 Theoretical relation between the depth of indentation of the tissue and the applied force

In conclusion, it is possible to determine the indentation depth necessary for the piezoelectric actuator, based on the Hertz contact theory and evaluation of the material properties. Example of such relationship is shown in the Figure 4.13. The Young's modulus of

the soft material is estimated to $E = 60\ kPa$ and Poisson's ratio v equal to 0.48. For comparison purposes, the same relationship obtained experimentally is presented for six polymer samples (marked on the Figure 4.14 as: A, B, C, D, E and F).
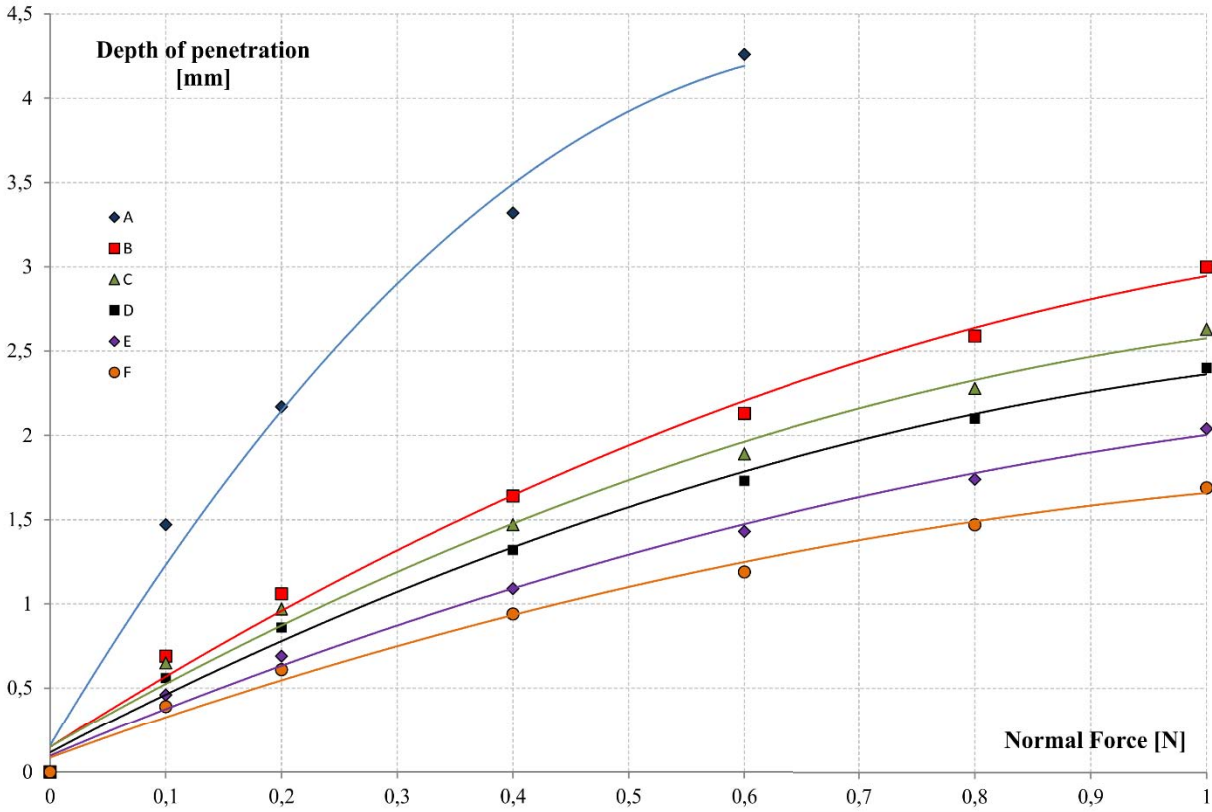
Figure 4.14 Experimental relation between depth of indentation and the applied normal force obtained for group of six polymers

4.3.3 Tangential force loading

When a tangential force F_T is applied on one of the solids in contact, a shear stress distribution $q(x, y)$ appears on the contact area:

$$q(r) = q_0 \sqrt{1 - \frac{r^2}{a^2}} \tag{4.70}$$

where: q_0 is average shear stress and r is polar coordinate:

$$q_0 = \frac{F_T}{2\pi a^2} \tag{4.71}$$

$$r^2 = x^2 + y^2 \tag{4.72}$$

If both solids in contact are elastic, the total displacement is proportional to the tangential force F_T and can be formulated as:

$$\delta_t = \left(\frac{2 - v_1}{G_1} + \frac{2 - v_2}{G_2} \right) \frac{F_T}{8a} \tag{4.73}$$

Moreover, the distribution of shear stress $q(x, y)$ is proportional to the distribution of normal pressure $p(x, y)$:

$$q(r) = \mu \cdot p(r) = \mu p_0 \sqrt{1 - \frac{r^2}{a^2}} \tag{4.74}$$

where μ is the friction coefficient described by Coulomb's law, which can be discretized by the Amontons principle:

$$\mu(x, y) = \left| \frac{q(x, y)}{p(x, y)} \right| = const \tag{4.75}$$

4.3.4 Quasi-static friction coefficient

We define a local friction coefficient μ_{local}, which is constant and depends on the mechanical properties of materials (local approach to friction according to the principle of Coulomb and Amontons). We also define a macroscopic coefficient of friction $\mu(t)$ which depends on the dynamic imposed on the contact and which evolves in time. The evolution of $\mu(t)$ is explained in the following paragraphs.

$$\mu_{local} = \left|\frac{q(x,y,t)}{p(x,y,t)}\right| = const \tag{4.76}$$

$$\mu(t) = \left|\frac{F_T}{F_N}\right| \tag{4.77}$$

When two solids in contact are subjected to a tangential force F_T which is lower than the normal force F_N multiplied by the coefficient of friction μ ($F_T < \mu \cdot F_N$), no macroscopic slippage is present ($\delta = 0$). The contact is static. However when loading by the tangential force F_T, micro-slippage occurs on the periphery of the contact. In the center, the solids are deformed without relative movement and adhere to each other (stick). The phenomenon of partial slippage is presented in the work of R.D. Mindlin [48] which explains the nonlinear behavior of the friction coefficient.

The moment when slip between two solids is created, is referred to as quasi-static contact (initial sliding). The case considered, a sphere/plane contact submitted to a tangential displacement δ, is presented in Figure 4.15. The system goes from a static state to a dynamic state through a transition phase (preliminary displacements) where adhesion and sliding areas coexists. Pressed together, the two surfaces are subjected to a pressure field $p(x, y, t)$ calculated according to the Hertz theory. This forms a circular contact area of radius a. A very low relative tangential displacement δ between these two solids results in the creation of a shear field $q(x, y, t)$ on the inside of the contact area. Expression of the shear field for adhesion or sliding is given by the relationships:

- Total slip:

$$q'(x,y) = -sign(\delta) \cdot \mu \cdot p_0 \cdot \sqrt{1 - \frac{x^2 + y^2}{a^2}} \qquad (4.78)$$

- Total stick:

$$q''(x,y) = -sign(\delta) \cdot \frac{p_0}{\sqrt{a^2 - x^2 - y^2}} \qquad (4.79)$$

The sign of the shear field is opposing the sign of the applied displacement δ. A total adhesion over the entire contact area implies infinite constraints on the periphery of the contact $(q(r = a) \to \infty)$ which is physically impossible. Micro-slippage appears in areas, where the local effective shear stress is greater or equal to the shear strain limit σ i.e. $q(x,y,t) \geq \mu.p\,(x,y,t)$. Thus there are two zones:

- an adhesion area (stick area): circular central area where there is no relative movement between the surfaces. The tangential stress q satisfies the relationship: $q(x,y,t) = q'' \leq \mu p(x,y,t) < \sigma$,
- slip area: exterior, ring-shaped area where the micro-slippage appears and the tangential stress q satisfies the relationship: $q(x,y,t) = q' = \mu p(x,y,t) > \sigma$.
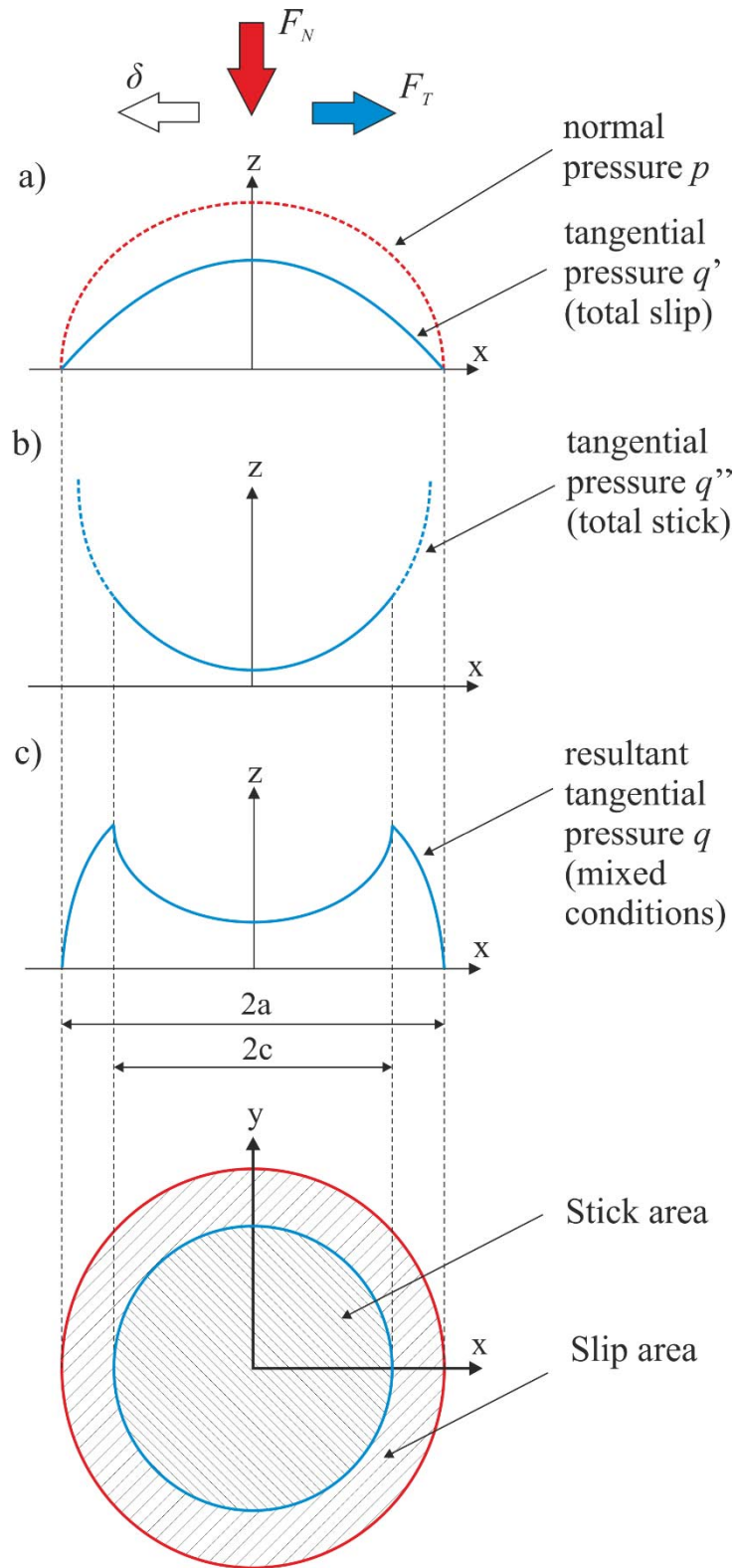
Figure 4.15 Pressure distribution for sphere/plane contact

The shear stress is different depending on the position in the contact area. The typical pressure distribution is shown in Figure 4.15. It results from the superposition of the different pressures and reaches a maximum at the transition from adhesion (stick) to slip zone. This position does not coincide with the maximum normal pressure p_0 which is at the center of the contact. The outcome of the tangential force load F_T can be described by integration over the surface of the contact:

$$F_T(t) = \int_S q(x, y, t) dx dy \qquad (4.80)$$

Although a relative motion exists, the points at contacting surfaces do not move with respect to each other. It's due to elastic accommodation of materials, which ensures that deformation (few micrometers). As soon as contact is deformed plastically, the distance between centers of each solid d is: $d > \delta_t$, the nature of the system becomes dynamic. The material points move against each other and the total slip is maintained. When the normal load F_N is kept constant and the displacement $\delta(t)$ begins, tangential effort F_T increases up to an asymptote $F_{T\infty}$. The point where $F_T = F_{T\infty}$ is called transition displacement δ_t. The F_T evolution is symmetrical with respect to displacement. In Figure 4.16 the evolution of F_T as a function of δ is shown. Three zones can be distinguished:

- For small displacements $\delta \ll \delta_t$, the response of tangential effort is linear. The stiffness of the contact is the proportionality coefficient:

$$F_T(t) = C \cdot \delta \qquad (4.81)$$

$$C = \frac{8a}{\dfrac{2 - \nu_1}{G_1} + \dfrac{2 - \nu_2}{G_2}} \qquad (4.82)$$

$$\delta_C = \frac{F_{T\infty}}{C} = \frac{\mu F_n}{8a} \cdot \left(\frac{2 - \nu_1}{G_1} + \frac{2 - \nu_2}{G_2} \right) \qquad (4.83)$$

where: C – contact stiffness, δ_C – critical slip, G_i – shear module of i solid and ν_i – Poisson coefficient of i solid. This zone is called: zero slip zone or stick zone.

It produces micro-slips, but their participation in friction is minor. The length of this zone is minimal.

- For displacements inferior to transition displacement $\delta < \delta_t$ the response of tangential stress is elliptic. This zone corresponds to mixed conditions of slip. The relation between the inner radius c of the contact ring (Figure 4.15) and the displacement was calculated by [48]:

$$\delta = \frac{3}{16} \cdot \mu F_N \cdot \left(\frac{2 - v_1}{G_1} + \frac{2 - v_2}{G_2} \right) \cdot \frac{a^2 - c^2}{a^3}$$ (4.84)

The transition displacement δ_t can be calculated for $c = 0$, which gives:

$$\delta_t = \frac{3}{16} \cdot \frac{\mu F_N}{a} \cdot \left(\frac{2 - v_1}{G_1} + \frac{2 - v_2}{G_2} \right)$$ (4.85)

- For bigger displacement $\delta > \delta_t$, the response of the tangential stress is constant and does not depend on the length of the slip. This zone corresponds to a total slip between two solids.
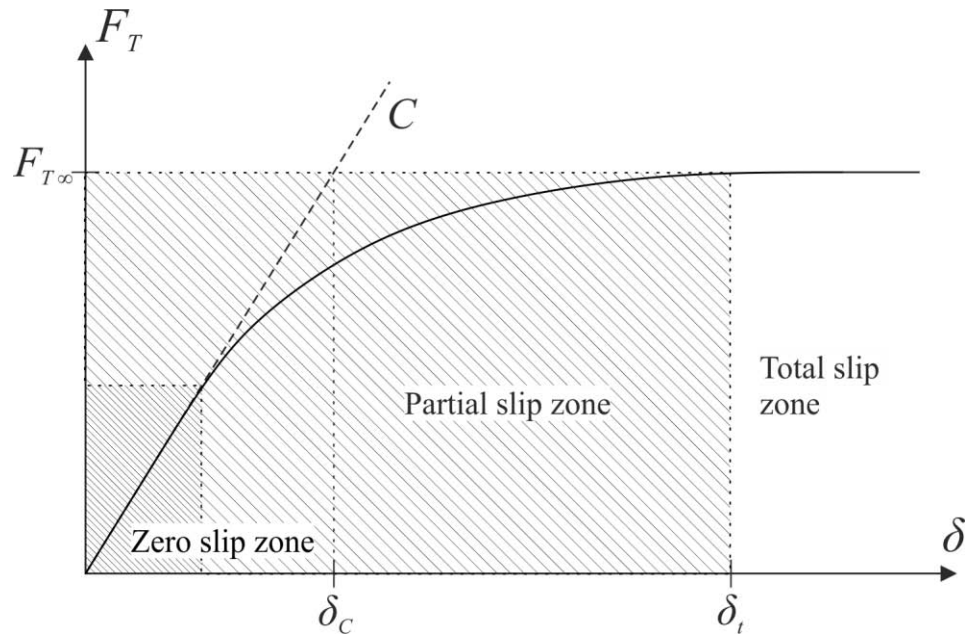
Figure 4.16 Zones of slippage in relation to the relative displacement

The solicitation, where small displacements in the order of transitional displacement δ_t (a few μm) are imposed, is called "fretting". Such conditions of solicitation are often the result of external disturbance (noise, vibration) and are the origin of numerous failures. Fretting is analyzed mostly as a harmful phenomenon, but can be favorably diverted for the reduction of friction between two surfaces. In the case of piezoelectric devices, such technique is called an electroactive lubrication [52], [53].

In the following chapter of thesis, first three working modes and associated resonance frequencies of unimorph transducer are analyzed. The first resonance corresponds to a bending movement of the unimorph. The free end of the device moves in quasi-normal way with respect to the tested sample (in approximation, considered as an elastic surface). The amplitude of those deflections is in the dozens of μm scale, proportional to the voltage supplied to the active layer (in approximation). The second working mode for the next resonance frequency corresponds to the tangential movement of the free end of unimorph transducer. The amplitude of deflection for this mode is smaller compared with the first mode. Thus, the area of operation depicted in Figure 4.16 is situated in the zero slip zone for this resonance frequency.

4.4 Conclusions

The main focus in this chapter was pointed on analytical study of the piezoelectric unimorph transducer. It had the following steps: static calculations of tip deflection, dynamic description in terms of equivalent circuits, and finally, an assessment of the contact conditions based on the Hertz theory.

The starting general case study was later simplified to one piezoelectric layer, one passive layer and electrode layer – an unimorph transducer, which is considered in the thesis. The influence of the geometric parameters on the free end deflection of the unimorph was demonstrated. Considering the two dimensional nature of the calculation, only the length of active layer l_1, the thickness of passive and active layers, h_p and h_a, respectively, were examined. This is adequate, since those parameters affect mostly the deflection of the transducer. The range of values for geometric parameters was chosen, based on the requirements for the piezoelectric transducer formulated in section 3.1 and technical limitations connected with manufacturing process. The results of static calculations of tip deflection will be compared with numerical (FEM method) static analysis results in the following chapter.

In section 4.2, the dynamic behavior of the unimorph transducer was described using analogies between electrical and mechanical quantities in the terms of equivalent circuits, i.e., classic Mason equivalent circuit. It gave the possibility of characterization of piezoelectric plate loaded by acoustic impedances at each of two faces. The electrical port was linked to the mechanical ones by ideal transformer. The general case of Mason circuit was later simplified to *RLC* circuit valid for the transducer working in the conditions of resonance, which is the case performance of the unimorph transducer. Such circuit can describe dynamics of the device for each of the resonant modes considered. The derived final circuit gave the possibility of expressing the properties of the contact with the tested material by passive components, added in series to the previous circuit. By comparative study of the equivalent circuits for unloaded unimorph, and one being in contact with the material, it is possible to assess the mechanical properties of contact such as: stiffness/compliance or viscosity.

Section 4.3 included the description of the contact between the unimorph transducer and the tested material. For both of the unimorph's geometries considered in this thesis, the indentation device was hemisphere of different radius. Considering that the tested sample was a cube of dimensions large enough, while compared with the deflection generated by the piezoelectric transducer, the contact conditions could be described by the classic mechanics theory developed by H. Hertz. A case of normal force loading was considered, including the description of contact area and pressure distribution within. Similar profiles of depth of indentation vs. normal force were obtained from the calculation as from the experimental characterization of six polymers. Tangential force loading was also considered. It leaded to the description of quasi-static friction coefficient and the definition of contact areas, where slip and stick phenomena can be observed. This concluded in the fact that piezoelectric devices, generating μm range displacement, located themselves in linear, zero-slip or partial slip zone of contact.

In the following chapter the two considered structures (geometries) of the unimorph piezoelectric transducer will be studied, using the 3D numerical approach (FEM simulation), to verify the results of the analytical study.

5 NUMERICAL (FEM) ANALYSIS

In this chapter a numerical approach to study unimorph transducer is presented. At first, 3D geometrical models of the considered unimorph transducers are developed. Next, using the Finite Element Method (FEM) analysis, the performance of the two unimorph transducer structures (called prototype "I" and prototype "II") is assessed.

5.1 Description of the parametric model

The model of a unimorph sensor/actuator with its dimensions is presented in (Figure 5.1). It is built of an active layer (piezoelectric material), a passive layer (elastic material) and an indentation device (rigid half sphere) attached to the free end of the transducer.
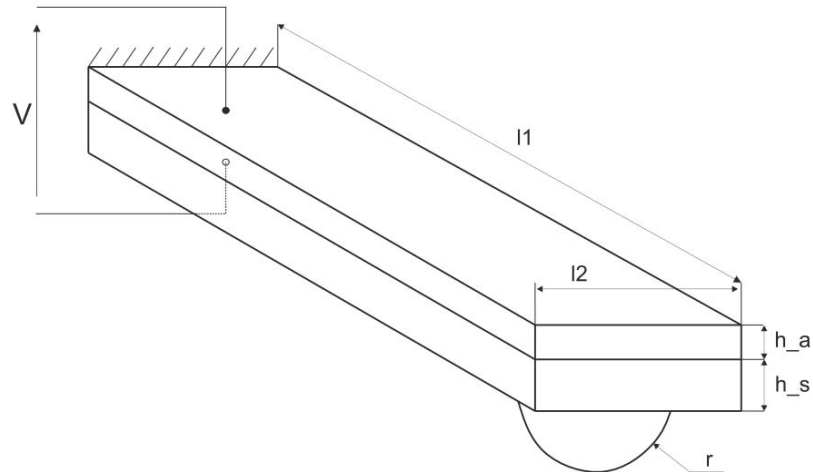
Figure 5.1 3D geometrical model of the considered unimorph transducer

The first part of the numerical model development for the unimorph transducer is based on 3D geometrical model. It was generated from a script in the APDL language (Appendix A1) as well as an Inventor CAD model imported to Workbench software [4], [3]. Having built the geometry, the three geometric parts (active layer, passive layer and the sphere) were connected (bonded) to form a suitable model for the unimorph transducer. Then, the material properties were assigned to the model. The precise description of this part is described in the next paragraph.

Finally, the model have be discretized. The accuracy of the finite element method depends on the quality of the mesh, since it is a crucial part of the calculation process. ANSYS software

has an automatic mesh generator, which can be further upgraded by manual adjustment of the mesh density. In addition, it can be controlled by defining mesh points, mesh lines or mesh surfaces which, subsequently, are used to indicate the local density of the mesh. In the case of the considered unimorph transducer, since it is a relatively simple model, it is enough to use the automatic mesh generator, with refined sizing of the active and passive layer, and also of the indentation sphere. The base of the transducer is set to the default size of finite elements. The meshed geometric model is shown in Figure 5.2.
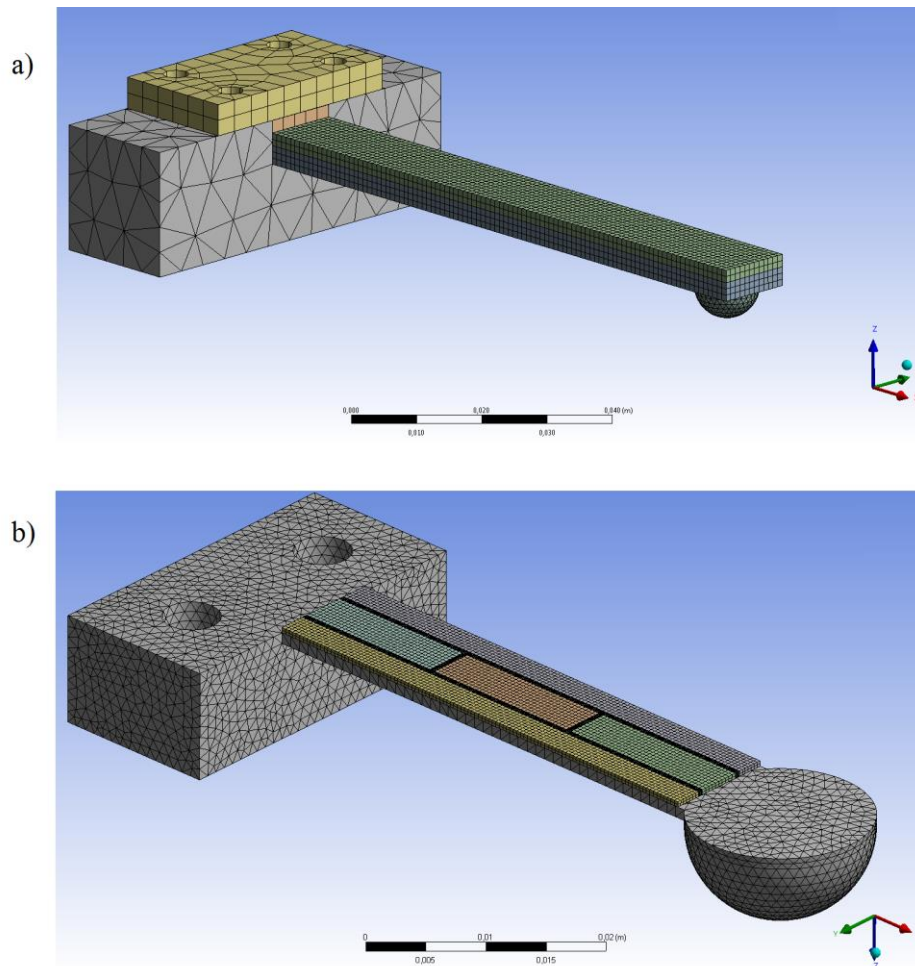
Figure 5.2 Meshed models of unimorph transducers: a) prototype "I", b) prototype "II"

To verify the chosen mesh density, the size of the elements was changed and the effect on resonant frequencies of the transducer was analyzed. The chosen number of elements is 4305 for the prototype "I". It is shown in row denoted by bold digits in Table 5.1.

Table 5.1 Influence of the number of finite elements on frequency of the first three resonance frequencies

Number of elements	I resonance frequency [Hz]	II resonance frequency [Hz]	III resonance frequency [Hz]
2991	261,04	612,76	1666,7
4305	**260,82**	**612,18**	**1665,1**
7571	260,63	611,81	1663,8
14748	260,17	610,95	1660,8
32766	259,86	610,33	1658,8
57504	259,75	609,98	1658,1

The obtained results agree with theory, since with increasing number of finite elements, the natural frequencies are decreasing. The relative difference between calculated frequencies is obtained using:

$$\frac{f_R - f_{RD}}{f_{RD}} \cdot 100\% \tag{5.1}$$

where: f_R – frequency for given number of finite elements; f_{RD} – frequency for chosen number of finite elements.
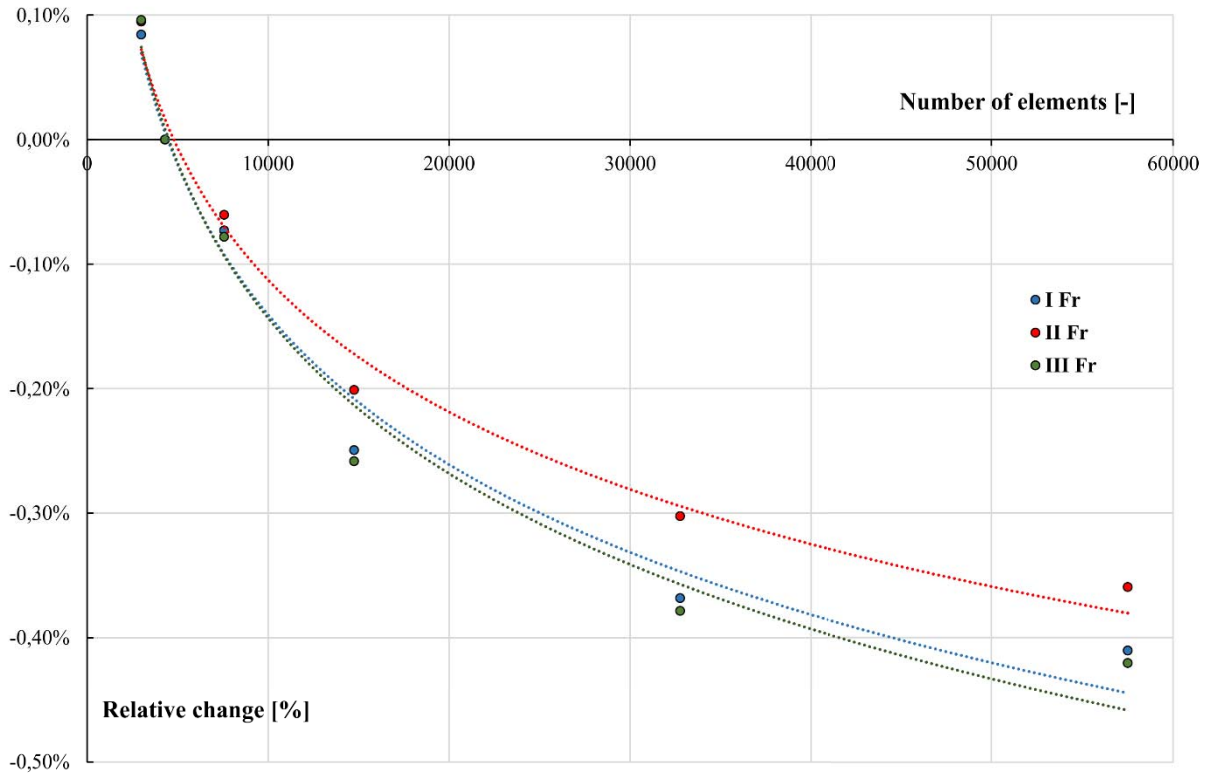
Figure 5.3 Relative change of the natural frequencies of transducer vs. number of the finite elements - unimorph transducer "I"

The plots illustrating a relative change for resonance frequencies is shown in Figure 5.3. It should be noticed, that the maximum obtained difference is 0,42 %. Such a small value does not justify the choice of greater number of finite elements, considering the longer time and higher computer power needed for the calculations. Simulation time for the largest mesh density was over ten times longer than for the chosen mesh density. APDL script for the mesh density testing is given in Appendix A2.

5.2 Definition of used materials

Calculations of piezoelectric transducer require definition of material properties: permittivity (or dielectric constants), the piezoelectric coefficient matrix and the elastic coefficient matrix [18]. The permittivity values represent the diagonal components ε_{11}, ε_{22}, ε_{33} respectively of the permittivity matrix ε^S. This matrix specifies the relative permittivity values. The superscript 'S' indicates that the constants are evaluated at constant strain. The piezoelectric matrix can be defined as a piezoelectric stress matrix **e** or a strain matrix **d**. The matrix **e** is usually associated with the input of anisotropic elasticity in the form of the stiffness matrix **c**, while **d** is associated with the compliance matrix **s**. The elastic coefficients matrix (6x6 symmetric matrix) specifies the stiffness **c** or compliance **s** coefficients. Below the piezoelectric stress and stiffness matrix are presented for the case of transversally polarized ceramics in the unimorph bending transducer (the ANSYS format of coefficients is taken into account).

$$e = \begin{bmatrix} 0 & 0 & e_{13} \\ 0 & 0 & e_{13} \\ 0 & 0 & e_{33} \\ 0 & 0 & 0 \\ 0 & e_{15} & 0 \\ e_{15} & 0 & 0 \end{bmatrix} \tag{5.2}$$

$$C^E = \begin{bmatrix} c_{11} & c_{12} & c_{13} & 0 & 0 & 0 \\ 0 & c_{22} & c_{13} & 0 & 0 & 0 \\ 0 & 0 & c_{33} & 0 & 0 & 0 \\ 0 & 0 & 0 & c_{66} & 0 & 0 \\ 0 & 0 & 0 & 0 & c_{44} & 0 \\ 0 & 0 & 0 & 0 & 0 & c_{44} \end{bmatrix} \tag{5.3}$$

Four piezoelectric materials were used for the active layer: P1-89 and PZT-401 ceramics (in the case of the prototype "I") and NCE-40 ceramics in the case of prototype "II". These are representative examples of the hard doped PZT materials produced by different manufactures. Ceramics of this group are particularly useful for a wide spectrum of applications ranging from combined resonant transducers for medical and flow measurements to accelerometers, pressure sensors, and non-destructive testing (NDT). Set of material properties necessary for the full definition of piezoelectric ceramics is given in the Table 5.2. Brass is used for the elastic element of the prototype "I". Its indentation device is made of steel sphere (100C6).

Table 5.2 Properties of PZT ceramics used for the FEM calculations

Property	P1-89	P1-91	PTZ-401	NCE-40
$C_{11}^E [10^{10} \cdot N/m^2]$	15.37	12.1	11.7	11.7
$C_{12}^E [10^{10} \cdot N/m^2]$	8.23	7.63	5.67	5.83
$C_{13}^E [10^{10} \cdot N/m^2]$	8.05	7.31	5.38	5.44
$C_{33}^E [10^{10} \cdot N/m^2]$	13.04	11.3	9.74	9.25
$C_{44}^E [10^{10} \cdot N/m^2]$	4.59	3.36	2.56	3.18
$C_{66}^E [10^{10} \cdot N/m^2]$	3.56	2.23	3.06	3.31
$d_{31} [10^{-10} \cdot m/V]$	-1.08	-2.47	-1.32	-1.40
$d_{33} [10^{-10} \cdot m/V]$	2.40	6.00	3.15	3.20
$d_{15} [10^{-10} \cdot m/V]$	2.80	5.09	5.11	5.00
$\varepsilon_{11}^S/\varepsilon_0$	1550	1820	1550	1550
$\varepsilon_{33}^S/\varepsilon_0$	1150	1460	1395	1250
$\rho [kg/m^3]$	7650	7410	7600	7750

5.3 Static simulation – prototype "I"

At the first step of the simulation, the visualization of the static tip deflection of the unimorph was done. When the active piezoelectric layer is connected to a voltage source, it contracts or elongates (depending on the polarization and the voltage applied to the electrodes) along the *x*-axis. The deformation of piezoelectric plate with specified dimensions (length l_1=0.1 *m*, width l_2= 0.012 *m* and thickness h_a = 0.002 *m*), in each plane is given in Table 5.3. The plate is fixed at non-electrode face.

Table 5.3 Deformation of piezoelectric plate and unimorph transducer with respect to different axis

Axis	Maximal deformation - piezoelectric plate only [m]	Maximal deformation - whole structure[m]
x	$10.848 \cdot 10^{-7}$	$1.724 \cdot 10^{-6}$
y	$6.554 \cdot 10^{-8}$	$7.06 \cdot 10^{-8}$
z	$2.575 \cdot 10^{-8}$	$15.691 \cdot 10^{-6}$

When the passive layer is bonded to piezoelectric active layer, the whole structure exhibits a bending deformation, if the voltage is supplied to the electrodes. In the Figure 5.4 deformations of the piezoelectric layer and the complete actuator are shown. The calculated values of deformation of unimorph transducer of active length l_1=0.1 m, width l_2= 0.012 m and thickness of active and passive layers, respectively, h_a = 0.002 m and h_p=0.003 m, in each plane are given in Table 5.3. The transducer is fixed at the bottom face of the base.
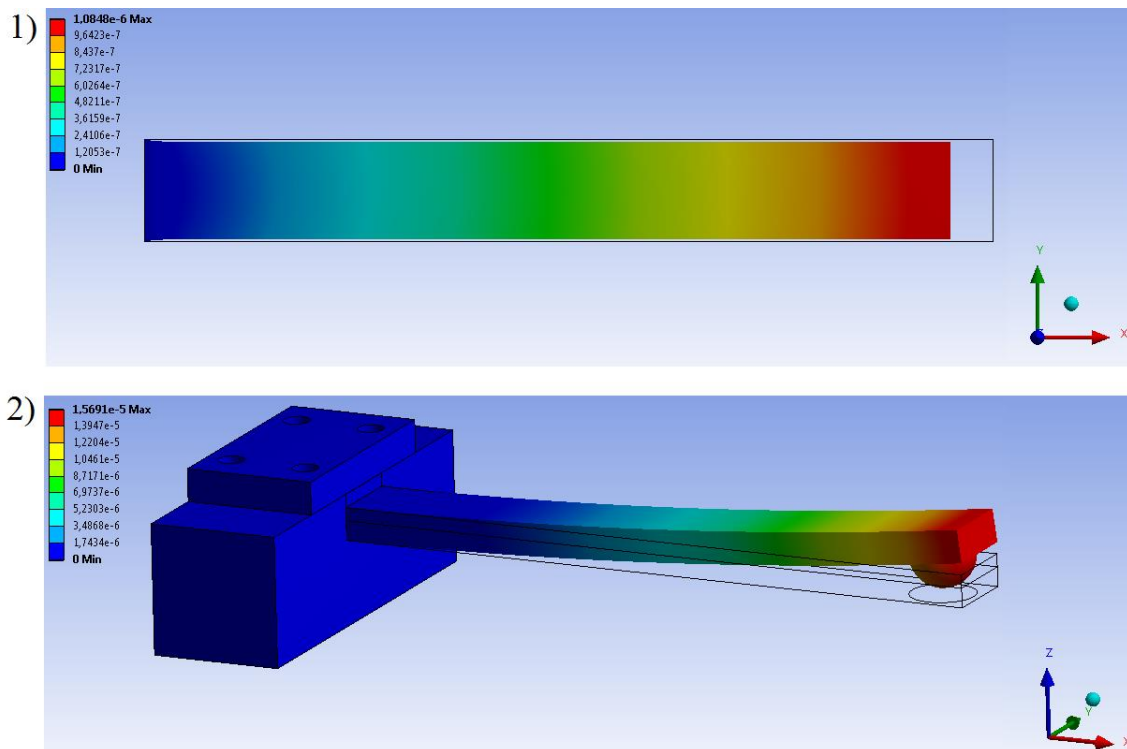
Figure 5.4 Results of static simulation: deformation of the P1-89 active layer (upper figure) and the bending movement of the whole unimorph transducer with fixed base (lower figure) – prototype "I"
(the scale of deformation is extended for clarity)

5.3.1 Deformation vs. active length l_1

The static simulation was carried out to verify maximal deformations of the unloaded transducer for different geometrical parameters. Chosen variations of l_1, l_2, h_s, h_a, and r were simulated. Piezoelectric layer was supplied by 200 V DC voltage. The deformation was calculated at the transducer's free end (which corresponds to maximum value). Its component along z-axis, relating to the normal excitation of the skin's surface (depth of the skin penetration), was the most interesting. The influence of changes of l_1 parameter on unimorph's deformation δ is shown in Figure 5.5.
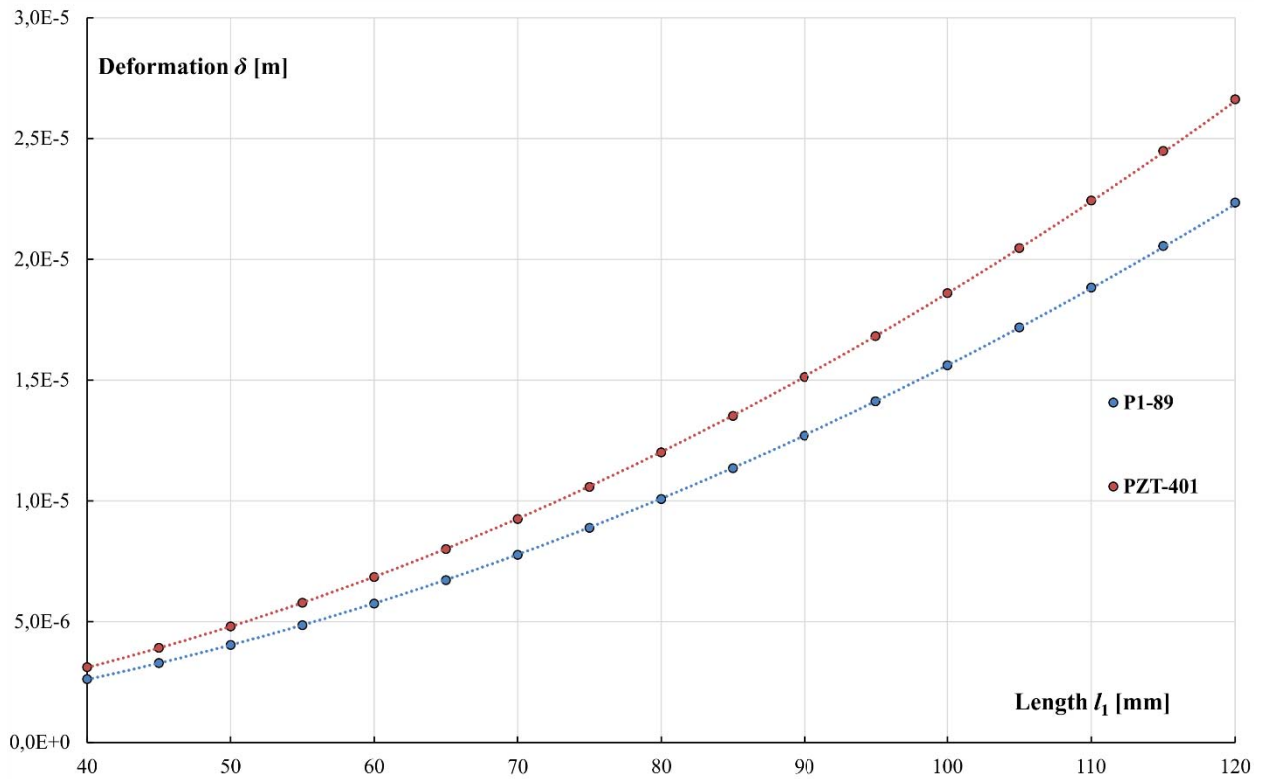
Figure 5.5 Results of static simulation: deformation vs. length l_1 of the active layer
- unloaded prototype "I"

Considering requirements for the transducer described in the section 3.1, the active length l_1 in the range of $100 - 120$ mm is the most appropriate. The maximal deflection at the state of resonance, depending on the quality factor Q of the transducer, does not exceed assumed 1 mm. Furthermore, the use of newer generation of hard doped piezoceramics (PZT-401) gives near 16 % gain in deformation compared to P1-89 piezoceramics. The comparison between analytical calculations of tip deflection and FEM static simulation result for PZT-401 active

101

layer is shown in Figure 5.6. There is good agreement between them, with relative error not exceeding 3 % in the considered range of l_1 parameter.
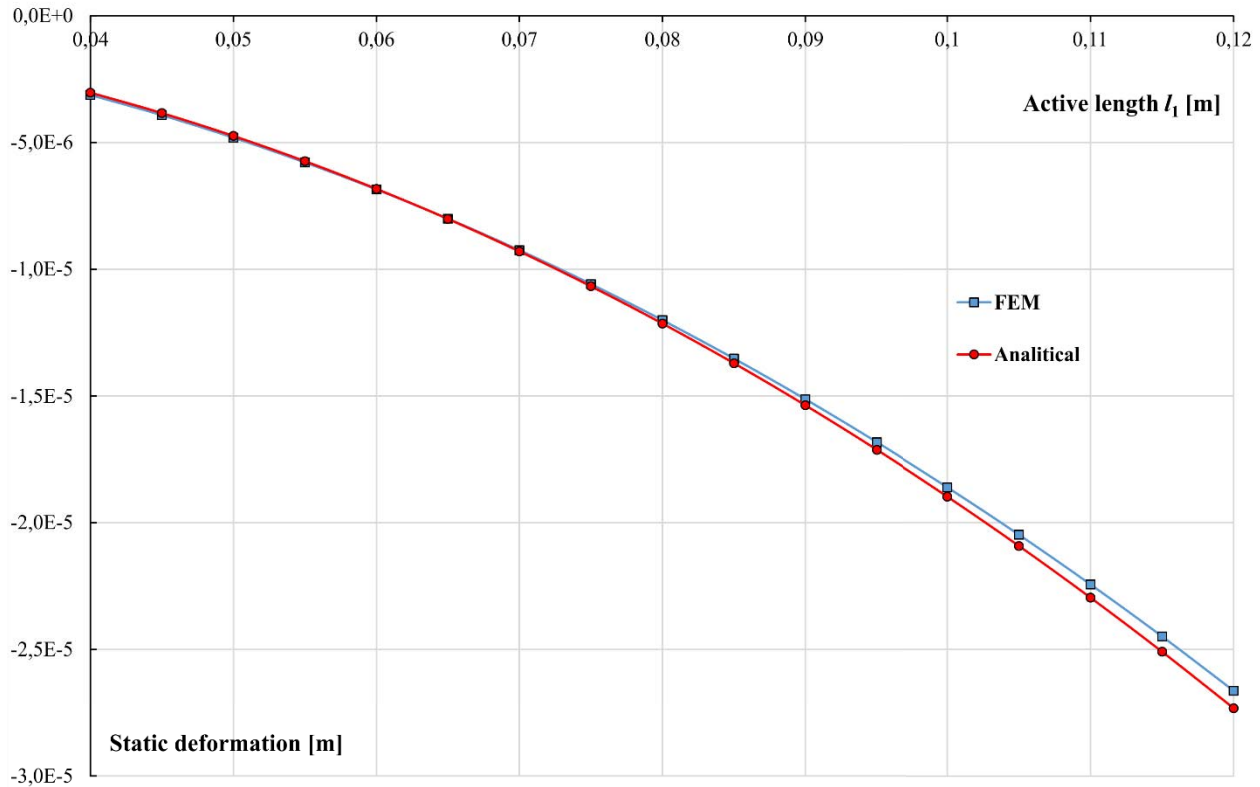
Figure 5.6 Comparison of analytical and FEM calculation results for static deformation vs. active length l_1 – prototype "I" (for PZT-401 active layer)

5.3.2 Deformation vs. remaining dimensions

The change in δ as a function of active width l_2 is a linear function. The relative values do not exceed 3% and do not considerably affect the overall performance of the transducer in the desired range of l_1 parameter (Figure 5.7). Figure 5.8 shows the influence of different thicknesses of active and passive layers – h_a and h_p, respectively, on the deformation of the unimorph. Only the results for PZT-401 active layer are shown, for clarity reasons. Considering the desired deformation level, only $h_a \in\ <1;3>$ and $h_s \in<2;4>\ mm$ were investigated. The diameter of the indentation device r does not affect the deformation much (1.5% relative change in δ - Figure 5.9). Nevertheless, considering the contact between the sphere and tested material, larger r (greater contact area) is desired.
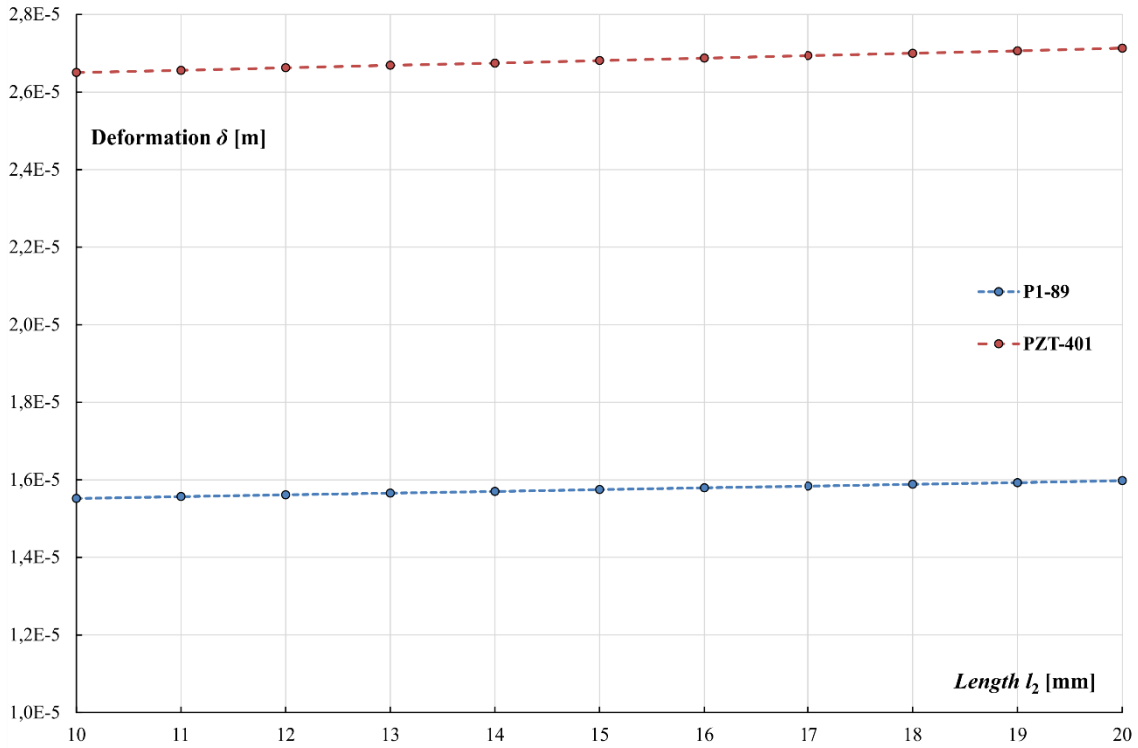
Figure 5.7 Deformation vs. width l_2 of the active layer - unloaded prototype "I"
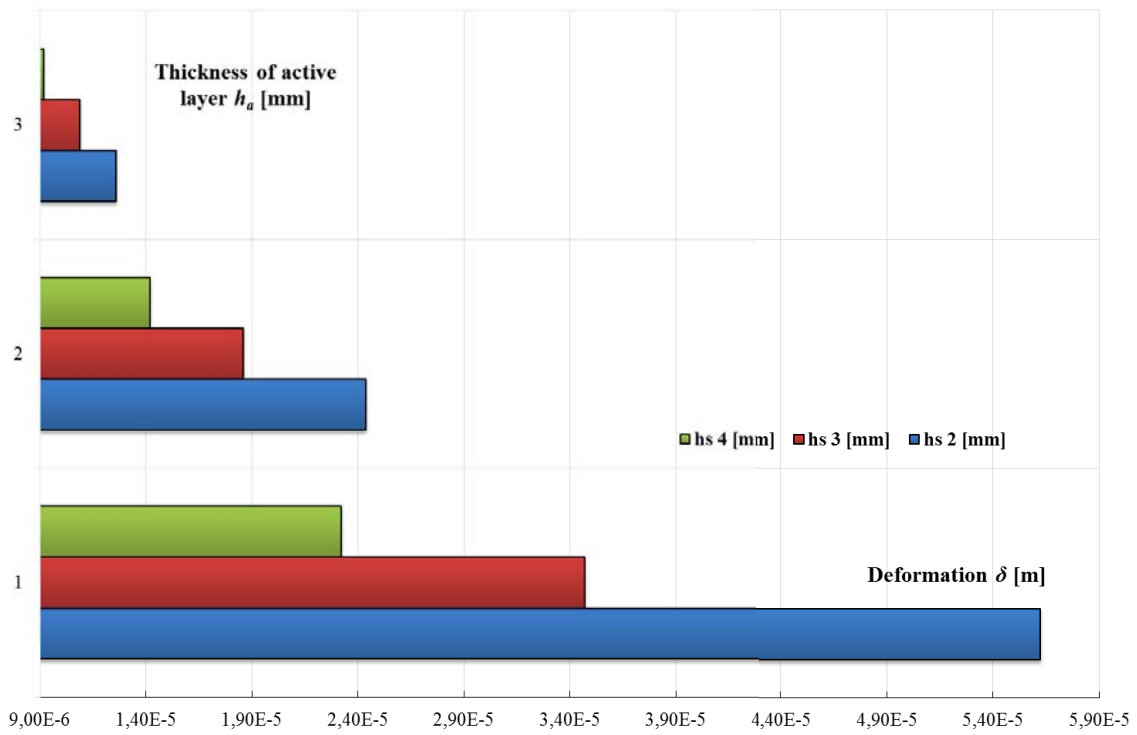
Figure 5.8 Deformation vs. active layer thickness h_a, for different values of thickness of passive layer h_s - unloaded prototype "I" (using PZT-401 active layer)

103
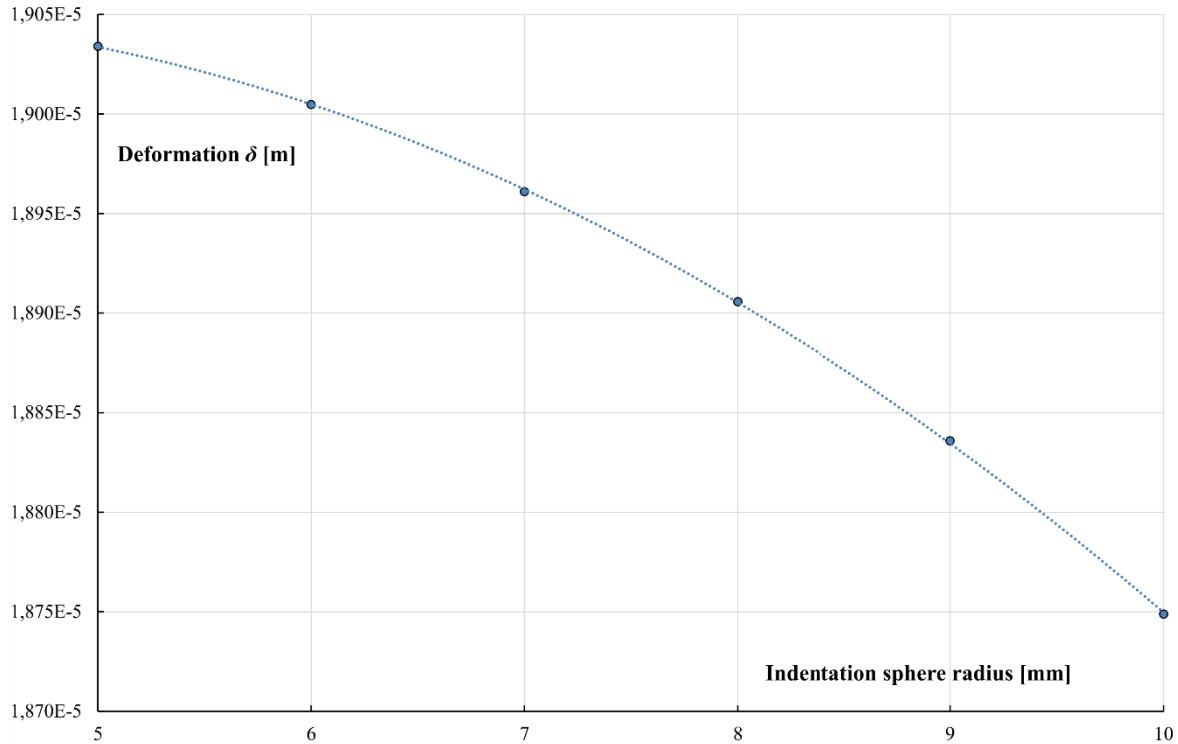
Figure 5.9 Deformation vs. indentation sphere radius *r* - unloaded prototype "I" (PZT-401 active layer)

5.4 Modal simulation – prototype I

At the next stage of study, the modal simulation were carried out. The main goal was to determine the vibration characteristics of the unimorph structure, which included the natural frequencies (eigen-frequencies) and mode shapes (eigen-vectors) for a given geometric set. The simulation was made for the frequencies from $200Hz$ to $27kHz$, which comprised sensitivity range of skin receptors. The first three modes represented basic movement of the indentation sphere in each direction: the first mode – quasi-normal deformation (*z*-axis); second mode – deformation in *y*-axis; third mode – deformation in *x*-axis. The modal simulation was carried out for 6 basic geometric sets:

- *I –* $l_1 = 40$, $l_2 = 12$, $h_s = 2$, $h_a = 1$, $r = 5\ mm$
- *II –* $l_1 = 60$, $l_2 = 12$, $h_s = 2$, $h_a = 1$, $r = 5\ mm$
- *III –* $l_1 = 100$, $l_2 = 12$, $h_s = 3$, $h_a = 2$, $r = 5\ mm$
- *IV –* $l_1 = 100$, $l_2 = 20$, $h_s = 3$, $h_a = 2$, $r = 8\ mm$
- *V –* $l_1 = 120$, $l_2 = 12$, $h_s = 3$, $h_a = 2$, $r = 5\ mm$
- *VI –* $l_1 = 120$, $l_2 = 20$, $h_s = 3$, $h_a = 2$, $r = 8\ mm$

The resonance F_r and anti-resonance F_a frequency values for those sets are given in the Table 5.4.

Table 5.4 Results of modal simulation for different geometrical sets – prototype "I"

	Mode number	P1-89 active layer		Pzt-401 active layer	
Geometric scenario		F_r **[Hz]**	F_a **[Hz]**	F_r **[Hz]**	F_a **[Hz]**
I	1	857	883	822	849
	2	3101	3152	3025	3073
	3	5619	5633	5388	5407
II	1	398	410	382	394
	2	1514	1540	1477	1502
	3	2715	2794	2605	2689
III	1	261	268	250	257
	2	613	625	595	607
	3	1667	1710	1595	1643
IV	1	243	250	232	240
	2	916	935	889	907
	3	1633	1678	1562	1613
V	1	183	188	176	181
	2	433	442	420	428
	3	1167	1197	1117	1150
VI	1	172	176	164	169
	2	656	670	639	650
	3	1141	1172	1092	1126

Set III gave a good compromise between acceptable deformation values (shown in Figure 5.5) and resonance frequencies values, that are low enough for the considered application. Mode shapes corresponding to the extracted resonance frequencies are shown in the Figure 5.10.
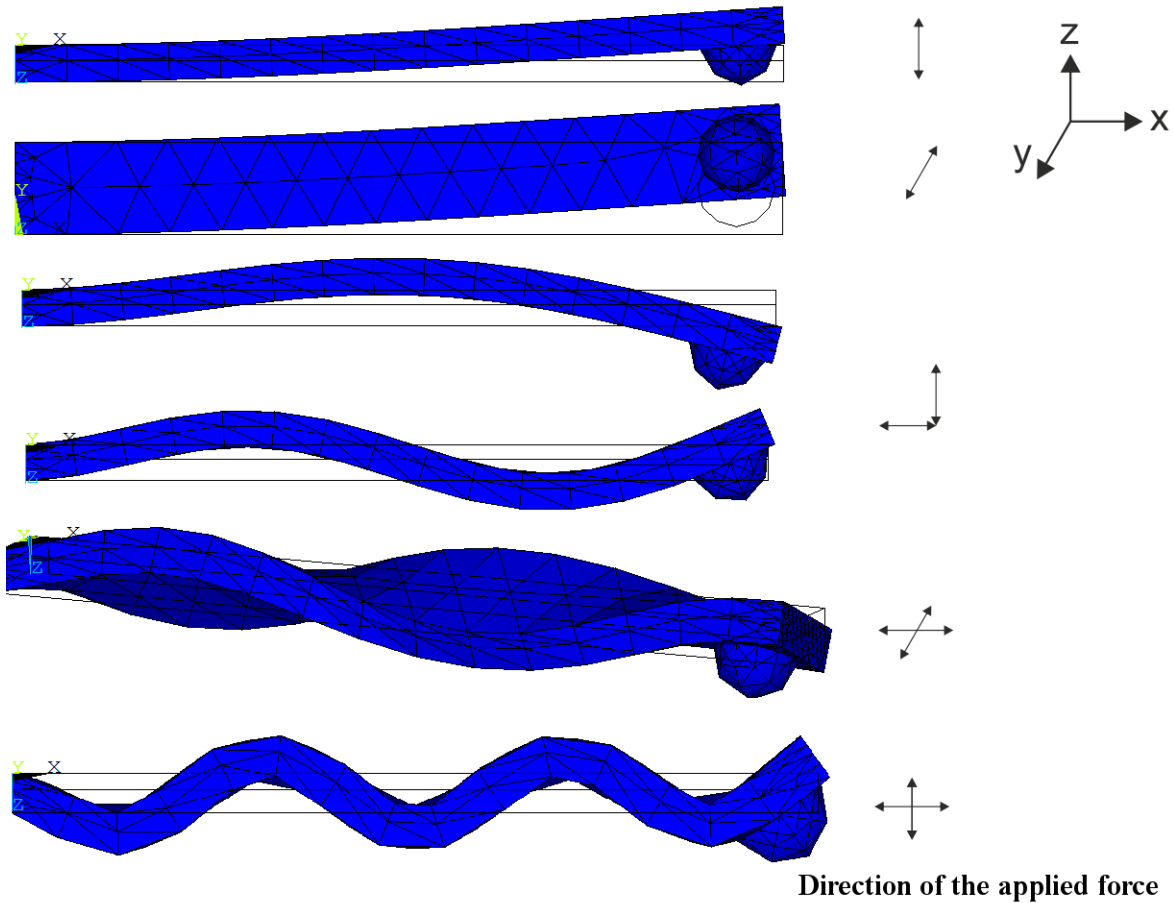
Figure 5.10 Results of FEM modal analysis: deformation of the bimorph corresponding to its natural
resonance frequencies – prototype "I"
(arrows on the right of each mode indicate the direction of the force applied on the tested material)

For each of the transducer's natural frequencies, the indentation force is acting in different directions and causes a different contact surface. This contributes to varying conditions of friction and sliding between the spherical indenter and characterized sample. Piezoelectric transducers, generally characterized by low amplitude of vibration, work in the area of partial slip, since the contact area is often greater than the vibration amplitude. Under these conditions, the coefficient of friction of the sphere/surface contact may change depending on the mode in question. Slip and stick areas, as well as the quasi-static friction coefficient, were described more precisely in sections 4.3.3 and 4.3.4. The above facts stress the impact of the choice of the resonance mode of the transducer on the mechanical contact between the indenter and the sample. Therefore, the right choice of working mode of the transducer is very important, since it can allow or significantly facilitate the measurement of mechanical properties of soft tissues.

5.5 Static simulation – prototype "II"

During the static analysis of the unimorph structure, different materials for active and passive layers were tested. The passive layer was integrated with indentation hemisphere and the base. Materials assigned to it were steel and aluminum. Active layer consisted of PZT-401 and NCE-40 piezoelectric ceramics of different manufactures. The active layer was connected to a DC voltage source of 200 V. The structure was fixed at the bottom of the base. The deformation was measured along z axis, and it corresponded to the normal excitation of the tissue's surface.

The most suitable geometric dimensions of the model were chosen based on the maximal deformation at the free end of the unimorph, the admissible levels of stress for piezoelectric ceramics as well as resonant frequencies low enough for the application. The parametric analysis was carried out for unsectorized active layer. The influence of changing the active length l_1 on the free end deformation is shown in Figure 5.11.
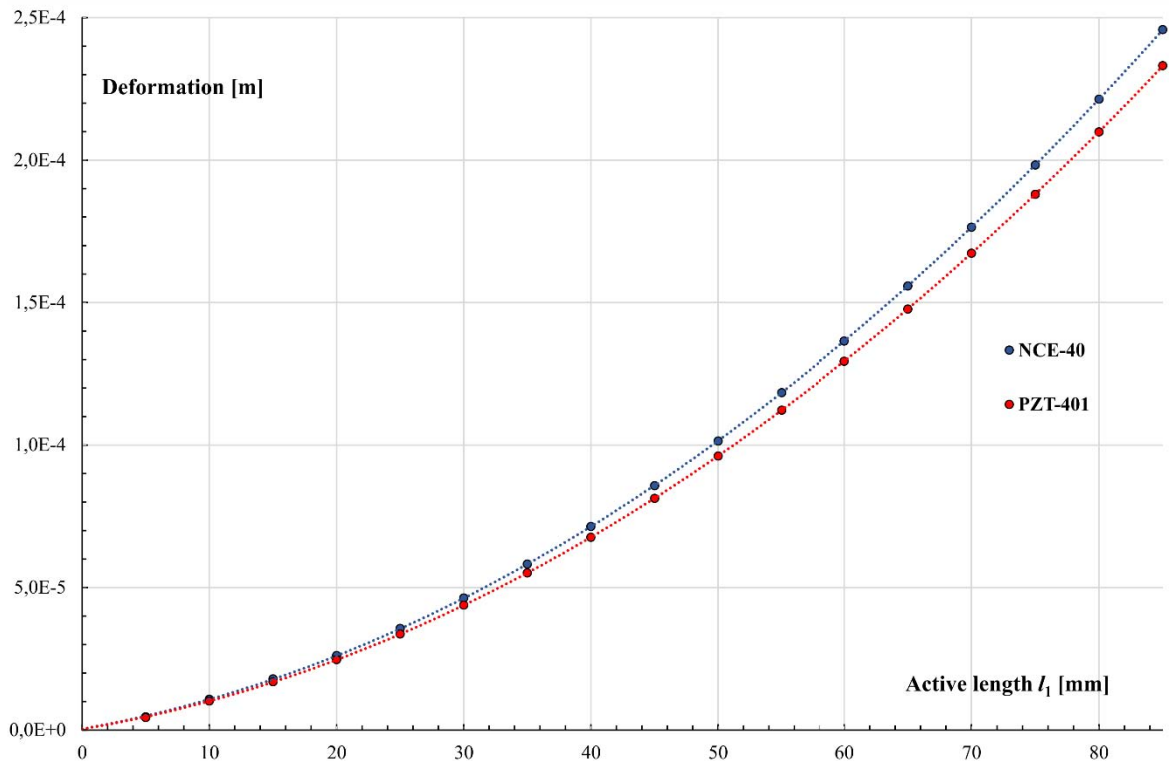
Figure 5.11 Deformation at the free end vs. active length l_1 – prototype "II"
(for two types of piezoelectric ceramics)

The deformations shown in the Figure 5.11 were obtained for the unsectorized active layer. They were approximately 27 % higher than in the case of sectorized active layer, which is understandable, considering the area needed for isolation between the sectors. Furthermore, changing the piezoelectric material did not gave a much improvement. This also agrees with material data of the same class of piezoelectric materials, showing little over 6% change at transducer's performance. Finally, NCE-40 ceramics were chosen for the prototype "II" assembly.

The results of static simulation for unimorph transducer with sectorized active layer is given in Table 5.5. The data points were obtained for geometry "II" of the transducer with the following parameters: $l_1 = 45$ mm, $l_2 = 10$ mm, $h_a = 0.5$ mm, $h_s = 1$ mm, and $r = 8$ mm.

Table 5.5 Results of static simulation for sectorized active layer – prototype "II"

Active material	Passive material	Maximal deformation [m]	Equivalent Stress (Von-Mises) [Pa]
PZT-401	Aluminum	$6.44 \cdot 10^{-5}$	$1.38 \cdot 10^7$
PZT-401	Steel	$5.04 \cdot 10^{-5}$	$1.31 \cdot 10^7$
NCE-40	Aluminum	$6.76 \cdot 10^{-5}$	$1.39 \cdot 10^7$
NCE-40	Steel	$5.28 \cdot 10^{-5}$	$1.51 \cdot 10^7$

Depending on the number of sectors which were supplied by voltage, the deformation of the transducer was changing, with maximum of 67.6 μm (for NCE-40 ceramics and aluminum passive layer). Those values could be related to a maximal deflection at the state of resonance using the quality factor Q. The static bending deformation and equivalent stress distribution are illustrated in the Figure 5.12.
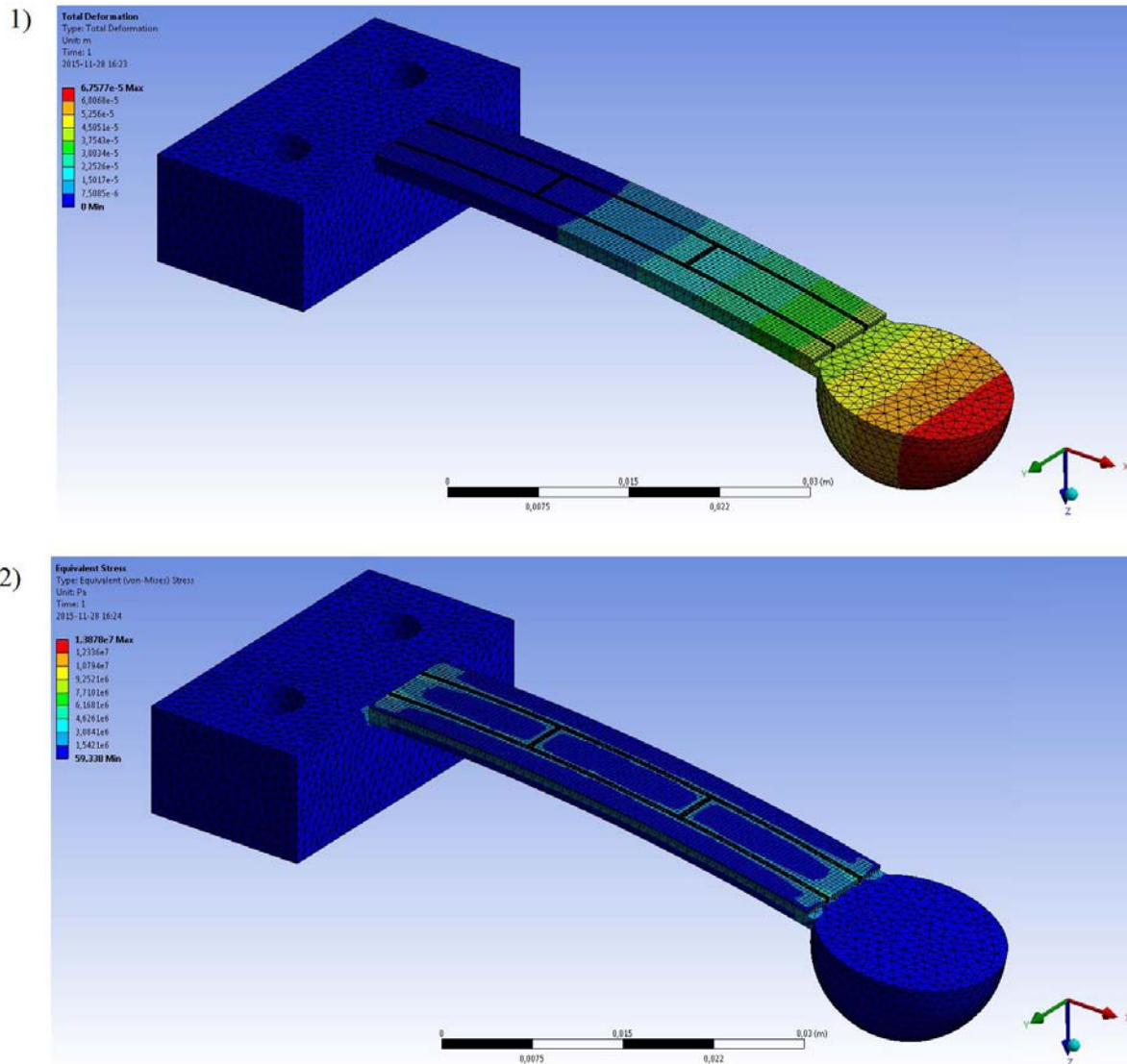
Figure 5.12 The static, bending deformation 1) and Von-Mises equivalent stress distribution 2) - prototype "II"(passive layer made of aluminum and active layer made of NCE-40 ceramics) (the scale is extended for clarity)

5.6 Modal simulation – prototype II

The other design requirements were tested by modal analysis. The aim was to determine the vibration characteristics of the considered structure, including natural frequencies, mode shapes and participation factors (the amount of a mode participates in a given direction).

Three basic natural frequencies were calculated. Each of those corresponded to a deformation in different direction (axis). The first resonant mode was the bending movement in the z-axis direction, which is normal to the plane of tested material. The second one was the

torsion deformation (the tip of spherical indenter-probe is moving in the *y*-axis). The third resonant mode was linked to a "wave" movement of the transducer, which caused the probe to move in the direction aligned with the *x*-axis.

Moreover, for each natural frequency of the transducer, the indentation sphere and tested material generate different contact surfaces. This contributes to varying conditions of friction and sliding between the spherical indenter and sample to characterize, as has been described in sections 4.3.4 and 0. To establish frequency values of resonance and anti-resonance for each mode of transducer, boundary conditions of model had to be defined accordingly:

- resonance – electromechanical impedance becomes minimum, $Z{\rightarrow}0$, the voltage on both electrodes is set to 0 (short-circuit state),
- anti-resonance – electromechanical impedance becomes maximum, $Z{\rightarrow}\infty$, voltage is not defined (open circuit state) [30].

The resonance and anti-resonance frequencies were obtained for geometry "II" of the transducer with the following parameters: $l_1 = 45$ *mm*, $l_2{=}10$ *mm*, $h_a = 0.5$ *mm*, $h_s{=}1$ *mm*, and $r{=}8$ *mm*.

Table 5.6 Frequencies of resonance and anti-resonance for first three working modes - prototype "II"

Active material	Passive material	F_r I [Hz]	F_a I [Hz]	F_r II [Hz]	F_a II [Hz]	F_r III [Hz]	F_a III [Hz]
PZT-401	Aluminum	162.91	165.13	861.62	867.23	1415.3	1435.1
PZT-401	Steel	132.84	134.83	769.04	771.9	1329	1349.9
NCE-40	Aluminum	162.37	165	862.77	869.45	1329	1430.4
NCE-40	Steel	132.39	134.77	772.06	775.45	1323.1	1347.9

Deformations corresponding to frequencies given by the Table 5.6 are shown in the Figure 5.13. The amplitude of deformations obtained using modal simulation, by definition it does not represent real values; they are scaled with mass or unity matrix instead. Depending on the frequency of the supply voltage, the bending transducer can produce movement in each axis. This property is quite interesting considering the characterization of the mechanical properties of soft materials, where different kind of movement can be used in evaluating different quantities. Moreover, the highest value of resonant frequency is below the required threshold of 1500 *Hz* specified in chapter 3.
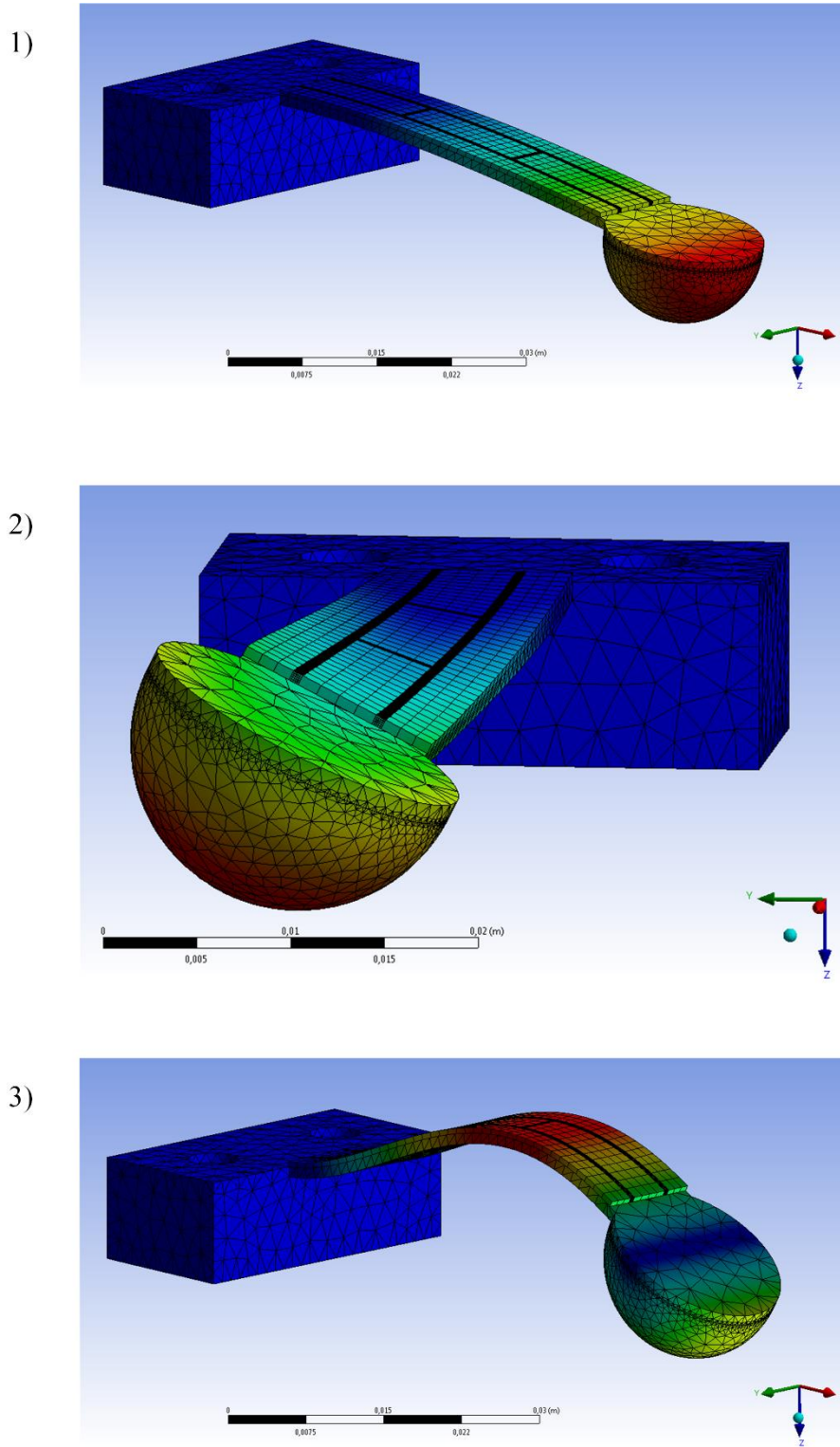
Figure 5.13 Results of modal simulation: first three natural frequencies and corresponding deformations
1) first mode - bending movement; 2) second mode - torsional movement; 3) third mode – "wave" movement –
prototype "II" (the amplitude of deformations is extended for clarity)

5.7 Conclusions

The main focus in this chapter was pointed on assessment of the chosen structure of piezoelectric bending transducer, using Finite Element Method (Ansys Mechanical and Workbench software). The key aspects of the analysis were following: the calculations of maximal deformation at the free end of unimorph transducer for different materials and different geometric parameters, as well as determining the resonance frequencies and vibrational (shape) modes.

The numerical model for FEM analysis was parametric and developed in APDL script language. Moreover, 3D model of the transducer was built in Inventor software linked to Workbench. This allowed relatively easy variation of the geometry and parameters of the analysis.

For the static analysis of the unimorph's transducer, its general principle of operation was graphically demonstrated. This part of numeric analysis has demonstrated that different geometric parameters have the influence on the static deformation of the transducer. Moreover, different piezoceramics were tested in the active layer. No longer available, P1-89 ceramics were compared to modern PZT-401 ceramics. The results have shown, that PZT-401 has approximately 16% higher deformation, than P1-89 ceramics.

Design requirements specified for operating frequencies of the unimorph transducer were verified with modal analysis results. The first three resonance frequencies were of special interest, due to the character of the movement of the indentation hemisphere at the free end of the transducer. It should be noticed, that piezoelectric actuators, generally characterized by low amplitude of vibration, work in the area of partial slip, since the contact area is often greater than the vibration amplitude. Under those conditions, the coefficient of friction of the sphere/surface contact may change depending on the mode shape in question (Figure 4.16). This property can serve as a method to tune the deformations of the transducer, to meet the specific requirements of the measurement of mechanical properties of materials. Concluding, the most suitable working mode for the desired application was the first one – due to generation of normal deformation with the highest amplitude. Nevertheless, the operation at the higher natural frequencies of unimorph transducer was verified experimentally, since it has interesting friction-sliding influence on the conditions of the measurement.

112

6 EXPERIMENTAL VERIFICATION

In this chapter experimental verification of two manufactured unimorph piezoelectric transducers is described. They are referred to as: prototype transducer "I", and prototype transducer "II". First, a description of the measurement methods and test bench are presented. The test bench can cover the following measurements: deformation, indentation depth, shift of resonance frequency, and electromechanical impedance.

6.1 Measurement methods and test bench

The prototype transducer "I", shown in Figure 6.1, has an active layer (P1-89 ceramic) and a brass, passive layer glued together. The hemispherical indenter is made of 100C6 steel. The geometrical dimensions are as follows: unimorph length - l_1=0.1 m, width - l_2=0.012 m, height of the active layer - h_a=0.002 m, height of the passive layer - h_s=0.003 m and radius of the indentation device - r=0.005 m. The prototype transducer "II" has of a passive layer, indentation hemisphere and base CNC milled from one block of aluminum. The active layer was made of Noliac NCE-40 piezoelectric ceramics. The overall dimensions are 40% lower compared with the first prototype. The thickness of the active layer was reduced to h_a=0.0005 m, and the passive layer - h_s=0.001 m. The radius of indentation sphere, on the other hand, is increased to r=0.008 m.

Both prototypes were attached to adjustable stand to allow controllable contact conditions between the indentation hemisphere and the material to characterize. The tested samples were positioned on an electronic balance to measure the normal force acting on their surface. The test bench is shown in Figure 6.2.
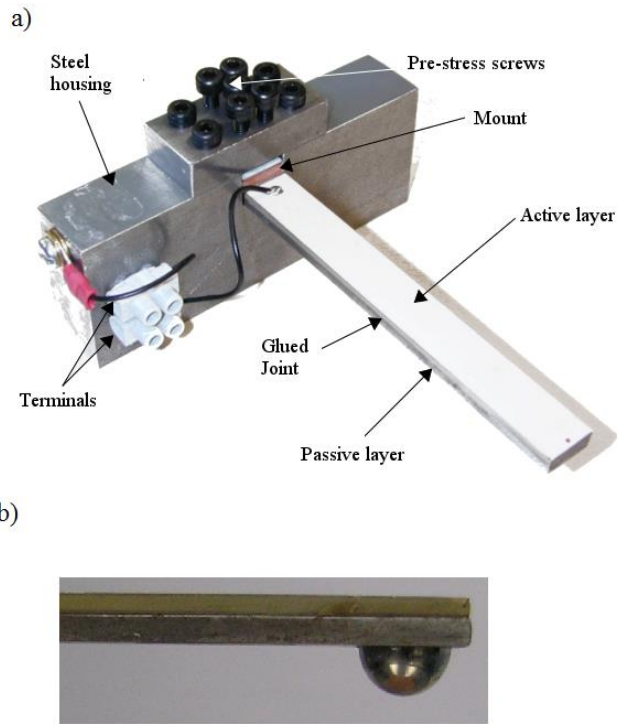
Figure 6.1 Prototype transducer "I": without the hemisphere, a) with the indentation sphere b)
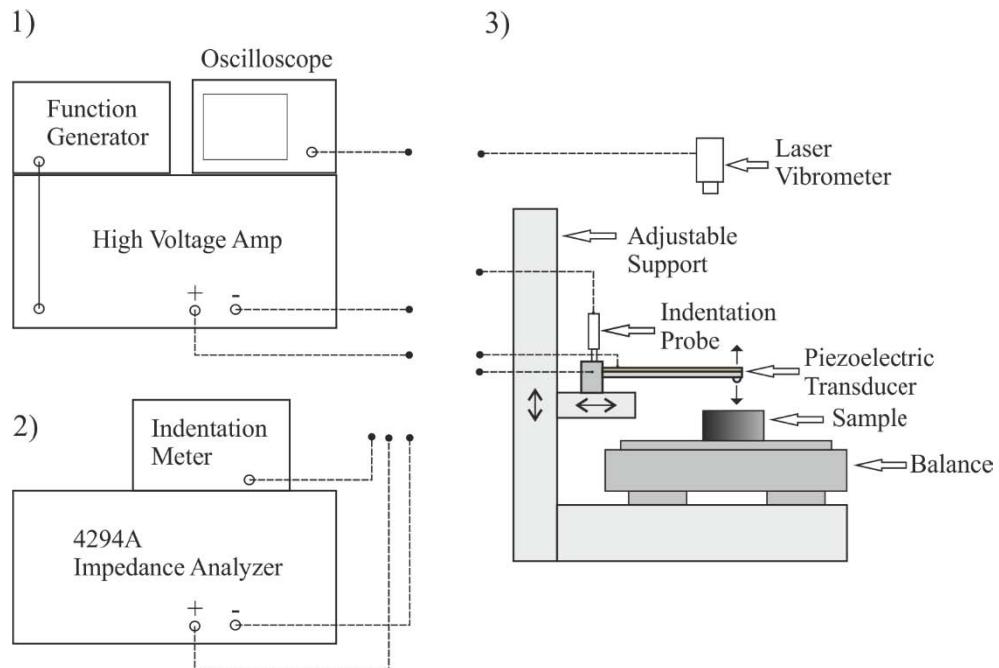
Figure 6.2 Test bench for the experimental analysis for a unimorph transducer: 1) supply chain for measurement of deformations 2) instruments for measurement of impedance 3) adjustable support with unimorph transducer and test samples placed on a balance; indentation and laser vibrometry probes

6.1.1 Measurement of maximal deformations

The first stage of measurements covered detection of the resonant frequencies of the unimorph transducer and the corresponding maximum deformations at the free end of the unimorph. This stage was conducted for unloaded transducer, i.e. there was no contact between the indentation hemisphere and the tested material. Measurement equipment has the following instruments:

- Tektronix AFG320 function generator;
- Physikinstrumente E-472 Modular High-Voltage Amplifier / Controller;
- Polytec CLV laser vibrometry system;
- Tektronix oscilloscope.

The function generator is set to output low voltage of sinusoidal singal (< 10 V) at desired frequency. Due to this, it was possible to generate frequency sweeps in order to determine the resonance frequency of the system. The signal from function generator was feeding the high-voltage amplifier designed for piezoelectric applications. The amplifed signal was supplied to the transducer. The voltage amplitude was set at 200 V, but it should be noted, that from the point of ceramic's thickness ($h_a = 2$ mm), voltage level of 2 kV didn't produce risks of depolarization or generation of electric arc.

The deformation of the piezoelectric unimorph transdcuer shoud vary between single μm to fraction of mm, depending on the voltage and frequency supplied. To measure such small level of movement, laser vibrometer system was used. Such systems work according to the principle of laser interferometry. The laser beam, with a certain frequency f_0 , strikes a point on the vibrating object. Light reflected from that point goes back to the sensor head. The back-scattered light is shifted in frequency (Doppler effect). This frequency shift f_D is proportional to the velocity of the vibrating object.

$$f_D = 2|v|/\lambda \tag{6.1}$$

To distinguish between movement towards and away from the sensor head an offset frequency f_B is added onto the backscattered light. The resulting frequency seen by the photo detector becomes $f = f_B + f_D$, where the sign in this equation depends upon the direction of

movement of the object. The frequency f on the photo diode, is linked to the vibration velocity by the simple relationship.

$$f = f_B + 2v/\lambda \tag{6.2}$$

where: λ - the wavelength of the HeNe laser utilized in the LDV system, which is a highly stable physical constant (0.6328 μm). The frequency f seen by the photo detector is then demodulated into a voltage U proportional to the vibration velocity v [47]. The displacement value can be calculated thanks to:

$$A = \frac{U \cdot Cal}{2\pi F} \tag{6.3}$$

where: U – voltaged proportional to vibration velocity, measured on the oscilloscope [V], Cal – calibration level [$mm/s/V$], F – working frequency [Hz].

The registered vibrations, coresponded to the maximal deflection of the unimorph transducer (at the free end) for its first rezonance frequency. Simplified laser measurement system is shown in Figure 6.3.
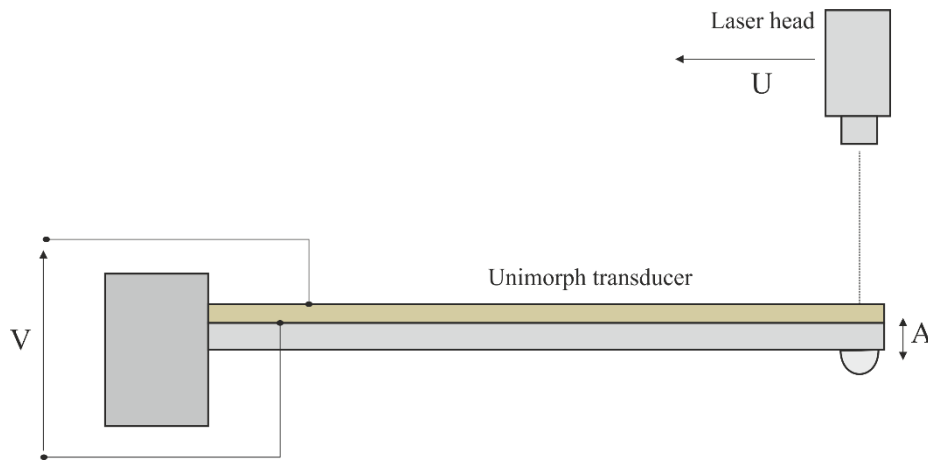
Figure 6.3 Simplified illustration of measurement of maximal deformations at the free end of unimorph transducer; A – value of deformation [m], U – voltage output from laser vibrometer [V], V – supply voltage [V]

6.1.2 Measurement of frequency shifts

The next stage of experimental analysis was measurement of resonant frequency shifts due to the contact of indentation hemisphere with material's surface. Adjustable stand was used to control the normal force F_N acting on the tested material. The value of F_N was calculated, using the mass of the structure, shown by the electronic balance.

116

$$F_N = (m_x - m_i)g \qquad (6.4)$$

where: F_N – normal force acting on the sample, m_x, m_i – total mass, mass of the sample, respectively, g – gravitational acceleration.

The values of chosen normal force F_N, were in the range specified in chapter 3 (below 1 N). For each material and force level, resonant frequency was registered. Due to the function generator and laser measurement of vibrations, the maximal deformations of unimorph working in resonance conditions, can be obtained with sufficient precision.

The frequency/deformation characteristics obtained for each tested material should be compared with the results of unloaded unimorph transducer (not in contact with the material). The resulting resonant frequency shift might, therefore, serve as a discriminant of mechanical contact between the transducer and each tested material sample. As a consequence, it might be used to differentiate the mechanical properties of those material samples.

6.1.3 Measurements of impedance

The final part of the experimental analysis included the detection of the electromechanical impedance characteristics of unimorph transducer. Especially, the variation of the impedance between the unloaded and loaded (in contact with the sample) states of unimorph transducer is interesting in terms of assessment of contact conditions, and finally mechanical properties of tested samples.

The measurement method is based on exciting the unimorph transducer by a series of frequencies, typically around the mechanical resonance of the unimorph structure. The result is a unimorph's response in a form of impedance function of those frequencies. The variations of the impedance of the transducer interacting with the tested material are functions of physical properties of the contact:

- stiffness of the contact, depending on the applied force and tested material,
- friction forces at the interface between intender and the material (sphere/plane contact conditions).

Those variations may be related to material properties using appropriate models [58]. Thus, the electromechanical impedance response of the system can be referred to as an electrical signature of the mechanical properties of the material.

Agilent 4294A impedance analyzer was used to measure the impedance characteristics. It was capable of outputting voltage signal of 1 V RMS level in the frequency range $f \in < 40\ Hz; 110\ MHz >$ [29]. The frequencies corresponding to the series and parallel resonances were observed. Moreover, the impedance and admittance matrices were used to calculate the lumped parameters describing the electromechanical behavior and represented by the equivalent circuit of the transducer (section 4.2). Concluding, to show the electromechanical impedance variations, it was enough to observe the evolution of equivalent circuit parameters between: the unloaded transducer state and loaded transducer state, i.e. in contact with each of the tested materials. For each of the materials and set of normal forces applied, the response of the transducer was registered by the impedance analyzer.

6.1.4 Tested material samples

For the verification process of the proposed method, two groups of material samples with mechanical properties comparable to human skin, were used to test/verify the prototype transducers. The mechanical properties of these materials were provided by the LTDS laboratory (Table 6.1). They were obtained for a normal force of 20 mN and a slide speed of $50\ \frac{\mu m}{s}$.

Table 6.1 Material properties of the first group of polymers used in the measurement analysis

Polymer symbol	Stiffness [N/m]	Young Modulus [MPa]
A	58.5	0.0586
B	103	0.154
C	119	0.199
D	134	0.208
E	164	0.297
F	220	0.482

The basic properties of the second batch of polymer materials, which was used for the impedance measurements of the unimorph transducer, are shown in Table 6.2.

Table 6.2 Material properties of the second group of polymers

Polymer Symbol	Viscosity [kPas/s]	Stiffness [N/m]	Young Modulus [kPa]
G	6000	35	10000
Y	8000	45	25000
R	30000	105	50000

The final measurements of equivalent circuit parameters, derived using the Bode and Nyquist plots, were carried out for both groups of polymers. The first group of 6 polymers was tested under normal force $F_N \in < 0.1; 0.6 > N$, while the second group of 3 polymers was tested under normal force $F_N = 0.05 \, N$.

6.2 Measurement results

6.2.1 Deformations characteristics

The resonant frequency corresponding to the first mode of the prototype transducer "I" (the bending movement of unimorph), was found at 236 *Hz*. With voltage level at 200 *V* the maximal deformation at this frequency reached 0.472 *mm*. The value of the deformation in the *z*-axis obtained from static analysis in Ansys was as follows: $\delta_{Ansys} = 15.691 \cdot 10^{-6} \, m$. To compare those two values, the quality coefficient *Q* can be used.

$$Q = \frac{1}{R_1} \sqrt{\frac{L_1}{C_1}} = 36.65 \qquad (6.5)$$

$$\delta_{Resonance} = \delta_{Ansys} \cdot Q = 0.575 \, mm \qquad (6.6)$$

The equivalent circuit parameters: R_1, L_1, C_1 were derived from impedance measurements of the unloaded prototype transducer "I" (described in detail in section 6.1.3). The calculated value $\delta_{Resonance}$ is comparable with the one obtained from the measurement. Also the registered resonance frequency is comparable with the results of modal FEM analysis (261 *Hz*). The difference could be accounted to screwed connections between the transducer and the base, as well as glued joint between active and passive layers. The graph illustrating

the deformations at frequencies around the first mechanical resonance of the prototype transducer "I" is shown in Figure 6.4.
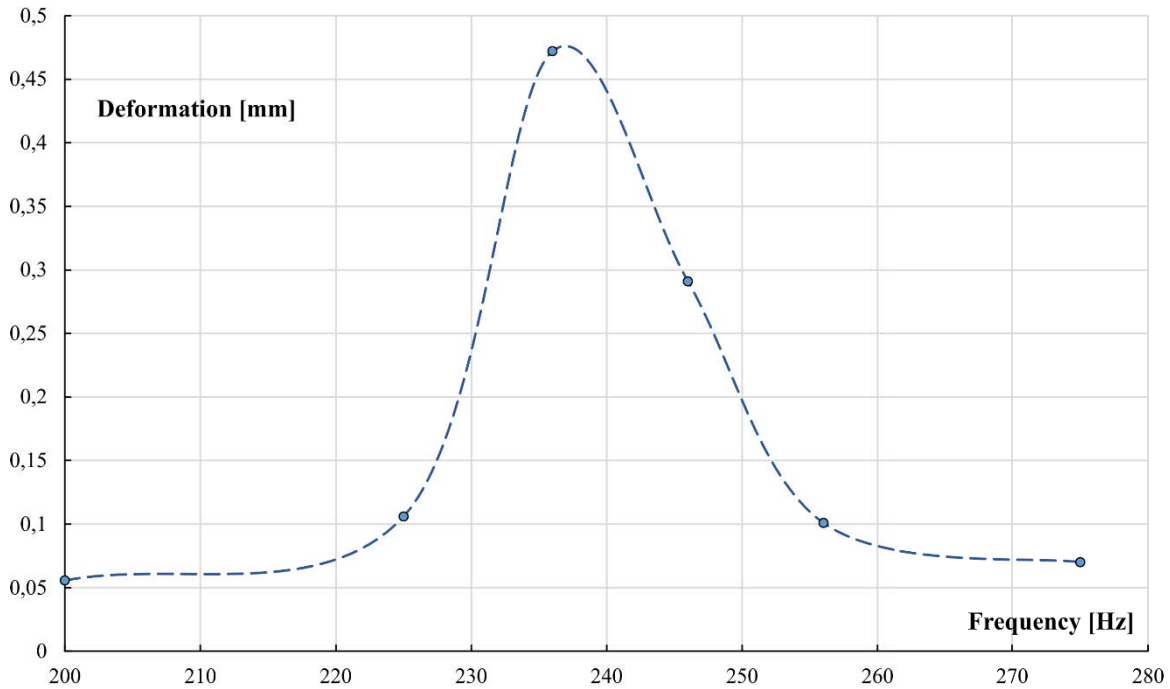
Figure 6.4 Deformations at the free end of prototype transducer "I" near resonance frequency

6.2.2 Frequency shift characteristics

The frequency shift characteristics given in Table 6.3, were measured for the prototype transducer "I". The indentation hemisphere was in contact with tested material samples (group of 6 polymers described in section 6.1.4) with different applied normal force F_N in the range of <0.1;1> N. The voltage supplied to the electrodes was set at 200 V. At this range of F_N the frequency shift is visible, but it is not possible to differentiate the tested material samples solely based on this criterion. Similar frequency shift for each of the polymer samples may be a result of the contact mechanics between the probe and samples. For example, the evolution of equivalent circuit parameters of the transducer, particularly due to temperature rise, could be the cause. The frequencies of resonance and anti-resonance are depended on the L_1 and C_1 parameters. If the ratio of those quantities remains the same, the frequencies of resonance will not change either.

Aside from the frequency shifts, it is possible to observe the relative values of unimorph's deformation (compared with the deformation of unloaded transducer $\delta = 0.472$ *mm*). In the Figure 6.5 are shown relative deformations of prototype transducer "I", as a function of the normal force applied on the sample. The differences are not significant, yet it is possible to discern the tested materials apart for $F_N = 0.1$ *N* and 0.6 *N*.

Table 6.3 Measurement results of frequency shift measurement for prototype transducer "I" in contact with different materials

	F_N [N]	f_R [Hz]	δ [mm]		F_N [N]	f_R [Hz]	δ [mm]		F_N [N]	f_R [Hz]	δ [mm]
Mat A	0.1	239	0.30	**Mat B**	0.1	239	0.333	**Mat C**	0.1	239	0.346
	0.2	239	0.275		0.2	239	0.311		0.2	240	0.326
	0.4	241	0.267		0.4	240	0.282		0.4	240	0.305
	0.6	241	0.221		0.6	241	0.261		0.6	241	0.266
	0.7	243	0.216		0.8	242	0.266		0.8	241	0.254
					1	243	0.249		1	242	0.245
Mat D	F_N [N]	f_R [Hz]	δ [mm]	**Mat E**	F_N [N]	f_R [Hz]	δ [mm]	**Mat F**	F_N [N]	f_R [Hz]	δ [mm]
	0.1	239	0.346		0.1	239	0.383		0.1	239	0.353
	0.2	239	0.328		0.2	240	0.332		0.2	240	0.335
	0.4	240	0.297		0.4	240	0.298		0.4	241	0.307
	0.6	240	0.275		0.6	241	0.281		0.6	242	0.288
	0.8	241	0.269		0.8	241	0.267		0.8	243	0.277
	1	242	0.261		1	242	0.255		1	244	0.276
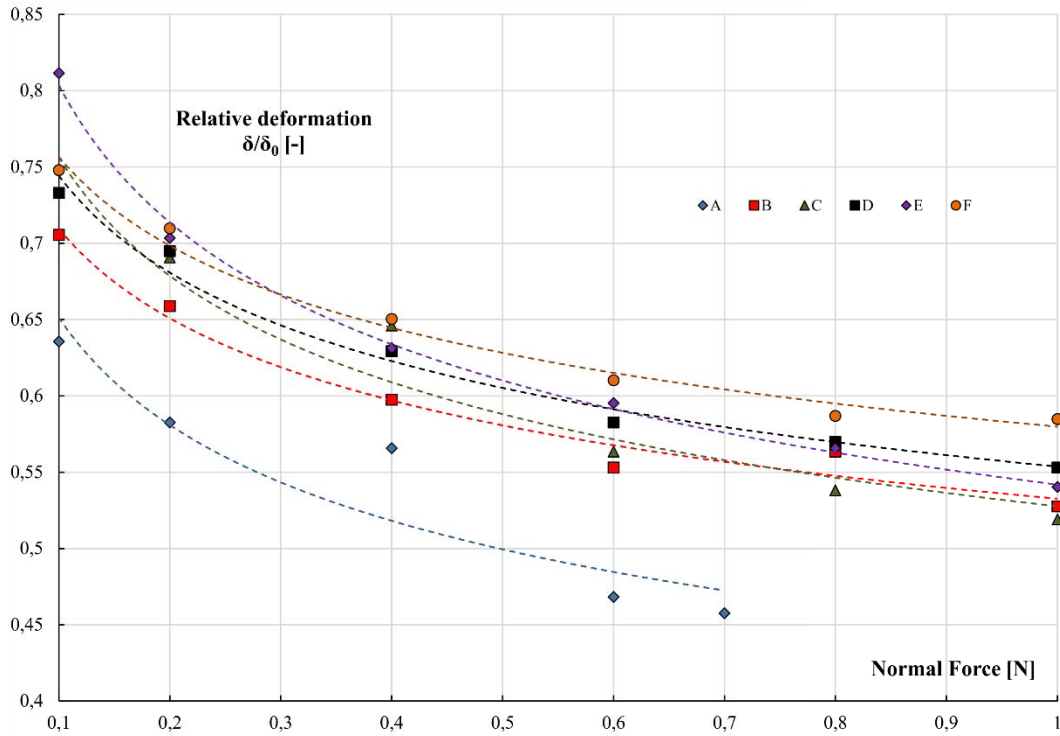
Figure 6.5 Relative deformation vs. normal force applied on different sample materials
- prototype transducer "I"

6.2.3 Electromechanical impedance

The measurement of impedance of the prototype transducers "I" and "II" began with examination of the work modes at the desired frequency range. Based on the input derived from modal FEM analysis results, the resonances of both prototype transducers were measured. The full considered frequency bands prototypes "I" and prototype "II" are shown in Figure 6.6 and Figure 6.7, respectively. Those results were used to determine the most suitable resonance frequencies to characterize the polymer samples (whether it was high amplitude of deformation, or the interesting motional character of the resonant mode).
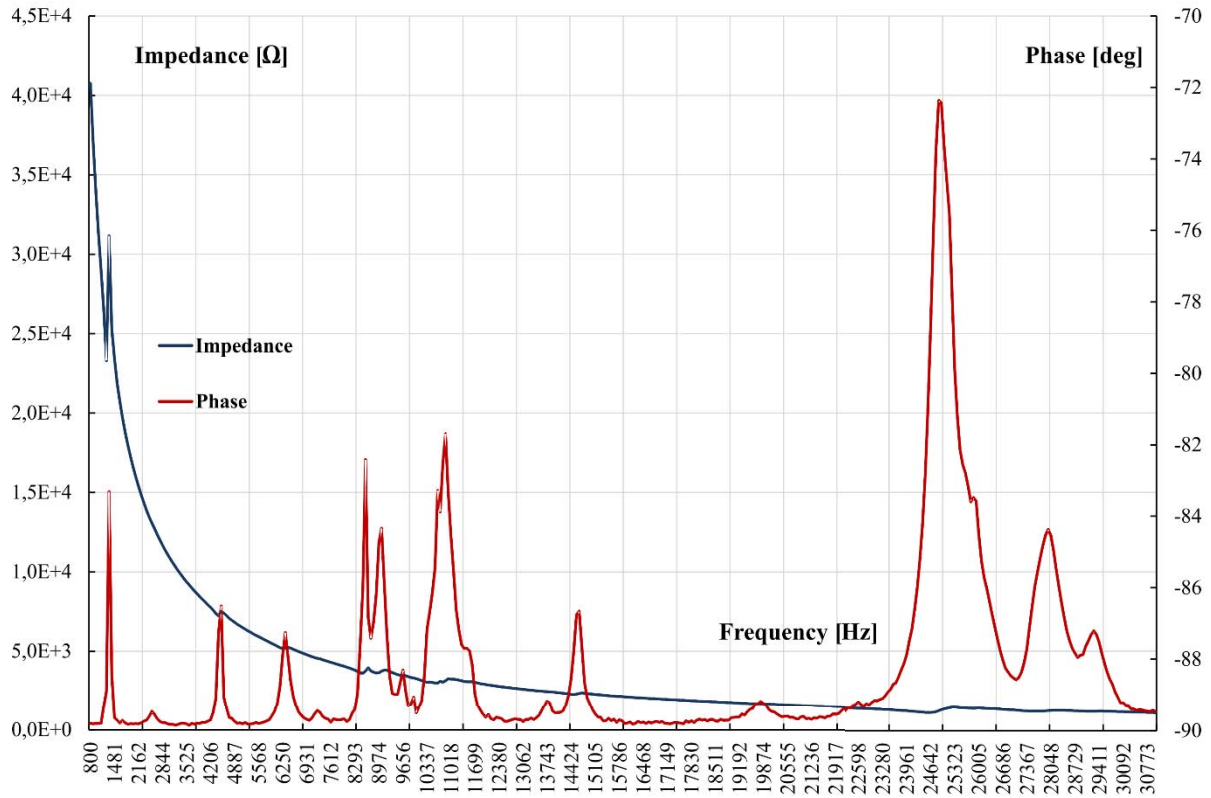
Figure 6.6 Impedance and phase characteristics including the required frequency spectrum
- prototype transducer "I"
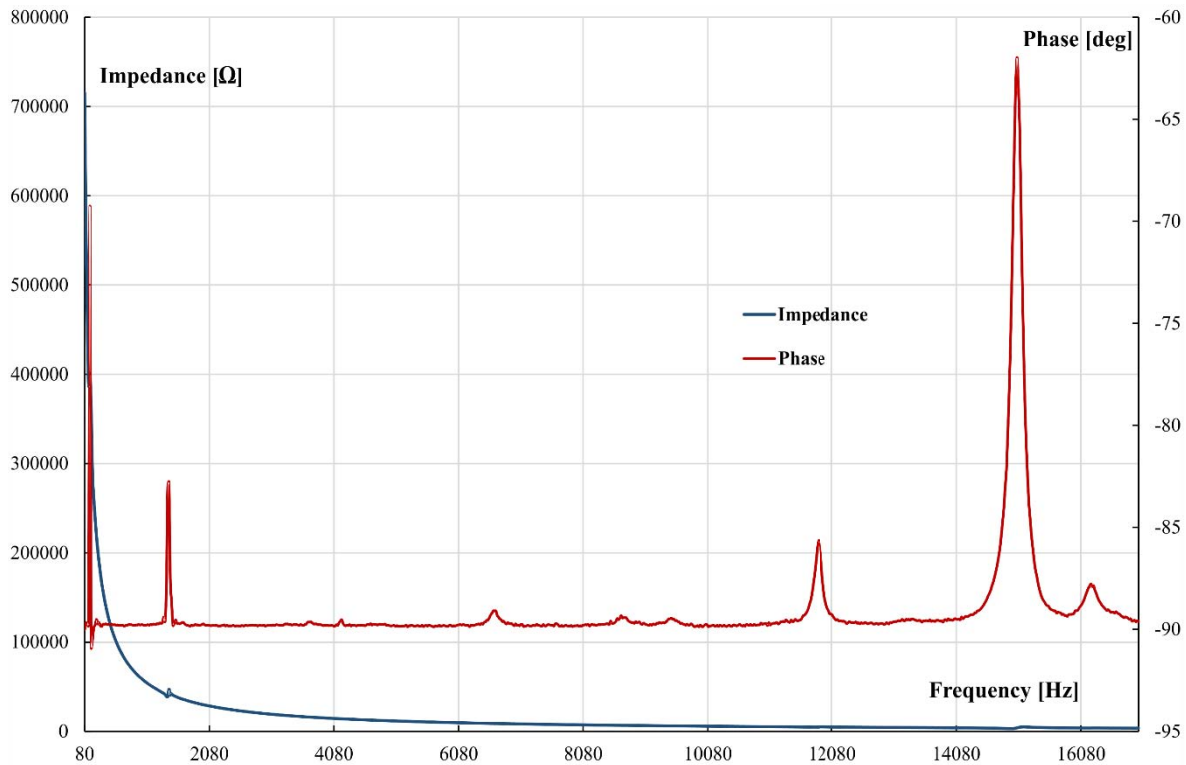
Figure 6.7 Impedance and phase characteristics including the required frequency spectrum
- prototype transducer "II"

Figure 6.8 and Figure 6.9 are shown impedance (admittance) and phase characteristics for frequencies in the vicinity of first resonance of both prototypes. The vibrational mode of the prototype transducers, associated with this frequency was of special importance, due to the character of the movement. The unimorph's free end (for both prototypes) was vibrating in a quasi-normal manner with respect to the tested material's surface, therefore it was the main work mode of the transducer, considering the indentation method. Moreover, the amplitude of the vibrations for first resonance frequency was the highest, compared with the higher order modes.

It should be noticed, that the value of resonance frequency of the prototype "II" was measured at 161 Hz, which corresponds well with the results of the FEM modal simulation (Table 5.6).

a)

b)
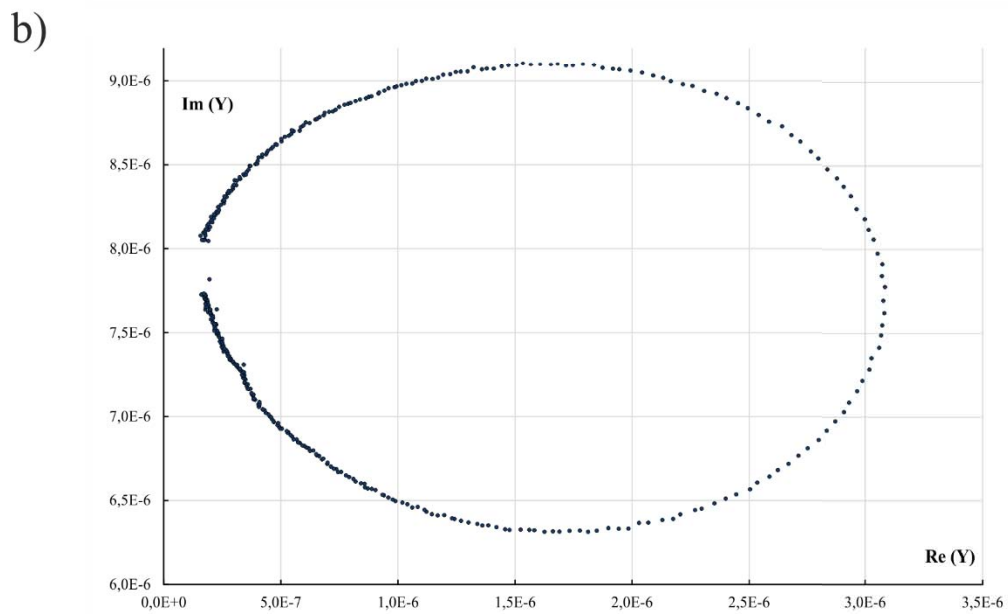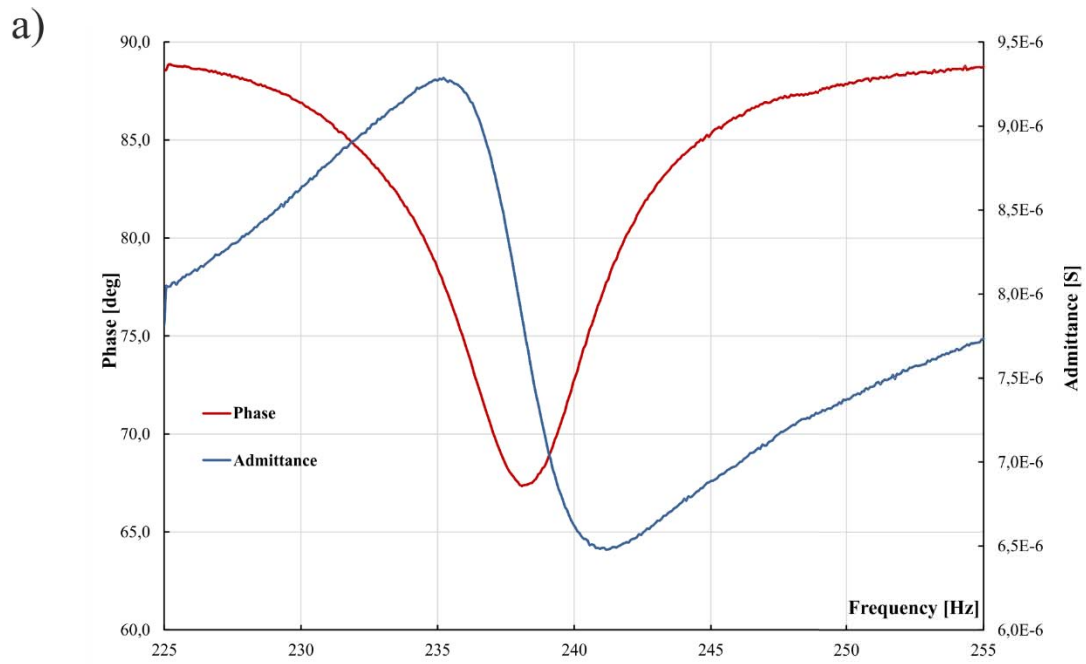
Figure 6.8 Bode (a), and Nyquist (b) plots for unloaded transducer state, near the first frequency of resonance - prototype "I"
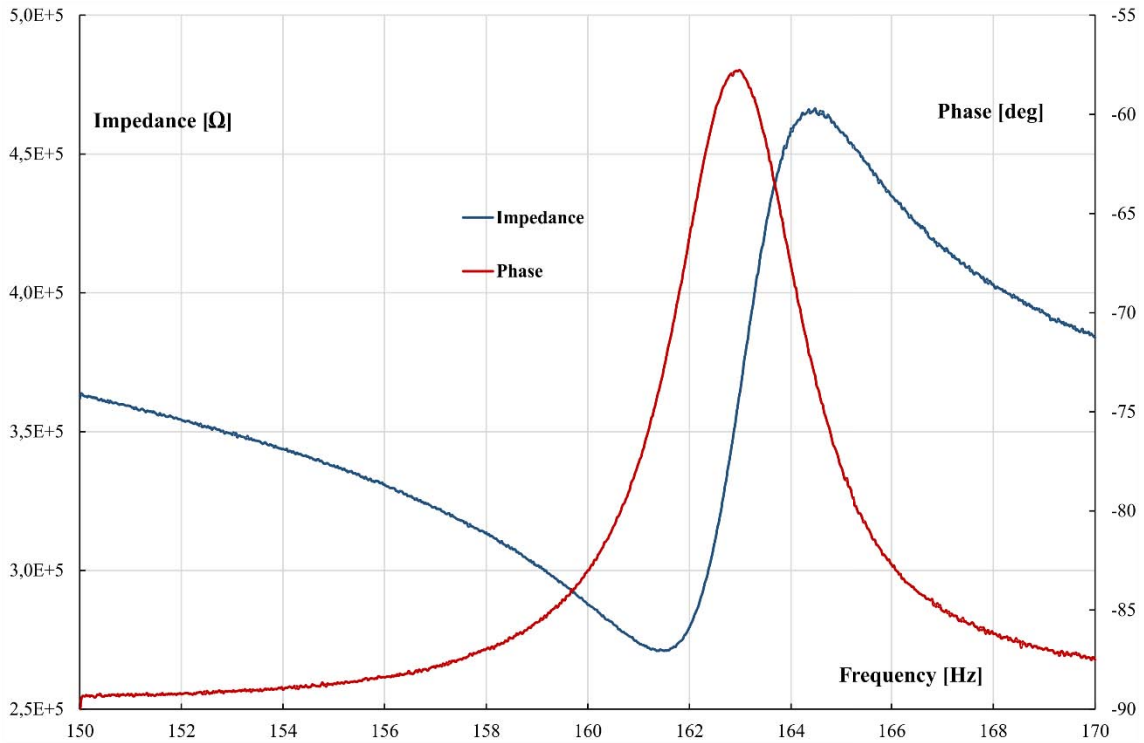
Figure 6.9 Bode (a), and Nyquist (b) plots for unloaded transducer state, near the first frequency of resonance - prototype "II"

The Bode and Nyquist diagrams were used to determine the parameters of the equivalent circuit for the piezoelectric transducer working near the resonance frequency, as it was described in section 4.2. The parameters of the tested materials were derived by comparing the results of the unloaded prototype transducer "I" and in contact with the materials. Two of them were particularly interesting. The resistance R_M modeling the contact friction losses and capacitance C_M which is an image of contact stiffness [6]. These two parameters will be discussed more in the next section of this chapter.

After the preliminary experimental examination of basic natural resonance frequencies of the prototype transducer "I", two of them were taken into further consideration. The first one (f_R =236Hz), due to its high deformation amplitude and a normal mode of operation. The other one, working in the ultrasonic frequency band (f_R=24.76kHz), was chosen due to its high sensitivity to measured quantities.

6.2.4 Equivalent circuit parameters

The measurement of equivalent circuit parameters R_M and C_M was divided between two resonance modes. Detection of the contact friction (resistance R_M) was made with the frequency f_R=236 Hz, while the contact stiffness inversely proportional to capacitance C_M was measured at f_R=24.76 kHz. This choice can be justified by the mechanical properties of the polymer samples. Submitted to low-frequency excitation at ambient temperature, polymers exhibit a predominantly elastic behavior (suitable for measuring friction and therefore resistance R_M). Subjected to a high frequency force at a room temperature, the polymer does not exhibit such a behavior and as a result, the high frequencies are more suitable for the detection of different mechanical properties, such as stiffness. Identified parameters for the resonance frequency f_R=24.76 kHz are listed in Table 6.4. Results of measurement for f_R=236 Hz are given in Appendix A3.

Table 6.4 Measurement results of equivalent circuit parameters for resonance frequency f_R=24.76 kHz and normal force F_N=0.1 N - prototype unimorph "I"

Material	Z [kΩ]	f$_R$ [Hz]	R$_M$ [kΩ]	L$_M$ [kH]	1/C$_M$ [V/C]	Δf [Hz]
No load	1.144	24.761	0	0	0	0
A	1.145	24.768	30	5.062	$1.25 \cdot 10^8$	7
B	1.144	24.761	13	8.314	$1.97 \cdot 10^8$	0
C	1.144	24.758	97	11.194	$2.54 \cdot 10^8$	-3
D	1.145	24.735	127	10.85	$2.36 \cdot 10^8$	-26
E	1.145	24.729	99	20.936	$4.83 \cdot 10^8$	-32
F	1.145	24.725	96	27.496	$6.42 \cdot 10^8$	-36
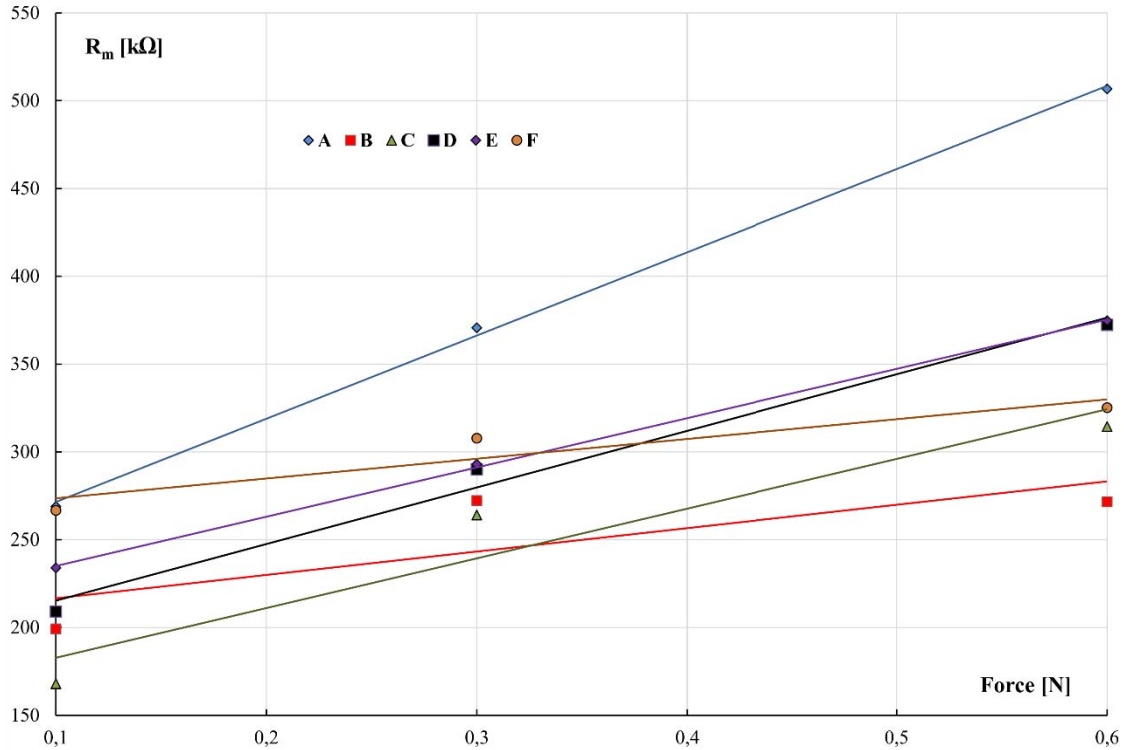
Figure 6.10 Evolution of the equivalent circuit's resistance R_m for different tested material samples

In Figure 6.10, the plotted evolution of equivalent circuit's resistance R_M is shown. The value of R_M is rising with the augmentation of F_N, which corresponds with the theory – R_M models the friction losses. Based on the $\tan\alpha$ (R_M/F_N) it is possible to differentiate tested material samples. On general basis, the prototype transducer "I" is sensitive to variations of contact resistance, and in consequence to the frictional properties of tested samples. This feature could be used to estimate the age of the tissue (by quantifying the loss of elasticity) in a comparative manner.
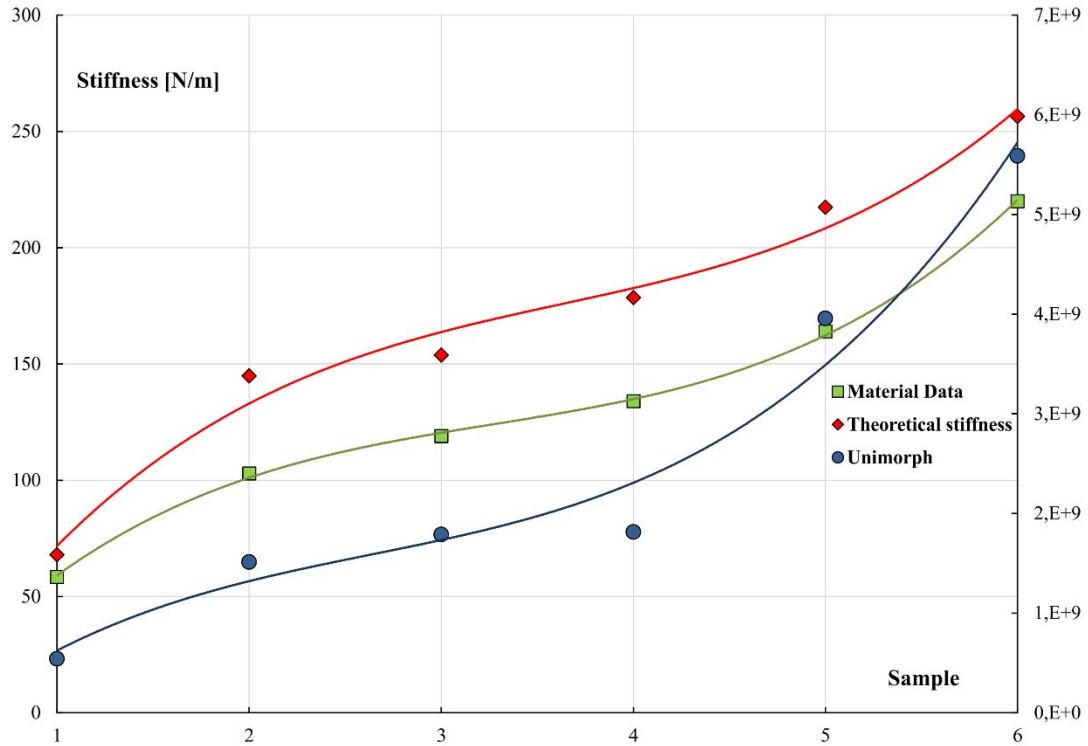
Figure 6.11 Comparison of stiffness plots for 6 tested polymers derived using: the impedance characterization of unimorph transducer (blue trace), theoretical calculations based on Hertz contact theory (red trace) and material data (green trace)

In the Figure 6.11, stiffness plots for 6 polymer samples are presented (tested under normal force of F_N=0.1 N and f_R=24.76 kHz). Green plot is based on the material data obtained from LTDS laboratory. Red is the theoretical stiffness K which is calculated from the equation below:

$$K_{theor} = \frac{F_N}{\delta} \tag{6.7}$$

Both of them show comparable values of stiffness, while blue trace (obtained by a transducer impedance characterization) gives similar behavior and evolution of polymer stiffness, but different absolute values.
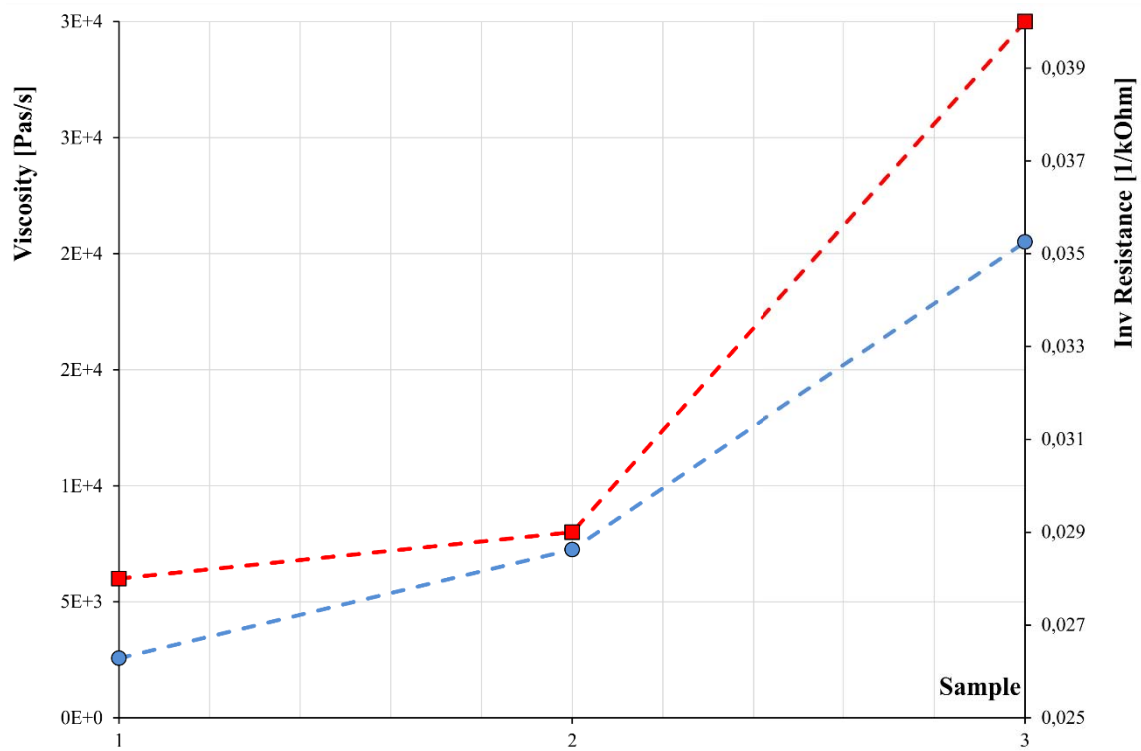
Figure 6.12 Evolution of the unimorph transducer's equivalent circuit resistance R_M (blue trace) and viscosity of 3 polymer samples (red trace) under the normal force of 0.05N
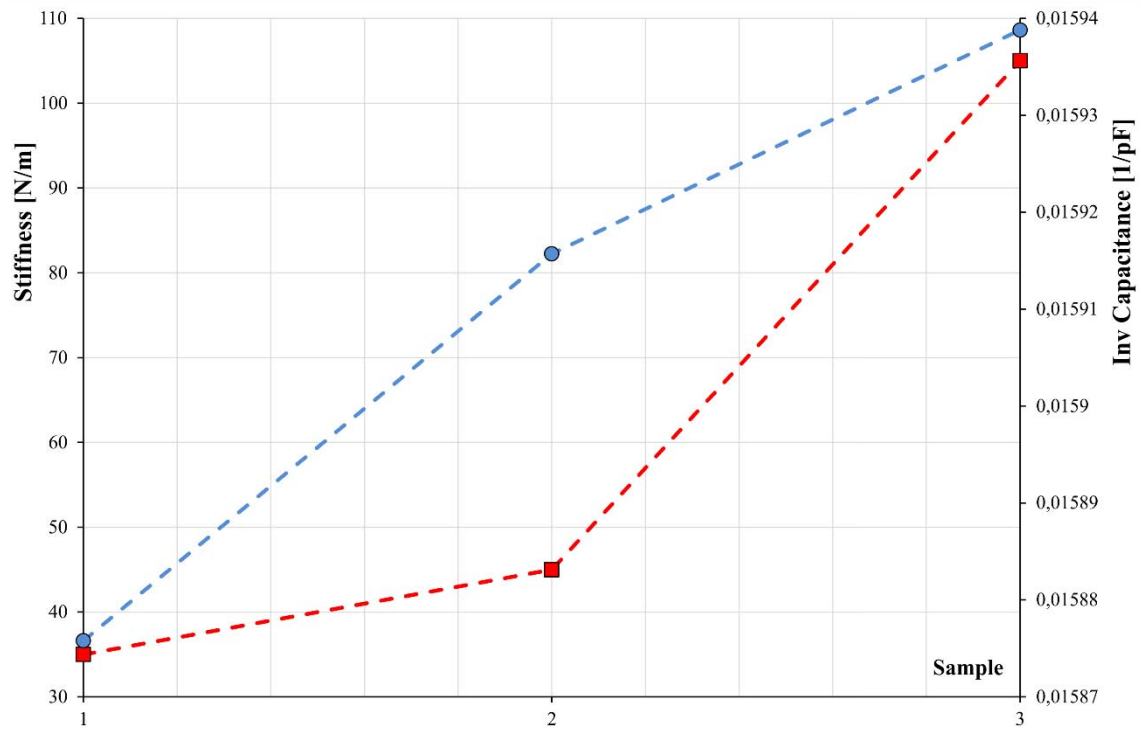
Figure 6.13 Evolution of the unimorph transducer's equivalent circuit capacitance C_M (blue trace) and stiffness of 3 polymer samples (red trace) under the normal force of 0.05N

130

Figure 6.12 and Figure 6.13 are presented the comparisons between the equivalent circuit resistance R_M and polymer viscosity (Figure 6.12), and equivalent circuit capacitance C_M and polymer stiffness (Figure 6.13) under the normal force of F_N=0.05N, for a group of 3 polymer samples. Similarities between the material data and the evolution of equivalent circuit's parameters should be noted. The calculated theoretical stiffness and the one obtained from LTDS laboratory have the same range of values. This means that the polymers were tested in similar external conditions to a static indentation. The stiffness image calculated from the response of the transducer – conditions similar to a dynamic indentation, contains different values. You can observe, however, a similar evolution. The same behavior but different values may be due to the result of the geometry of the indenter, which differs between the prototype unimorph transducer "I" and the test apparatus of the LTDS laboratory. Another reason for this discrepancy seems to be due to insufficient electromechanical conversion factor of the considered transducer, and also due to the impedance analyzer's low level of test voltage (< 1 V).

6.3 Conclusions

The results presented in this chapter confirmed that, unimorph sensor/actuator can differentiate tested materials, based on the values of equivalent circuit's resistance R_M and capacitance C_M,. The prototype transducer "I" is sensitive to variations of contact friction and contact stiffness, which can be related to viscosity and stiffness properties of tested materials. Such a distinction can serve as a method for tissue's age estimation (quantification of the elasticity loss) or as a detection of abnormal skin states (situations of excessive friction or abnormal skin fragility: eczema, scars, epidermolysis bullosa).

The main conclusion concerning the performance of the prototype unimorph "I" can be described as follows: at this stage of the research, the transducer can be used to give the evolution of the mechanical properties of the tested materials (subject to various external conditions). The mechanical properties can be expressed qualitatively, but not quantitatively, unless a reference sample is used. Nevertheless, the measurement results are promising, and can be used as a base an introduction to further future research.

7 FINAL CONCLUSIONS

The main goal of the dissertation was following: development a new concept, implementation and analysis of the piezoelectric resonant sensor/actuator for measuring the aging process of human skin. The research work has been carried out at the university of technology NP-ENSEEIHT-LAPLACE, Toulouse, France, and at the Gdansk University of Technology, Faculty of Electrical and Control Engineering, Research Unit of Power Electronics and Electrical Machines, Gdańsk, Poland.

7.1 Research results and achievements

The main focus of initial stages of research work covered study on the piezoelectric phenomenon, existing piezoelectric materials and their basic physical structure. Various types of piezoelectric transducers applied in the fields of medicine and bioengineering were reviewed. A special attention was devoted to the application of piezoelectric transducers for the measurement of soft tissues, including human skin. Serving the role of a theoretical background, the basic properties of the human skin were addressed. Finally, the methods for mechanical description of the skin were presented. The general requirements for the developed transducer were formulated on the basis of human skin's properties and indentation method for measurement of skin's mechanical properties.

A concept of transducer for the characterization of mechanical properties of soft tissues was developed. The piezoelectric resonant, bending transducer, referred to as "unimorph transducer" was chosen considering different topologies of piezoelectric benders based on the fulfillment of the formulated requirements: sufficient depth of tissue's penetration, suitable frequency range, generated force below 1 N, compact dimensions and relatively simple electro-mechanical structure.

The innovation of the project lies in the integration of the dynamic indentation method by using a unimorph transducer as an indentation device. This allows the use of a number of favorable electromechanical properties of piezoelectric transducers, i.e. high sensitivity, generation of vibrations in a wide frequency range, control of the measurement conditions by changing the work mode of the transducer, description of the measurement system by the electromechanical impedance methods. Piezoelectric transducers, due to their properties, are

likely to replace many of the current solutions for the measurement of mechanical quantities characterizing soft tissues.

Chosen structure of the piezoelectric unimorph transducer was described using analytical approach. It covered static calculations of tip deflection, dynamic description in the form of equivalent circuits (using modified Mason's circuit) and finally, assessment of the contact conditions based on the Hertz theory.

Using the theory of elasticity and Airy stress function, equations and boundary conditions describing the static 2D problem of multilayer bending transducer were equations were derived. Next, the general case study was simplified to one piezoelectric layer, one passive layer and electrode layer – an unimorph transducer. The influence of the geometric parameters on the free end deflection of the unimorph transducer was analyzed, and then the results were compared to the static deflection, determined using FEM analysis (Ansys software). Sufficient agreement between analytical and numerical results was proved.

Also, the dynamic behavior of the unimorph transducer was described using equivalent circuits. Classic Mason equivalent circuit was presented and then simplified to RLC circuit valid for the transducer working in the conditions of resonance. It presented dynamics of the unimorph transducer. Such circuit described dynamics of this device for each of the considered resonant modes. The final circuit gave the possibility of expressing the properties of the contact with the tested material by passive components added in series to the previous circuit. Comparative study of equivalent circuits for unloaded unimorph and loaded transducer being in contact with the material, gave the possibility to assess the mechanical properties of contact such as: stiffness/compliance or viscosity by equivalent circuit parameters.

The last part of analytical analysis covered the modeling of the contact between the unimorph transducer and the tested material, based on the classic mechanics theory developed by H. Hertz. A case of normal force loading was considered, including the description of contact area and pressure distribution within. Similar profiles of depth of indentation vs. normal force were obtained using the analytical calculation and the experimental characterization of the six polymers. Tangential loading force was also considered. It gave the description of quasi-static friction coefficient and the definition of contact areas where slip and

stick phenomena can be observed. It proved the fact that piezoelectric devices, generating μm range displacement, located themselves in linear, zero-slip or partial slip zone of contact.

The next stage of research project covered the numerical (FEM) analysis of parametric virtual 3D model of the transducer elaborated in Inventor software linked to Ansys Workbench. During the static analysis the unimorph's general principle of operation was graphically demonstrated. This part of numeric analysis has demonstrated the influence of different geometric parameters on the static deformation of the transducer. Moreover, different piezoceramics were tested for the active layer. Design requirements associated with operating frequencies of the unimorph transducer were tested using modal analysis. First three resonance frequencies were of special interest, due to the character of the movement of the indentation hemisphere at the free end of the transducer. For the geometry "I", the third resonance frequency f_{RIII} was above the required threshold of 1500 Hz (1667 Hz), while f_{RIII} for the geometry "II", was lower, at 1329 Hz.

The final stage of thesis involved the experimental verification of the developed analytical and numerical models and the prototype unimorph transducers. The results covered measurement of maximal deformations at the free end of the unloaded transducer working at first resonance frequency. Those values were compared with the analytical and numerical results with sufficient acuracy. The first prototype reached the following performance:

- $\delta_0 = 0.472$ mm
- $F_R = 236$ Hz

The last part of the experimental analysis covered the detection of the electromechanical impedance characteristics of both prototype unimorph transducers. After the preliminary inspection of the main resonance modes, the variation of impedance between the unloaded and loaded (in contact with the sample) unimorph sensor/actuator was verified in terms of contact conditions assessment, and finally the mechanical properties of tested polymer samples. The variation of the impedance was measured in terms of equivalent circuit parameters. It was registered at two main resonant modes:

- $f_R = 236$ Hz - due to its high deformation amplitude and a normal mode of operation, measurement R_M values were compared to the given data of contact friction and viscosity of the used polymers;

- f_R=24.76 *kHz*, ultrasonic mode due to its high sensitivity to variations of C_M (C_M was compared to given data of contact stiffness).

The electromechanical impedance analysis of the prototype unimorph transducer "I" showed that this type of piezoelectric structure can be used to evaluate the mechanical properties of soft tissues, such as: stiffness and viscosity. The evolution (variation) of modified Mason equivalent circuit's parameters for the unimorph transducer being in contact with the tested samples gives similar effect to the evolution of stiffness and viscosity taken from material data and analytical calculations. However, this type of analysis gives information about the relative values of material properties and their evolution. The acurate values of the mechanical parameters is not possible to obtain, without using a reference sample.

The main contributions of the dissertation:

- Specification of the requirements for the piezoelectric transducer for measurement of mechanical properties of soft tissues.
- Concept development of the piezoelectric unimorph transducer.
- Static characterization of the unimorph transducer using 2D analytical approach (deformation analysis in terms of the geometry and physical properties of the transducer).
- Development of a virtual model of the transducer (in operating mode – being in contact with tested material) using CAD techniques.
- Numerical (FEM ANSYS software) analysis of the virtual model of the piezoelectric unimorph transducer.
- Manufacturing the modified prototype of unimorph transducer using CNC technology and advanced piezoelectric ceramic materials.
- Verification of the unimorph transducer prototypes using laser interferometry and measurements of electromechanical impedance variations.
- Determination of the equivalent circuit's parameters for the prototype transducer (in operating mode – being in contact with tested material).

7.2 Future research works

The main future research goals can be specified as follows.

The extended experimental verification of the prototype unimorph transducer "II". In the frame of this thesis only the preliminary impedance characterization of the unloaded transducer was carried out. Those results, appeared promising, while compared with the prototype transducer "I" (lower frequencies of resonance, potentially higher vibrational amplitudes). The most important part of the measurement should cover the comparison of unloaded and loaded transducer.

The impedance measurement at the conditions of higher supplied voltage of the transducer, than the output voltage level of the impedance analyzer.

Design and manufacturing of dedicated laboratory test bench for experimental verification of the bending piezoelectric transducers. Such test bench should have the following parts: signal generator, dedicated resonant power amplifier (considering the wide frequency band and capacitive nature of piezoelectric devices) and measurement probes with high sensitivity. The whole measurement system should be controlled by interface developed in Matlab or LabView software.

LIST OF FIGURES

137

138

139

LIST OF TABLES

BIBLIOGRAPHY

[1]   A. Favier: Étude et validation d'un dispositif de caractérisation des tissus mous par mesure d'impédance acoustique. Rapport de Stage, LAPLACE, Toulouse, 2010

[2]   Advanced PhD - The Center for Advanced Studies - the development of interdisciplinary doctoral studies at the Gdansk University of Technology in the key areas of the Europe 2020 Strategy - http://advancedphd.pg.gda.pl/en, 2014

[3]   Ansys Workbench platform: http://www.ansys.com/Products/ Workflow+Technology/ANSYS+Workbench+Platform, 2014

[4]   Autodesk 3D Design Software: www.autodesk.com, 2014

[5]   B. Jaffe, R.S. Roth, S. Marzullo: Piezoelectric properties of lead zirconate-lead titanate solid-solution ceramic ware. J Appl Phys 25, 1954, p. 809–810.

[6]   B. Nogarede: Moteurs piézoélectriques. Techniques l'Ingénieur, traite Génie électrique, 1996

[7]   C. Nadal: Contribution à la conception et la modélisation transformateurs piézoélectriques dédiés à la génération de plasma, PhD Thesis, INP Toulouse, 2011

[8]   C. Pailler-Mattei, H. Zahouani: Analysis of adhesive behavior of human skin in vivo by an indentation test. Tribology International 39, 2006, p. 12–21

[9]   C. Pailler-Mattei, S. Bec, H. Zahouani: In vivo measurements of the elastic mechanical properties of human skin by indentation tests, Medical Engineering & Physics 30 (5), 2008, pp. 599–606

[10]   C. Pailler-Mattei, S. Pavan, R. Vargiolu, F. Pirot, F. Falson, H. Zahouani: Contribution of stratum corneum in determining bio-tribological properties of the human skin. 16th International Conference on Wear of Materials, Wear 263 (712), 2007, pp. 1038 – 1043

[11]   D. Zhou: Experimental Investigation of Non-linear Constitutive Behaviour of PZT Piezoceramics. Forschungszentrum Karlsruhe, Wissenschaftliche Berichte, FZKA 6869, PhD Thesis, pp. 6-12, 2003.

[12]   Erasmus Gdansk University of Technology: http://pg.edu.pl/international/o-programie, 2014

[13]   Exelis: Electro-Ceramic Products and Material Specification, 2013

[14]   Ferroperm Piezoceramics. Product Specification

[15]   G. Fleury, R. Berriet, L. O. Baron, B. Huguenin: New piezocomposite transducers for therapeutic ultrasound. Ultrasound Med Biol, 26(1), 2000, pp. 153-9

[16]   G. Lippman: Principe de la conservation de l'électricité. Ann Chimie Phys, 24, 1881, p. 145.

[17]   H. Han, J. Kim: Active muscle stiffness sensor based on piezoelectric resonance for muscle contraction estimation. Sensors and Actuators A, 194, 2013, pp. 212-219

[18]   H. Kawai: The piezoelectricity of poly(vinylidene fluoride). Japanese Journal of Applied Physics, 1969, 8, pp. 975

[19]   H. V. Tran, F. Charleux, A. Ehrlacher, M. C. Ho Ba Tho: Propriétés mécaniques multi-couches de la peau humaine in vivo. Colloque National en Calcul des Structures, 2005

[20]   H.J. Xiang, Z.F. Shi: Static analysis for multi-layered piezoelectric cantilevers. International Journal of Solids and Structures 45, 2008, pp. 113-128

[21]   J. Curie, P. Curie: Développement, par pression, de l'électricité polaire dans les cristaux hémièdres faces ' inclinées. C R Acad Sci Gen 91, 1880, p. 294–295.

[22]   J. Curie, P. Curie: Sur l'électricité polaire dans les cristaux hémièdres ' faces inclinées. C R Acad Sci Gen 91, 1880, p. 383–386.

[23]   J. G. Smits: The constituent equations of piezoelectric heterogeneous bimorphs. Proceedings of IEEE Ultrasonics Symposium, vol. 3, 1990, pp. 1275 - 1278

[24]   J. Tichý, J. Erhart, E. Kittinger, J. Prívratská: Fundamentals of Piezoelectric Sensorics, Springer, 2010.

[25]   K. Junwu, Y. Zhigang, P. Taijiang, C. Guangming, W. Boda: Design and test of a high-performance piezoelectric micropump for drug delivery. Sensors and Actuators, Volume 121, Issue 1, 2005, pp. 156–161

[26]   K. L. Johnson: Contact mechanics, Cambridge University Press, 1985, pp. 84-104

[27]   K. N. Malizos, M. E. Hantes, V. Protopappas, A. Papachristos: Low-intensity pulsed ultrasound for bone healing: An overview. Injury, Int. J. Care Injured, 37S, 2006, pp. 56-62

[28]   K. Suresh, G. Uma, M. Umapathy: Design of a resonance-based mass sensor using a self-sensing piezoelectric actuator. Smart Materials and Structures, 21 (2), 2012, 025015

[29]   KEYSIGHT Technologies: www.keysight.com /en/pd1000000858%3Aepsg%3Apro-pn-4294A/precision-impedance-analyzer-40-hz-to-110-mhz?cc=PL&lc=eng, 2014

[30]   L. Dalessandro, D. Rosato: Finite-element analysis of the frequency response of a metallic cantilever coupled with a piezoelectric transducer. IEEE Trans. on Instrumentation and Measurement, vol. 54, no. 5, 2005, pp. 1881-1891

[31]   L. Diez, H. Calas, A. Ramos, A-A. T. Gomez Alvarez-Arenas: Ultrasonic properties of bio-compatible silicone rubbers for matching transit-time piezoelectric transducers for blood flow estimation in coronary vessels. Ultrasonics Symposium (IUS), 2011 IEEE International, 2011, pp. 852–855.

[32]   L. Garbuio : Etude du phénomène de lubrification électroactive à l'aide d'actionneurs piézoélectriques. Application à la réduction des forces de frottement sec dans un moteur à combustion interne, PhD Thesis, INP Toulouse, 2006

[33]   L. Zhang: Analytical Modeling And Design Optimization Of Piezoelectric Bimorph Energy Harvester. PhD Thesis, University of Alabama, 2010

[34]   LAPLACE - Laboratoire Plasma et Conversion d'Energie: www.laplace.univtlse.fr, 2014

[35]   M. Budinger: Contribution à la conception et à la modélisation d'actionneurs piézoélectriques cylindriques à deux degrés de liberté de type rotation et translation. PhD Thesis, INP Toulouse, 2003

[36]   M. Jung, K. Kim, J-H. Lee: Micromachined ultrasonic transducer using piezoelectric pvdf film to measure the mechanical properties of bio cells, Sensors, IEEE, 2009, pp. 1225–1228.

[37]   M. L. Laquieze: Propriétés mécaniques de la peau et méthodes d'évaluation au regard du vieillissement cutané. Phd Thesis, Universite Montpellier, 2008

[38]   M. O'Donnell, L.J. Busse, J.G. Miller: 1. Piezoelectric Transducers, In: Methods in Experimental Physics. Academic Press, Volume 19, 1981, Pages 29-65

[39] M. S. Fleming, W. Luo: The anatomy, function, and development of mammalian Aβ low-threshold mechanoreceptors. Frontiers in Biology, Vol. 8, Issue 4, 2013, pp. 408-420

[40] M. S. Holi, S. Radhakrishnan, S. Swaranamani, N. A. Jayavelan: Quantitative ultrasound technique for the assessment of osteoporosis and prediction of fracture risk. J. Pure Appl. Ultrason. 27, 2005, pp. 55-60

[41] M. S. Vijaya: Piezoelectric Materials and Devices, CRC Press, 2013.

[42] M. Tanaka, C. Jiyon, Y. Chiba, Y. Tanahashi, S. Chonan: Development of a tactile sensor for monitoring prostate conditions. Japan, 2004, pp.185-188

[43] M. Wiertlewski, J. Lozada, V. Hayward: The spatial spectrum of tangential skin displacement can encode tactual texture. IEEE Transactions on Robotics 27, (3), 2011, pp. 461–472

[44] N. B. Smith: Perspectives on transdermal ultrasound mediated drug delivery. International Journal of Nanomedicine,Vol. 2, No. 4, 2007, pp. 585–594

[45] O. A. Lindahl, S. Omata, K. A. Angquist: A tactile sensor for detection of physical properties of human skin in vivo. Journal of Medical Engineering & Technology 01/1998, 22(4), pp. 147 – 53

[46] P. Dineva, D. Gross, R. Müller, T. Rangelov: Dynamic Fracture of Piezoelectric Materials. Springer, 2014.

[47] Polytec: CLV – Compact Laser Vibrometer. Manual

[48] R. D. Mindlin: Compliance of Elastic Bodies in Contact. ASME Trans. J. Appl. Mech., 16, 1949, pp. 259-268

[49] R. G. Ballas: Piezoelectric Multilayer Beam Bending Actuators, Springer, 2007.

[50] R. Okuno, M. Yokoe, K. Akazawa, K. Abe, S. Sakoda: Finger Taps Movement Acceleration Measurement System for Quantitative Diagnosis of Parkinson's disease. EMBS 28th Annual International Conference of the IEEE '06, 2006, pp. 6623 – 6626

[51] Research Unit of Power Electronics and Electrical Machines, Gdansk University of Technology, Faculty of Electrical and Control Engineering: http://eia.pg.edu.pl/kelime, 2014

[52] Rouchon J.-F., Harribey D., Tran D.H., Ryndzionek R., Sienkiewicz Ł., Ronkowski M., Michna M., Kostro G.: Assembling and testing of hybrid piezoelectric motor

based on electroactive lubrication principle. Archives of Electrical Engineering, vol. 62(2), pp. 237-249 (2013).

[53] Rouchon J.-F., Harribey D., Tran D.H., Ryndzionek R., Sienkiewicz Ł, Ronkowski M.: Hybrid piezoelectric motor based on electroactive lubrication principle. Prace Naukowe Instytutu Maszyn i Napędów Elektrycznych Politechniki Wrocławskiej, no. 66, p. 326-332, 2012.

[54] Ryndzionek R., Rouchon J-F., Ronkowski M., Michna M., Sienkiewicz Ł.: Design, modelling and analysis of a new type of piezoelectric motor. Multicell piezoelectric motor. IECON 2013 - 39th Annual Conference of the IEEE, pp. 3910-3915, Nov. 2013.

[55] Ryndzionek R., Sienkiewicz Ł., Ronkowski M., Szłabowicz W ., Grzywacz M.: Piezoelectric motors of simple and multi-motions systems: Review of chosen topologies and motion controls. Wiadomości Elektrotechniczne 2011-11.

[56] Ryndzionek R., Sienkiewicz Ł., Ronkowski M., Szłabowicz W ., Grzywacz M.: Review of chosen topologies of piezoelectric actuators. Zeszyty Problemowe - Maszyny Elektryczne, no. 92, p. 115-120, 2011.

[57] S. Mahmoodi, M. F. Daqaq, N. Jalili: On the nonlinear-flexural response of piezoelectrically driven microcantilever sensors. Sensors and Actuators A: Physical 153 (2), 2009, pp. 171 – 179

[58] S.-F. Ling, Y. Xie: Detecting mechanical impedance of structures using the sensing capability of a piezoceramic inertial actuator. Sensors and Actuators A: Physical 93 (3), 2001, pp. 243 – 249

[59] Sienkiewicz Ł., Rouchon J.-F., Ronkowski M., Kostro G.: Design and simulation of a new prototype of piezoelectric cantilever sensor/actuator for analysis of the soft tissues properties. Zeszyty problemowe – Maszyny Elektryczne no. 104/2014 pp. 219-224.

[60] Sienkiewicz Ł., Rouchon J.-F., Ronkowski M.: Design and analysis of a piezoelectric resonant sensor/actuator for measuring the aging process of human skin. Zeszyty problemowe – Maszyny Elektryczne no. 100/2013 pp. 83-89.

[61] Sienkiewicz Ł., Rouchon J-F., Ronkowski M., Kostro G., Ryndzionek R.: Identification of the mechanical properties of the skin by electromechanical

impedance analysis of resonant piezoelectric actuator. IECON 2013 - 39th Annual Conference of the IEEE, pp. 3940-3945, Nov. 2013.

[62]   V. Jalkanen, B. M. Andersson, A. Bergh, B. Ljungberg, O. A. Lindahl: Resonance sensor measurements of stiffness variations in prostate tissue in vitro—a weighted tissue proportion model. Physiological Measurement 27, 2006, pp. 1373–1386

[63]   V. Jalkanen, B. M. Andersson, A. Bergh, B. Ljungberg, O. A. Lindahl: Prostate tissue stiffness as measured with a resonance sensor system: a study on silicone and human prostate tissue in vitro. Med Bio Eng Comput 44, 2006, pp. 593–603

[64]   V. L. Popov: Contact Mechanics and Friction Physical Principles and Applications, Springer, 2010, pp. 55-60

[65]   V. Monturet: Conception optimale des actionneurs piézoélectriques à l'aide d'une méthodologie de type « Problème Inverse » - Application au cas des actionneurs répartis. PhD Thesis, INP Toulouse, 2002

[66]   V. Sharapov: Piezoceramic Sensors, Springer, 2011

[67]   W. G. Hankel: Uber die aktinound piezoelektrischen eigen schaften des bergkrystalles und ihre beziehung zi den thermoelektrischen. Abh Sachs, 12, 1881, p. 457.

[68]   W. Hu: Experimental search for high Curie temperature piezoelectric ceramics with combinatorial approaches, PhD Thesis, Iowa State University, 2011

[69]   W. P. Mason: An Electromechanical Representation of a Piezoelectric Crystal Used as a Transducer. Proceedings of the Institute of Radio Engineers, vol.23, no.10, 1935, pp.1252-1263

[70]   W. Przyborowski : Podstawy Teorii Elektropiezomechanicznych Przetworników – Silników Piezoelektrycznych. Maszyny Elektryczne – Zeszyty Problemowe, vol.108, no. 4, 2015, pp. 1-6

[71]   W. Szłabowicz: Contribution au dimensionnement et a la réealisation d'actionneur piézoeléctrique a rotation de mode fort coupe pour applications aéronautiques. PhD Thesis, INP Toulouse, 2006

[72]   Wikipedia Commons: https://en.wikipedia.org/wiki/File:Skin.png

[73]   Y. Yanling, L. Shih-Fu, L. Yong: A dynamic indentation method for characterizing soft incompressible viscoelastic materials. Materials Science and Engineering A 379, 2004, p. 334–340

APPENDIXES

A1. APDL scripts for FEM static analysis in ANSYS Mechanical

```
! Type d'elements
ET,1,SOLID98,0                              ! 3-D COUPLED-FIELD SOLID
!----------------Parameters--------------------------------------------------------------
l1_b=0.02
l2_b=0.06
h_b=0.02
l1_s=0.1
l2_s=0.012
h_s=0.003
l1_a=0.1
l2_a=0.012
h_a=0.002
V=200                          ! Voltage applied on the ceramic [V]
R=0.005                                     ! radius of the ball [m]
! -------------Material definition-------3 PZT 401 4 P1-89 5 EC-67 ------
! --------------------------------------------------------------------------------------
EMUNIT,     EPZRO, 8.854187E-12
!-----------------------------------
! Steel 100C6                     |
! ----------------------------------
MP,EX,1,210E9                               ! MODULUS OF ELASTICITY
MP,NUXY,1,.3                                    ! POISSON RATIO
MP,DENS,1,8400                                     ! DENSITY
!-----------------------------------
! Passive - brass            |
! ----------------------------------
MP,EX,2,105E9                               !MODULUS OF ELASTICITY
MP,NUXY,2,.3                                    ! POISSON RATIO
MP,DENS,2,8400                                     ! DENSITY
!-----------------------------------
! Ceramique PZT 401 positive       |
! ----------------------------------
MP,   DENS,  3,     7600                            ! DENSITY
MP,   KXX,   3,     0
MP,   MURX,  3,     1
! [E] PIEZO MATRIX CONSTANTS
TB,   PIEZ,  3                                      ! DEFINE PIEZO. TABLE
TBDATA,      3,    -5.98                            ! e31
TBDATA,      6,    -5.98                            ! e31
TBDATA,      9,    16.5                             ! e33, Polarization sign
TBDATA,     14,    13.1                             ! e15
TBDATA,     16,    13.1                             ! e15

! PERMITTIVITY
MP,   PERX,  3,     794                             ! Eps_s_11
MP,   PERY,  3,     794                             ! Eps_s_11
MP,   PERZ,  3,     630                             ! Eps_s_33
! [C] STIFFNESS MATRIX FOR PZT 401
TB,ANEL,3
TBDATA,      1, 11.7e10,   5.67E10,     5.38E10 ! Ce11,Ce12,Ce13
TBDATA,      7, 11.7E10,   5.38e10                  ! Ce11,Ce13
TBDATA,     12,    9.74E10                     ! Ce33
TBDATA,     16, 3.06E10                             ! Ce66, Inversion
TBDATA,     19, 2.56E10                             ! Ce44
TBDATA,     21, 2.56E10                             ! Ce44
!-----------------------------------
! Ceramique P1-89 positive      |
! ----------------------------------
MP,   DENS,  4,     7650                            ! DENSITY
MP,   KXX,   4,     0
MP,   MURX,  4,     1
! [E] PIEZO MATRIX CONSTANTS
TB,   PIEZ,  4                                      ! DEFINE PIEZO. TABLE
TBDATA,      3,    -6.16                            ! e31
```

```
TBDATA,      6,     -6.16                                    ! e31
TBDATA,      9,     13.90                                    ! e33, Polarization sign
TBDATA,     14,     12.86                                    ! e15
TBDATA,     16,     12.86                                    ! e15
! PERMITTIVITY
MP,    PERX,  4,     1142                                    ! Eps_s_11
MP,    PERY,  4,     1142                                    ! Eps_s_11
MP,    PERZ,  4,     668                                     ! Eps_s_33
! [C] STIFFNESS MATRIX FOR P1-89
TB,ANEL,4
TBDATA,      1, 154E9,           82E9,    81E9               ! Ce11,Ce12,Ce13
TBDATA,      7, 154E9,        81E9                           ! Ce11,Ce13
TBDATA,     12,     130E9                                    ! Ce33
TBDATA,     16, 36E9                                         ! Ce66, inversion
TBDATA,     19, 46E9                                         ! Ce44
TBDATA,     21, 46E9                                         ! Ce44
!---------------------------------
! Ceramique EC-67 positive        |
! ---------------------------------
MP,   DENS,  5,     7500                                     ! DENSITY
MP,    KXX,  5,     0
MP,   MURX,  5,     1
! [E] PIEZO MATRIX CONSTANTS
TB,   PIEZ,  5                                               ! DEFINE PIEZO. TABLE
TBDATA,      3,     -9.91                                    ! e31
TBDATA,      6,     -9.91                                    ! e31
TBDATA,      9,     13.9                                     ! e33, Polarization sign
TBDATA,     14,     15.9                                     ! e15
TBDATA,     16,     15.9                                     ! e15
! PERMITTIVITY
MP,   PERX,  5,     1220                                     ! Eps_s_11
MP,   PERY,  5,     1220                                     ! Eps_s_11
MP,   PERZ,  5,     483                                      ! Eps_s_33
! [C] STIFFNESS MATRIX EC-67
TB,ANEL,5
TBDATA,      1, 114.9E9,         45.46E9,        30.08E9     ! Ce11,Ce12,Ce13
TBDATA,      7, 114.9E9,      30.08E9                                    ! Ce11,Ce13

TBDATA,     12,    84.28E9                                   ! Ce33
TBDATA,     16, 34.7E9                                       ! Ce66, inversion
TBDATA,     19, 43.9E9                                       ! Ce44
TBDATA,     21, 43.9E9                                       ! Ce44
!------------------------------------------------------------------------------------------
!---------------------------geometry-------------------------------------------------------
Block,-l1_b,0,l2_s/2,l2_b/2,0,h_a+h_s+0.002
Block,-l1_b,0,-l2_s/2,-l2_b/2,0,h_a+h_s+0.002
Block,-l1_b,0,l2_b/2,-l2_b/2,0,-h_b+h_a+h_s+0.002
Block,-l1_b,l1_s,l2_s/2,-l2_s/2,0,h_s
Block,-l1_b,l1_a,l2_a/2,-l2_a/2,h_s,h_s+h_a
Block,-l1_b,0,l2_s/2,-l2_s/2,h_s+h_a,h_s+h_a+0.002
Block,-l1_b,0,l2_s/2+0.0115,-l2_s/2-0.0115,h_s+h_a+0.002,h_s+h_a+0.007
!------joing the base volumes into one--------------------------------------------------------
FLST,2,5,6,ORDE,4
FITEM,2,1
FITEM,2,-3
FITEM,2,6
FITEM,2,-7
VADD,P51X
!-----------------------new work plane (moved zero_point and rotation of YZ plane 90°)
FLST,2,1,8
FITEM,2,l1_s-R-0.001,0,0
WPAVE,P51X
wprot,0,270,0
!-----------Sphere-----------
SPHERE,R, ,0,180,
!-----------gluing the sphere onto the sub
FLST,2,2,6,ORDE,2
FITEM,2,1
FITEM,2,4
VGLUE,P51X
!-----------gluing the piezo onto the sub
```

```
FLST,2,2,6,ORDE,2
FITEM,2,2
FITEM,2,5
VGLUE,P51X
!----------gluing sub to base
FLST,2,2,6,ORDE,2
FITEM,2,2
FITEM,2,8
VGLUE,P51X
!----------gluing piezo to podk
FLST,2,2,6,ORDE,2
FITEM,2,3
FITEM,2,5
VGLUE,P51X
!---------------------------------------------material attribution-steel------------
VSEL,S,,,1
VATT,1,,1,0
ALLSEL,ALL
VSEL,S,,,6
VATT,1,,1,0
ALLSEL,ALL
!-----------------------------material attribution-brass and piezo---------
VSEL,S,,,4
VATT,2,,1,0
ALLSEL,ALL
VSEL,S,,,2
VATT,4,,1,0
ALLSEL,ALL
/REPLOT
!------------------------------------------------------Mesh---------------------------
SMRT,6
MSHAPE,1,3D
MSHKEY,0
!*
SMRT,5
/UI,MESH,OFF
!!!!!!!!!!!!!!!
CM,_Y,VOLU
VSEL, , , ,         6
CM,_Y1,VOLU
CHKMSH,'VOLU'
CMSEL,S,_Y
!*
VMESH,_Y1
!*
CMDELE,_Y
CMDELE,_Y1
CMDELE,_Y2
!*
!-------------Precise mesh of active el-------------------
VPLOT
!!!!!
SMRT,1
FLST,5,3,6,ORDE,3
FITEM,5,1
FITEM,5,-2
FITEM,5,4
CM,_Y,VOLU
VSEL, , , ,P51X
CM,_Y1,VOLU
CHKMSH,'VOLU'
CMSEL,S,_Y
!*
VMESH,_Y1
!*
CMDELE,_Y
CMDELE,_Y1
CMDELE,_Y2
!*
/USER,  1
/VIEW,  1,  0.812542996121    , -0.491231059667    ,  0.313792806599
```

```
/ANG,    1,   -78.0527021903
/REPLO
!--------------------------SOLUTION--------------------------------------------------
FINISH                                          !static analysis
/SOL
!*
ANTYPE,0
!---------------zero displacement-----------------
FLST,2,1,5,ORDE,1
FITEM,2,13
/GO
DA,P51X,ALL,0
!---------------voltage-----------------------------
FLST,2,1,5,ORDE,1
FITEM,2,18
/GO
DA,P51X,VOLT,V
!-----------
FLST,2,2,5,ORDE,2
FITEM,2,35
FITEM,2,-36
/GO
DA,P51X,VOLT,0                                   !ground
!-----------solution--------------
/SOLU
SOLVE
!---------------------------POSTPROC-------------------------------------------------
/POST1
SET,LIST
PLDISP,2
```

A2.   APDL script for mesh density test in Ansys Mechanical

```
!----------------------------------------------mesh------------------------------------
FINISH
/PREP7
!*
ESIZE,0.12E-02
SMRTSIZE, ,1,1,2,15,28,1.5,1,1,4,0
!*
ESIZE,0.12E-02
SMRTSIZE, ,1,1,2,15,28,1.5,1,1,4,0
!!!!!!!!!!!!!!!!!!!!!!!!!!!!!!!!!!!!!
MSHAPE,1,3D
MSHKEY,0
!*
FLST,5,3,6,ORDE,3
FITEM,5,1
FITEM,5,-2
FITEM,5,4
CM,_Y,VOLU
VSEL, , , ,P51X
CM,_Y1,VOLU
CHKMSH,'VOLU'
CMSEL,S,_Y
!*
VMESH,_Y1
!*
CMDELE,_Y
CMDELE,_Y1
CMDELE,_Y2
!*
VPLOT
!*
ESIZE,0.1
SMRTSIZE, ,1,1,2,15,28,1.5,1,1,4,0
!*
ESIZE,0.1
SMRTSIZE, ,1,1,2,15,28,1.5,1,1,4,0
!*
```

```
CM,_Y,VOLU
VSEL, , , ,         6
CM,_Y1,VOLU
CHKMSH,'VOLU'
CMSEL,S,_Y
!*
VMESH,_Y1
!*
CMDELE,_Y
CMDELE,_Y1
CMDELE,_Y2
```
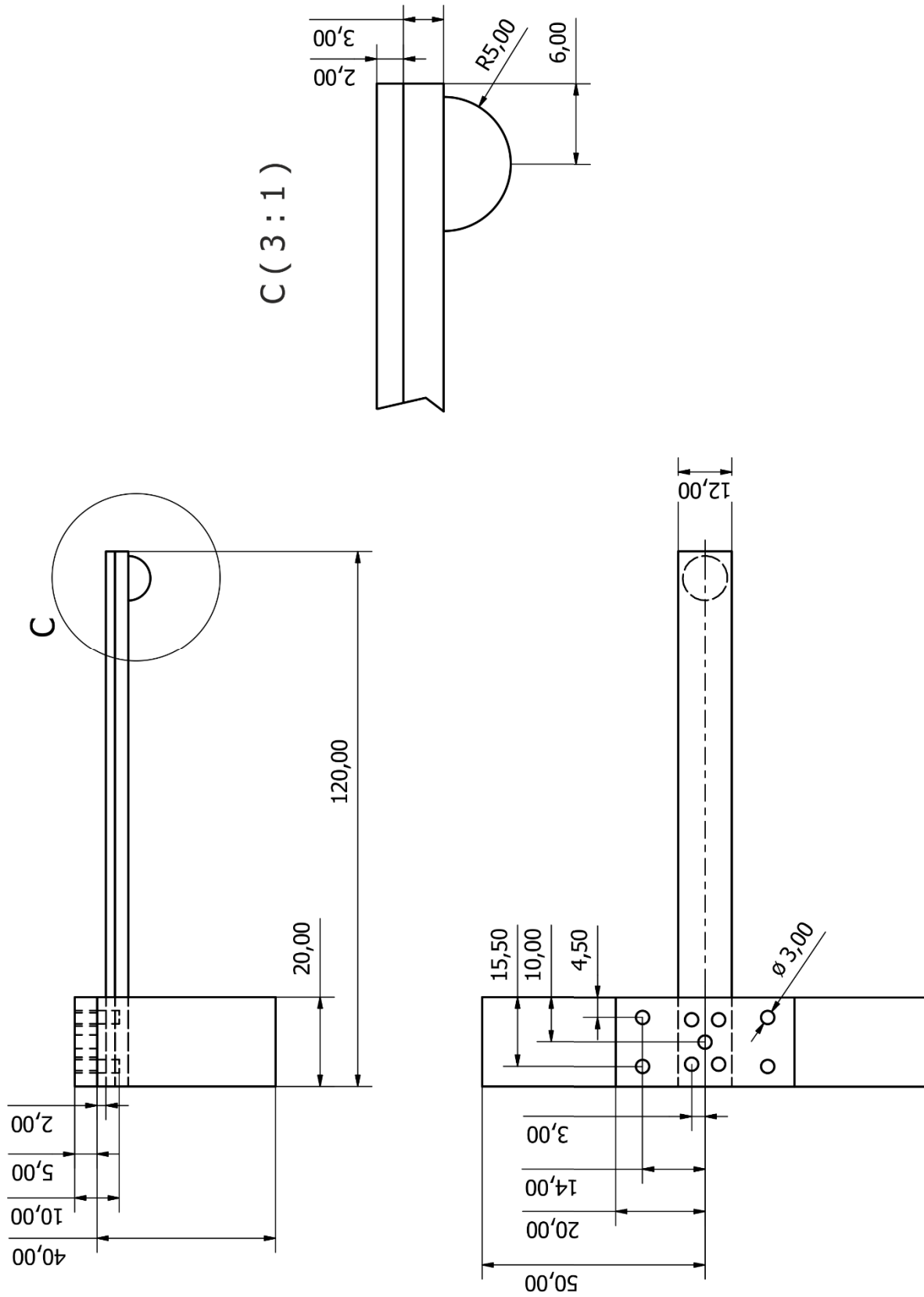
A3. Results of measurement of equivalent circuit resistance R_M for resonance frequency F_R=236 Hz and $F_N \in < 0.1; 0.6 > N$

Mat	$F[N]$	$Z[kΩ]$	$f[Hz]$	$R_1[kΩ]$	$L_1[kH]$	$C_1[pF]$	$C_0[nF]$	R_M [kΩ]	L_M [kH]	$1/C_M$	$ΔZ$ [kΩ]	$Δf[Hz]$
No load	-	**114.397**	**234.2**	**416.278**	**10.238**	**43.993**	**4.97**	**0**	**0**	**0**	**0**	**0**
A	0.1	124.565	232.3	685.178	9.122	50.183	4.93	268.9	-1.116	-2.80E9	10.168	-1.9
A	0.3	126.81	231.6	786.899	8.766	51.288	4.96	370.621	-1.472	-3.23E9	12.413	-2.59
A	0.6	129.1	230.6	923.041	8.528	52.905	4.96	506.763	-1.71	-3.83E9	14.703	-3.6
B	0.1	122.627	233.5	615.481	8.86	50.589	4.97	199.203	-1.378	-2.96E9	8.23	-0.7
B	0.3	124.499	232.4	688.499	8.999	49.743	4.97	272.221	-1.239	-2.63E9	10.102	-1.8
B	0.6	124.259	233.8	687.927	7.984	55.533	4.97	271.649	-2.254	-4.72E9	9.862	-0.4
C	0.1	121.476	233	584.283	8.227	54.255	4.97	168.005	-2.011	-4.30E9	7.079	-1.2
C	0.3	124.36	232.3	680.29	9.319	47.95	4.97	264.012	-0.919	-1.88E9	9.963	-1.9
C	0.6	125.5	232.1	730.732	8.789	50.697	4.97	314.454	-1.449	-3.01E9	11.103	-2.1
D	0.1	121.966	232.9	625.379	9.372	47.598	4.97	209.101	-0.866	-1.72E9	7.569	-1.3
D	0.3	123.399	232.7	706.262	9.555	46.614	4.97	289.984	-0.683	-1.28E9	9.002	-1.5
D	0.6	124.568	232.6	788.579	9.28	47.88	4.97	372.301	-0.958	-1.85E9	10.171	-1.6
E	0.1	121.403	233.6	650.197	9.041	49.294	4.97	233.919	-1.197	-2.44E9	7.006	-0.6
E	0.3	124.166	232.7	709.204	8.812	50.48	4.97	292.926	-1.426	-2.92E9	9.769	-1.456
E	0.6	124.473	233.5	790.972	8.721	50.78	4.97	374.694	-1.517	-3.04E9	10.076	-0.7
F	0.1	121.998	233.9	682.934	8.435	52.609	4.97	266.656	-1.803	-3.72E9	7.601	-0.26
F	0.3	124.147	233.7	724.054	8.729	50.629	4.97	307.776	-1.509	-2.98E9	9.75	-0.5
F	0.6	121.882	237.1	741.485	7.781	56.109	4.97	325.207	-2.457	-4.91E9	7.485	2.9

A4. Inventor technical drawing for prototype unimorph transducer "I"

153

A5.   Inventor technical drawing for prototype unimorph transducer "II"